Probing the Universe with Citizen Science and Gravitational Lensing

Dissertation

zur

Erlangung der naturwissenschaftlichen Doktorwürde

(Dr. sc. nat.)

vorgelegt der

Mathematisch-naturwissenschaftlichen Fakultät

der

Universität Zürich

von

Rafael Küng

von

Beinwil (Freiamt) AG

Promotionskommission

Prof. Dr. Prasenjit Saha (Leitung der Dissertation)
Prof. Dr. Philippe Jetzer (Vorsitz)
Prof. Dr. Romain Teyssier

Zürich, 2017

Summary

It is generally accepted that the universe is composed of about 70% dark energy, 25% dark matter and only 5% ordinary matter. It is, however, imperfectly understood how the universe progressed from nearly homogeneous, as seen in the cosmic microwave background, to the present day structure of groups and clusters of galaxies, arranged in sheets, filaments and voids. Galaxy formation mechanisms and the interplay between and distribution of dark and regular matter are under investigation.

In contrast to regular matter, dark matter does not interact with light and thus cannot be observed directly. It does, however, interact with spacetime, as Einstein's theory of general relativity directly relates the local curvature of spacetime to the matter content. Light from a background source passing such curved spacetime is deflected – an effect called gravitational lensing. If the effect of deflection is larger than its apparent angular size of the lensing object, *strong gravitational lensing* occurs, and two or even more images can possibly be seen. Luminous, opaque cores of galaxies are embedded in much larger, transparent dark matter halos, which makes galaxies excellent candidates for strong lensing. Light rays travelling through these dark halos can probe dark matter, allowing the formation mechanism theories to be tested.

Today a few hundred strong lenses are known. With ongoing and future surveys, covering a factor of a hundred vaster areas, this number is expected to increase by a hundredfold as well. Since those events are rare, gravitational lensing is difficult to find. There are, however, methods that can scale a hundredfold. For the next step in the analysis pipeline, creating models of the mass distribution of the lenses, there is not yet a process in place that can scale. This modelling is currently done manually by experts.

This work suggests involving citizen scientists in the modelling task. It develops a software framework to create models of gravitational lenses, using a novel and intuitive visual input method based on Fermat's principle. This allows citizen scientists to use this program collaboratively and become experienced lens modellers. The first part describes the design considerations and implementation details for building such software. The second part tests the implementation by giving a small group of volunteers fabricated, simulated lenses (sims) to model and comparing the results from the modelling process to the parameters used to produce the sims. We find that the volunteers perform comparably to a lensing expert and identify some areas for improvement. In the last part, the citizen scientists model a set of 58 newly found lens candidates. For each candidate, we present a selected best model with a set of diagnostics. Finally, we compare the total masses of these newly discovered lensing galaxies with their stellar masses. From this data, we can conclude that galaxies of masses a few times $10^{11}\,M_\odot$ are the most efficient producers of stars.

Zusammenfassung

Das Universum besteht aus 70% dunkler Energie, 25% dunkler Materie und 5% regulärer Materie. Es ist jedoch ungeklärt, wie sich aus dem homogenen Zustand des frühen Universums, wie mittels der kosmischen Hintergrundstrahlung beobachtet, die heutigen Strukturen mit Galaxien, Galaxiengruppen, Sheets, Filamenten und Voids bilden konnten. Gegenwärtig wird untersucht, wie sich Galaxien bilden, und dadurch wie dunkle und reguläre Materie interagieren und wie sich diese Materien im All verteilen.

Dunkle Materie interagiert nicht mit Licht und kann deshalb nicht direkt beobachtet werden. Allerdings beeinflusst sie direkt die Raumzeit. Einsteins Allgemeine Relativitätstheorie verbindet die Präsenz von Materie mit einer lokalen Krümmung der Raumzeit. Der *Gravitationslinseneffekt* beschreibt, dass Licht von einer Quelle hinter einer Masse durch die dadurch gekrümmte Raumzeit abgelenkt wird. Falls diese Ablenkung grösser ist als die räumliche Ausdehnung der ablenkenden Masse, lassen sich zwei oder mehrere Bilder derselben Quelle an unterschiedlichen Orten beobachten: der *starke Gravitationslinseneffekt*. Der sichtbar leuchtende, undurchsichtige Teil einer Galaxie ist eingebettet in einen grösseren Halo aus unsichtbarer dunkler Materie. Dies macht Galaxien zu exzellenten Kandidaten für den Gravitationslinseneffekt. Dadurch abgelenkte Lichtstrahlen sind hervorragende Instrumente, um dunkle Materie zu untersuchen und Entstehungstheorien von Galaxien zu testen.

Heute sind ein paar hundert solcher Linsen bekannt. Mit geplanten, neuen Observatorien können einen Faktor hundert grössere Bereiche des Himmels untersucht werden als bisher. Dadurch steigt die Zahl der potenziell entdeckbaren Linsen ebenfalls um einen Faktor hundert. Diese Linsen sind zwar schwierig zu finden, aber es gibt etablierte Methoden, die skalieren. Der nächste Schritt einer Analyse, das Modellieren der Massenverteilung dieser Linsen, wird heute aber noch manuell von Experten erledigt und skaliert deshalb nicht.

Diese Arbeit schlägt vor, Freiwillige (Citizen Scientists) in den Prozess des Modellierens miteinzubeziehen und stellt ein Programm zum Erstellen von Modellen vor. Es beruht auf einer neuen, intuitiven Eingabeform, angelehnt an das Prinzip von Fermat. Freiwillige erstellen Modelle im Team und werden dadurch zu erfahrenen Modellierern. Der erste Teil dieser Arbeit beschreibt die Überlegungen zum Design und der Implementierung dieses Programms. Der zweite Teil testet das Programm, indem eine Gruppe Freiwilliger einige simulierte Linsen modellieren. Die Parameter dieser Modelle werden mit den Eingabeparametern der Simulationen verglichen. Dies erlaubt die Qualität der erzeugten Modelle zu vergleichen und zu verifizieren. Für den letzten Abschnitt modellierten Freiwillige einige vor kurzem entdeckte Linsen. Die besten 58 resultierenden Gravitationslinsenmodelle werden, zusammen mit einigen neuen Diagnosekriterien, vorgestellt. Die totalen und stellaren Massen dieser Modelle erlauben die Überprüfung von Entstehungstheorien und den Schluss, dass Galaxien mit einer Masse von $10^{11}\,M_\odot$ am effizientesten Sterne produzieren.

Acknowledgements

Firstly, I would like to express my most profound gratitude to my supervisor *Prof. Dr Prasenjit Saha* for his never-ending support of my work, for his optimism, patience, motivation and energy. His immense knowledge and reassuring guidance helped me during my research and writing, with not only professional but also personal affairs. I consider myself particularly lucky to have him as my advisor and mentor for my Ph.D. study.

During my work, I had the great pleasure to meet many brilliant people, and I am very grateful to my colleagues who contributed immensely to my scientific research: *Dr Jonathan Coles*, *Dr Ignacio Ferreras*, *Dr Dominik Leier*, *Dr Phil Marshall*, *Dr Anupreeta More* and *Dr Aprajita Verma*; and the citizen scientists *Elisabeth Baeten*, *Claude Cornen*, *Christine Macmillan*, *Julianne K. Wilcox* and the whole community, without whom this work would not have been possible.

I want to express my special gratitude to *Prof. Dr Philippe Jetzer* for providing me with the opportunity to do my doctorate in his group at the University of Zurich. He also provided for and helped find funding that covered my salary and my many travel expenses for conferences and schools. I also greatly appreciate our many stimulating discussions that often extended beyond physics. I am also grateful to *Prof. Dr Ulrich Straumann* for my time at his side as a lecture assistant; it was an absolute pleasure. I would like to thank him also for insight behind the curtains of the faculty and, in particular, for his funding support in times of need. I am especially grateful to have earned the title and thrust of a quasi-experimental physicist – despite my theoretical education.

I particularly appreciate the great atmosphere I experienced with my office colleagues *Yannick Boetzel*, *Lionel Philippoz* and *Andreas Schärrer* which also extended to topics and activities outside of research and formed (ssh-ish) connections that will reach beyond academia. Moreover, I would like to thank *Carmelina Genovese*, *Esther Meier*, *Monika Röllin* and *Regina Schmid* of the Sekretariat for all their work; as well as the electronics lab and the workshop team, who always found some time to help with my stupid ideas; and the whole physics department.

Finally, I would like to thank my family: first and foremost, my mother *Maria Küng*, who never stopped supporting me; as did my grandparents *Emma* and *Isidor Ottiger* – thanks for the big inspiration they have been to me. Additionally, I thank my father *Adolf*, my sister *Sabine* and my brothers *Stefan* and *David*, not to forget the family of my godmother *Barbara Ursprung*, *Markus* and 'my' three little girls *Sara*, *Katrin* and *Franziska*. Last but not least, thank you to *Elizabeth Lopez Palos* for all your love, support and motivation.

Thank You.

Rafael Küng Zürich, September 21, 2017

Publications

Some of the following chapters are based on work already published.
Chapter 2 is published in Astronomy and Computing **23** *pp. 115–123* (Küng, 2018).
Chapter 3 is published in MNRAS **447** *pp. 2170–2180* (Küng et al., 2015).
Chapter 4 is published in MNRAS **474** *pp. 3700–3713* (Küng et al., 2018).

Table of Contents

Chapter 1

Introduction and Motivation

1.1 Gravitational lensing

In their famous experiment, Dyson, Eddington, and Davidson (1920) set out to measure the deflection of the positions of stars near a solar eclipse due to their light passing the gravitational field of the sun. They measured a deflection of the stars' positions as $1.61(31)''$, with just enough precision to deliver one of the earliest confirmations for Einstein's theory of general relativity.

Today, this effect of general relativity can be measured to a precision of $10^{-5}{}''$. It is not only measurable for the sun, but also for all the solar system gas giant planets – and not only close to the line of sight but all over the sky. Since the bodies in the solar system move around in the sky, this effect becomes time-dependent. Current day observations correct for this effect, to allow for more precise measurements (e.g., Gaia, see Crosta et al., 2015). What was a groundbreaking observation one hundred years ago became background noise to correct for.

If we consider objects at cosmological distances, a similar deflection occurs. However, it is not time-dependent. Due to the size of these extended objects, we can see a differential deflection – they are slightly stretched in one direction. This phenomenon can be used to study the large-scale structure (e.g., Kilbinger, 2015) as well as clusters of galaxies (e.g., Applegate et al., 2016). All of these are examples of *weak lensing* – where a single image of the observed structure is stretched and magnified.

On the other hand, there are phenomena where multiple images of a single object are observable. Imagine increasing the distance to the sun from 1 au to more than 550 au, the angular size of the sun would reduce to under $2''$ and thus be lower as the deflection. The deflection of the background light would be large enough for the light to curve around the sun on the near as well as on the far side; two or even more images of the same source would be visible (Landis, 2016). Even a telescope with poor resolution would at least see

a brightening of the source. Einstein (1936) wrote about lensing effects by stars, but he concluded: "there is no hope of observing this phenomenon directly". Today we have an automated photometry experiment including an early warning system in place that reports an average of two thousand such *microlensing* events each year (OGLE, Udalski, Szymanski, and Szymanski, 2015).

Lensing on larger and more massive objects than stars, called *strong lensing*, could be very well observable. In the same year, Zwicky (1937a) pointed out, that galaxies (which were called nebulae at the time) would produce multiple images that could be well resolved. The first observation of such a situation took more than forty years and was found by Walsh, Carswell, and Weymann (1979). Now, after another forty years, there are a few hundred lenses known. Recent studies, for example in the 155 $\deg^2$ CFHT LS[1], found on average more than one lens per square degree (More, Cabanac, et al., 2012; Gavazzi et al., 2014; Maturi, Mizera, and Seidel, 2014; More, Verma, et al., 2016; Paraficz et al., 2016). Extrapolation of this number with the area covered by the next generation of wide-field surveys, like KiDS[2], DES[3], LSST[4] or Euclid[5] lead to the plausible prediction of tens of thousands of strong lensing discoveries in the next five to ten years (Collett, 2015).

Strong lensing of galaxies that produces multiple images is very promising for science. The images can, however, only be seen if the deflection is larger than the apparent size of the object; otherwise, the light is blocked. By analysing the radial velocities of stars in galaxies, Bosma (1978) showed that the luminous, opaque centre of a galaxy is embedded in a dark, transparent halo that is much more massive than the core. Thus, galaxies with their dark but heavy halos are excellent candidates for gravitational lensing. These halos are thought to consist of an unknown form of matter, *Dark Matter*. The light passing these halos samples the distribution of this unknown constituent of the universe. Mapping these dark halos is the goal of this work.

1.2 Larger astrophysical context

To see why mapping dark halos is a significant problem, let us consider our current understanding of the universe. When the universe was less than 380 000 years old, it was a hot plasma of protons, neutrons, electrons and photons. Photons could not move freely, but scattered frequently with the free electrons and protons; thus, the universe was opaque. The interactions of baryons with photons led to acoustic oscillations in the density of the plasma (Eisenstein, 2005). The universe was then expanding further and thus cooling. At a critical point, the temperature dropped enough to allow primordial atoms to form, electrons were bound to atom cores, and thus photons decoupled. Since they were no longer scattered and

[1] Canada-France Hawaii Telescope Legacy Survey; 2003–2009; 155 $\deg^2$ (Cuillandre et al., 2012)

[2] Kilo-Degree Survey; operational since 2011; 1500 $\deg^2$ (Jong et al., 2013)

[3] Dark Energy Survey; operational since 2013; 5000 $\deg^2$ (Dark Energy Survey Collaboration, 2005)

[4] Large Synoptic Survey Telescope; planned first light in 2022; 18 000 $\deg^2$ (Ivezic et al., 2008)

[5] Spectroscopic All Sky Space Telescope; planned launch in 2020; 15 000 $\deg^2$ (Refregier et al., 2010; Laureijs et al., 2012)

could move freely, the universe became transparent (Peebles, 1968). The surface of the last scattering of photons is what we observe today as the Cosmic Microwave Background (CMB). It is imprinted with small density fluctuations – the acoustic oscillations happening at the moment of the last scattering. Those fluctuations in the CMB are the most distant objects or structures that we can and ever will be able to observe with photons.

Processes can be probed further back to the formation of light elements at their observable primaeval abundances (Cyburt et al., 2016). Earlier processes to the quantum gravity regime, fractions of a second after the Big Bang are also studied, but from the CMB we can deduct most of the current standard picture of the universe, the Lambda Cold Dark Matter (ΛCDM) model.

ΛCDM states that the universe contains a cosmological constant Λ corresponding to Dark Energy and Cold Dark Matter. The density parameter of Dark Energy Ω_Λ is 0.68, whereas the matter part splits up into Dark Matter Ω_c of 0.27 and baryonic (or regular) matter Ω_b of 0.05 and a negligible part of photon and neutrino radiation $\Omega_{rad} < 0.01$ (see Planck Collaboration et al., 2016). Historically, the first direct evidence for Dark Energy came from supernovae observations by Riess et al. (1998) and Perlmutter et al. (1999). The reason is that the effect of Dark Energy is much stronger in the late universe, when supernovae come into play, as opposed to the early epochs.

The CMB also reveals hints to the formation of large-scale structures. An analogue to the CMB fluctuations is seen in the large-scale structure of galaxies. Immediately after the observation of the CMB the *Dark Age* started. No radiation was emitted in this period, with the exception of the radiation of neutral hydrogen atoms with 21 cm wavelength due to the hyperfine spin-flip transition. Only now are we able to observe this epoch (Zaroubi et al., 2012). It is thought that during the Dark Ages the density fluctuations seen in the CMB grew through gravitational instabilities. Gas fell into the high-density regions, radiating away its potential energy and initially cooling as it fell in. Eventually the gas clumped into proto-stars. The ignition of this first generation of stars formed by gravitational collapse of hydrogen after hundreds of millions of years ended the period of darkness. These stars started to fuse heavier elements and re-ionised the interstellar medium. This was the beginning of the epoch that is currently ongoing, where structures on every scale can be observed including planetary systems, stars bound together in galaxies, groups and clusters of galaxies, and clusters arranged in sheets, filaments and voids.

Understanding the role of dark matter and baryonic matter (gas) is crucial to understand how the young universe evolved from the fluctuations in the CMB when 380 000 years old to the fully formed large-scale structures like stars and galaxies some 500 million years later. The general idea is as follows (consult for example Silk and Mamon, 2012, for a review).

As described, gas can fall into overdensities of the CMB fluctuations through radiative cooling and thus clump together to build stars. There are, however, feedback mechanisms leading to outwards pressure and thus stopping the infall. These mechanisms are currently under investigation but are thought to work as described in the following way.

Stellar populations include a range of stars with different masses. The more massive stars

burn up their fuel quickly and explode in a supernova after only a short lifetime (Baade and Zwicky, 1934). Supernovae heat up the interstellar medium (ISM), leading to pressure that counteracts gravitational attraction. In high-mass galaxies, gravitation can resist this, but in low-mass galaxies, the gravitation is too weak, and this pressure makes star formation inefficient. On the other hand, high-mass galaxies have very active supermassive black holes (SMBH) that form an active galactic nucleus (AGN). The AGN produces jets of material flowing outwards that disturb and inhibit further star formation processes and thus inhibit the formation of very heavy galaxies (Morganti, Tadhunter, and Oosterloo, 2005).

These feedback processes are, however, much debated. Galaxies where lensing occurs offer a special insight into the composition of galaxies, their baryonic and dark matter constituents and their distribution of matter. They provide valuable data to test the above-mentioned feedback theories (see, e.g., Koopmans et al., 2009; Leier, Ferreras, Saha, and Falco, 2011; Leier, Ferreras, and Saha, 2012; Leier, Ferreras, Saha, Charlot, et al., 2016; Bruderer et al., 2016)

The study of the lensing galaxies involves modelling their masses. This requirement was not widely discussed early on when lensing was nothing but a theory, but with the first lensing discoveries modelling quickly became an issue (Young, Deverill, et al., 1981; Young, Gunn, et al., 1981). Current day lens modelling has to be done individually by experts. This process, however, does not scale with the increase of tens of thousands of systems that is expected from current and next-generation surveys.

1.3 Introducing citizen science

Other research fields and projects have already faced the difficulty of an inadequate workforce and came up with an innovative solution. They asked for non-professional volunteers to participate in scientific research – citizen scientists. Before the professionalisation of the scientific community in the 19th century, one would now consider most scientists to be non-professional volunteers. With the advent of highly specialised equipment, especially in the natural sciences, research was professionalised and mostly took place inside universities. First projects reinvolving the non-professionals in research again – mostly for data collecting – date back to the beginning of the 20th century. A famous example, the CHRISTMAS BIRD COUNT, is the annual census of birds by volunteers organised by the National Audubon Society that started in 1900 and is ongoing (see, e.g., Butcher et al., 1990).

Modern communication technology, foremost the Internet, has allowed scientists to easily recruit large numbers of volunteers, distribute data and administer projects (Silvertown, 2009). One of the first projects making use of the new possibilities was the SETI@HOME project, released in 1999 (Werthimer et al., 2001), which inspired the STARDURST@HOME project (Westphal et al., 2005) and this, in turn, inspired the GALAXYZOO project (Lintott et al., 2008). The first was a distributed computing project where volunteers contributed the idle time of their computer, but there was no component of active participation involved. The second asked people to help identify stardust on images taken from a sample return

mission. The third invited citizen scientists to classify the morphologies of galaxies.

There is no unanimous definition of citizen science, and the distinction between distributed computing, clinical trials and amateur astronomy is vague. Haklay (2013) proposes four levels of citizen science: On the first level, volunteers are mostly passive sources of data and observation, as for example in the SETI@HOME project. The second level asks volunteers to contribute actively by solving a complex task, such as pattern recognition, classification or identification. The STARDUST@HOME and GALAXYZOO projects are categorised on this level. On the third level, volunteers are additionally involved in study design and the choice of research topics. The final level involves the citizen scientists in all stages, from the study design to the data analysis. Distributed computing projects are not considered citizen science by most researchers now. Kullenberg and Kasperowski (2016) report that citizen science is currently used mainly as a method of collecting and classifying data.

1.4 Development of SpaghettiLens

Strong gravitational lenses are a powerful tool for scientists, but they are rare and difficult to find. Several automated lens searching algorithms have been developed (Lenzen, Schindler, and Scherzer, 2004; Alard, 2006; Seidel and Bartelmann, 2007; More, Cabanac, et al., 2012; Gavazzi et al., 2014, among many other), but the resulting purity necessitates manual inspection of the results to reduce the generated samples by one or two orders of magnitude, as shown by Marshall, Verma, et al. (2016). That work introduces the SPACEWARPS project, which asks citizen scientists to help with the detection of gravitational lenses.

At one of the first preparatory meetings for what was later called the SPACEWARPS project in summer 2012 at the University of Zurich, the prospects of citizen science lens detection and modelling were discussed. There was a consensus among the invited scientists and the invited citizen scientists that existing modelling tools were not usable by citizen scientists. Various new tools were discussed (e.g., MOWGLI, presented in Naudus, Wallin, and Marshall, 2010), including a precursor program of SPAGHETTILENS developed by Sabah Ansari, Marion Baumgartner, Đorđe Mašović, Prasenjit Saha and the present author, using PIXELENS (Saha and Williams, 2004) as a backend. It was decided to develop a software stack for modelling as a lab project, a sub-project of SPACEWARPS that was later called SPAGHETTILENS by the volunteers.

The input method presented in the precursor was combined with a new backend by Jonathan Coles called GLASS (Coles, Read, and Saha, 2014), which improves on PIXELLENS and, in particular, implements a new sampling algorithm by Lubini and Coles (2012). In contrast to other tools, this program uses arrival time contours and Fermat's principle as a means of input. This idea is based on the presentation of lensing theory by Blandford and Narayan (1986) and is summarised as follows.

Typically, in the field of strong lensing, we consider the lens and the source to each lie in a plane perpendicular to the line of sight. They are separated from the observer by the angular diameter distances D_{OS} from the observer to the source, D_{OL} from the observer to the lens

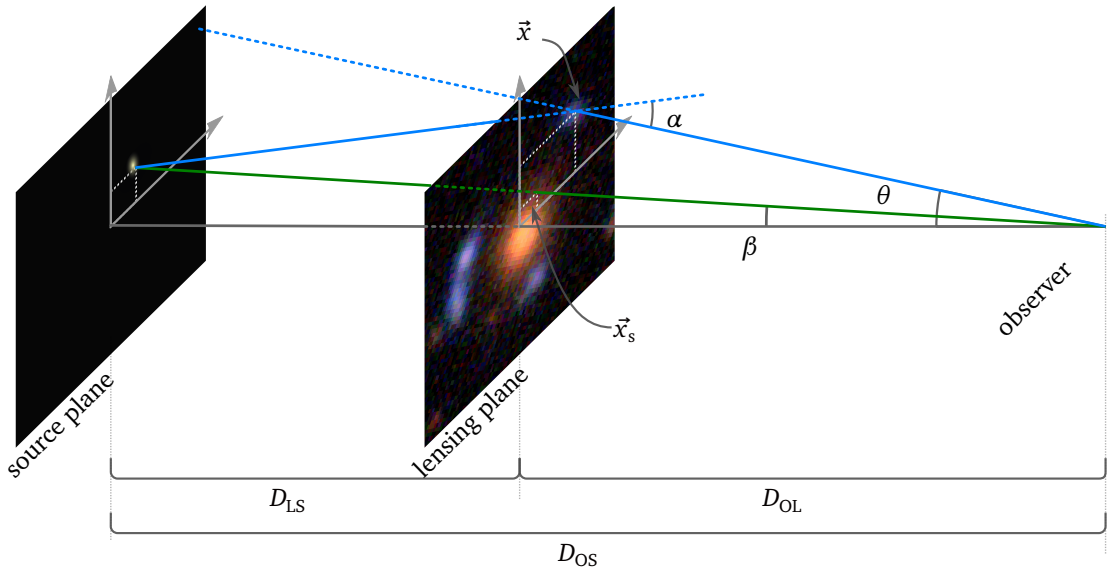

Figure 1.1: Usual layout of gravitational lensing.

and D_{LS} from the lens to the source. In the ΛCDM model, angular diameter distances D_{AB} are defined as:

$$D_{AB} = \frac{c}{H_0} \frac{1}{1+z_B} \int_{z_A}^{z_B} \frac{dz}{\sqrt{\Omega_M (1+z)^3 + \Omega_\Lambda}}, \tag{1.1}$$

From Figure 1.1, we can derive the lensing equation graphically on the plane of the source object using the angular separation from an arbitrarily chosen optical axis to the image on the sky $\vec{\theta}$ and to the actual position of the source $\vec{\beta}$, and the deflection angle $\vec{\alpha}$ due to lensing. Assuming small angles we arrive at:

$$\vec{\theta} D_{OS} = \vec{\beta} D_{OS} + \vec{\alpha} D_{LS} \tag{1.2}$$

Converting into angular separations on the lensing plane by applying $\vec{x} = D_{OL}\vec{\theta}$ and $\vec{x}_s = D_{OL}\vec{\beta}$ and rearranging for the deflection angle leads to:

$$\vec{\alpha} = (\vec{x} - \vec{x}_s) \frac{D_{OS}}{D_{LS} D_{OL}} \tag{1.3}$$

On the other hand, we know from the theory of general relativity that the deflection angle $\alpha_\bullet$ of a light ray with impact parameter b due to the potential $\Phi = -\frac{GM}{r}$ of a point mass M can be written as:

$$|\alpha_\bullet(b)| = \frac{4GM}{bc^2} \tag{1.4}$$

Equation (1.4) illustrates that $\alpha_\bullet$ is linear in M. This allows one to write the deflection of an extended lensing mass α as the sum of point masses. The deflection takes place mostly Δz

near the lens on the optical axis. Comparing the typical angular diameter distances to Δz, we can assume a *thin lens*, where $\Delta z \approx 0$, thus the light ray is only deflected at the point where it crosses the lensing plane. This justifies reducing the extended mass distribution $\rho(x, y, z)$ of the lens into a two dimensional surface density $\Sigma(\vec{x})$, the mass distribution projected onto the lensing plane $\Sigma(\vec{x}) = \int \rho(x, y, z)\mathrm{d}z$, using angular separation coordinates $\vec{x}$ on the lensing plane. Putting these observations together, we can rewrite Equation (1.4) for an extended, thin lens as:

$$\vec{\alpha} = \frac{4G}{c^2} \int \frac{(\vec{x} - \vec{x}')}{|\vec{x} - \vec{x}'|^2} \Sigma(\vec{x}')\mathrm{d}^2\vec{x}' \tag{1.5}$$

Combining Equation (1.5) and Equation (1.3) together and rearranging leads to:

$$0 = (\vec{x} - \vec{x}_\mathrm{s}) \frac{D_\mathrm{OS}}{D_\mathrm{LS} D_\mathrm{OL}} - \frac{4G}{c^2} \int \frac{(\vec{x} - \vec{x}')}{|\vec{x} - \vec{x}'|^2} \Sigma(\vec{x'})\mathrm{d}^2\vec{x}' \tag{1.6}$$

In integrating this expression, we note that this expression is the gradient of a scalar with the dimension of distance. Multiplying by $(1 + z_\mathrm{L})c^{-1}$ provides a time.

$$0 = \nabla \left[\frac{1 + z_\mathrm{L}}{c} \frac{1}{2} (\vec{x} - \vec{x}_\mathrm{s})^2 \frac{D_\mathrm{OS}}{D_\mathrm{LS} D_\mathrm{OL}} - \frac{1 + z_\mathrm{L}}{c} \frac{4G}{c^2} \int \log(\vec{x} - \vec{x}')\Sigma(\vec{x}')\mathrm{d}^2\vec{x}' \right] \tag{1.7}$$

The term in square brackets denotes the total light travel time $t(\vec{x})$ of a virtual light ray originating at the source, passing $\vec{x}$ on the lensing plane and arriving at the observer, which in this work is called *arrival time surface*. In particular, the first part of the bracket can be identified as the geometrical part t_geom, whereas the second part is a deflection due to a gravitational delay t_grav experienced from the gravitational potential of the lensing mass.

We can see that Equation (1.7) is basically Fermat's principle (Ghatak, 2010). The arrival time surface reveals the travel time for virtual photons. Real photons, however, only take paths that are stationary; those paths are where one can observe a lensed image. The arrival time surface provides an intuitive link between what is seen on a survey image and the result of the modelling process, the surface mass density $\Sigma(\vec{x})$. Even though Equation (1.7) looks complicated, the underlying idea can be easily explained graphically to citizen scientists– only the concept of stationary points and self-intersecting contour lines need to be explained; Section 2.3.1 with Figure 2.3 and Section 3.2 illustrate this explanation. This is the reasoning behind choosing this as an input method and choosing GLASS as the backend simulation program; Section 2.5.1 provides more details about GLASS. A general overview on and additional details about the implementation of these concepts follow in detail in Chapter 2.

After the implementation of a complete beta version and some internal testing, in summer 2013 the SPAGHETTILENS beta version was presented to the volunteers. Initial feedback was that the citizen scientists preferred to work collaboratively on creating models. This feature was implemented by giving the volunteers the possibility to iteratively load models created by other users and thus create refined versions of existing models. This leads to a tree of models whose branches explore the space of possible models. To test this feature, a

small group of volunteers started an effort to collaboratively model the SPACEWARPS lensing candidate J022409.5−105807. They published their findings in the form of a collaborative letter published on a now-defunct web page[6], and finally entered into the collection of models published in Küng et al. (2018), presented in Chapter 4.

Around the same time, in autumn 2013, we proposed a *sim modelling challenge* to test the beta version of the SPAGHETTILENS system in a real-world scenario. We drew 29 simulated lenses (sims) from a broader set and presented them to the volunteers for modelling. We counted the error rate in recovering image position and morphology and compared the recovered mass profile with the original one. The findings of this test were quite promising and are presented in Chapter 3, which was published in Küng et al. (2015).

The feedback from these early tests by volunteers and scientists and the investment in new server hardware motivated a general overhaul of the system until autumn 2014. Some minor changes on the user interface combined with a substantial redesign of the backend and the database eventually lead to the release of the first stable version of SPAGHETTILENS in summer 2015, with the setup that is presented in Chapter 2 and was published in Küng (2018).

With the new version running, the volunteers were asked to focus on creating models for all the lensing candidates identified by the SPACEWARPS project and published in More, Verma, et al. (2016). The resulting models of these candidate lenses are presented in Chapter 4 and they are published in Küng et al. (2018). It also proposes a set of diagnostic criteria to help volunteers assess their models. During the collection of these models, a few additional improvements were implemented:

- After the testing of SPAGHETTILENS with the sims, there was a tendency determined to recover mass profiles which were too shallow. This was addressed by increasing the pixel resolution of the models in the innermost regions.
- In a summer project in 2015, Lucy Oswald worked on fitting the non-parametric, pixelated ensemble of mass models created by SPAGHETTILENS to a single parametric model of an isothermal ellipsoid.
- SPAGHETTILENS generates synthetic images of the user input as a means for feedback to the user. These synthetic images are essentially renderings of the gradient of the arrival time surface. Work on a prototype for better synthetic images began to improve this feedback mechanism for the citizen scientists. The pixels of images on the lensing plane were mapped back on the source plane and merged to a source image. This image is then lensed by the model the user created and is displayed as feedback of the modelling process.

The details about these improvements are presented in Section 4.8. In spring 2015, the collaboration with Ignacio Ferreras started with the determination of the stellar mass for

[6] `http://letters.zooniverse.org`

modelled lenses by comparing photometric data of the lenses with M/L estimates from population synthesis models. The comparison between the halo mass and the stellar mass for all the models forms one of the main points of Chapter 4 and is presented in Figure 4.7. This is the main scientific result of this work.

Chapter 2

The SPAGHETTILENS Software Stack

Original title:
"SpaghettiLens: A software stack for modelling gravitational lenses by citizen scientists"

Rafael Küng[1]

[1] Physik-Institut, University of Zurich, Winterthurerstrasse 190, 8057 Zurich, Switzerland

Published in:
Astronomy and Computing, Vol. 23, pp. 115–123 (04/2018)

Abstract

The 2020s are expected to see tens of thousands of lens discoveries. Mass reconstruction or modeling of these lenses will be needed, but current modeling methods are time intensive for specialists and expert human resources do not scale. SPAGHETTILENS approaches this challenge with the help of experienced citizen scientist volunteers who have already been involved in finding lenses. A top level description is as follows. Citizen scientists look at data and provide a graphical input based on Fermat's principle which we call a Spaghetti Diagram. This input works as a model configuration. It is followed by the generation of the model, which is a compute intensive task done server side though a task distribution system. Model results are returned in graphical form to the citizen scientist, who examines and then either forwards them for forum discussion or rejects the model and retries. As well as configuring models, citizen scientists can also modify existing model configurations, which results in a version tree of models and makes the modeling process collaborative. SPAGHETTILENS is designed to be scalable and could be adopted to problems with similar characteristics. It is licensed under the MIT license, released at `http://labs.spacewarps.org` and the source code is available at `https://github.com/RafiKueng/SpaghettiLens`.

2.1 Introduction

The rate of discoveries of gravitationally lensing galaxies is increasing rapidly. As an example consider the Canada-France Hawaii Telescope Legacy Survey (CFHTLS, Cuillandre et al., 2012). Intensive searches using robotic and visual methods in the survey area of 155 $\deg^2$ have revealed on average more than one lens per square degree (More, Cabanac, et al., 2012; Gavazzi et al., 2014; Maturi, Mizera, and Seidel, 2014; More, Verma, et al., 2016; Paraficz et al., 2016). With ongoing surveys like (DES, KiDS) and next generation wide field surveys (Euclid, LSST, WFIRST) tens of thousands of lens candidates are to be expected (Collett, 2015).

Studies using galaxy lenses to study galaxy structure, dark matter and cosmological parameters (for example Koopmans et al., 2009; Leier, Ferreras, Saha, and Falco, 2011; Leier, Ferreras, and Saha, 2012; Sereno and Paraficz, 2014; Rathna Kumar, Stalin, and Prabhu, 2015; Leier, Ferreras, Saha, Charlot, et al., 2016; Bruderer et al., 2016) have so far only worked with up to tens of lenses. This is because modeling is intensive in terms of expert time. In other branches of lensing this is not the bottleneck. Microlensing deals with larger numbers of systems to be modelled, but they are less complex and modeling pipelines are already in place (Udalski, Szymanski, and Szymanski, 2015). In cluster lensing however the models can be very complex (e.g., Mohammed, Saha, and Liesenborgs, 2015; Mohammed, Saha, Williams, et al., 2016) but the number of systems is smaller.

The above considerations motivate a new strategy for modeling galaxy lenses especially. This is to provide tools for experienced but non professional volunteers who already participated in lens discovery through the SPACEWARPS citizen science project (Marshall, Verma, et al., 2016). This paper presents the software stack SPAGHETTILENS which has been developed to allow citizen scientists to model gravitational lenses collaboratively.

This software should also be easily adaptable to any other, reasonably similar problem. It solves the problem of letting the volunteers execute a computer intensive task that cannot be easily executed client side and relies on citizen scientists collaborating.

This paper is organized as follows. Section 2.2 shows an overview over the components and a short summary of the steps involved in creating a model. It includes three different perspectives which are detailed in the following sections. Section 2.3 elaborates on the important tasks from the point of view of a citizen scientist, introduces the concepts they have to know to do lens modeling and explains the user interface. Section 2.4 gives detailed information about implementation of the components of the software stack. Section 2.5 summarizes the underlying scientific concepts and the post processing of the data generated with this stack from the point of view of a scientist. Section 2.6 discusses feasibility of scaling up the SPAGHETTILENS system by orders of magnitudes for future runs and in Section 2.7 we add some concluding remarks.

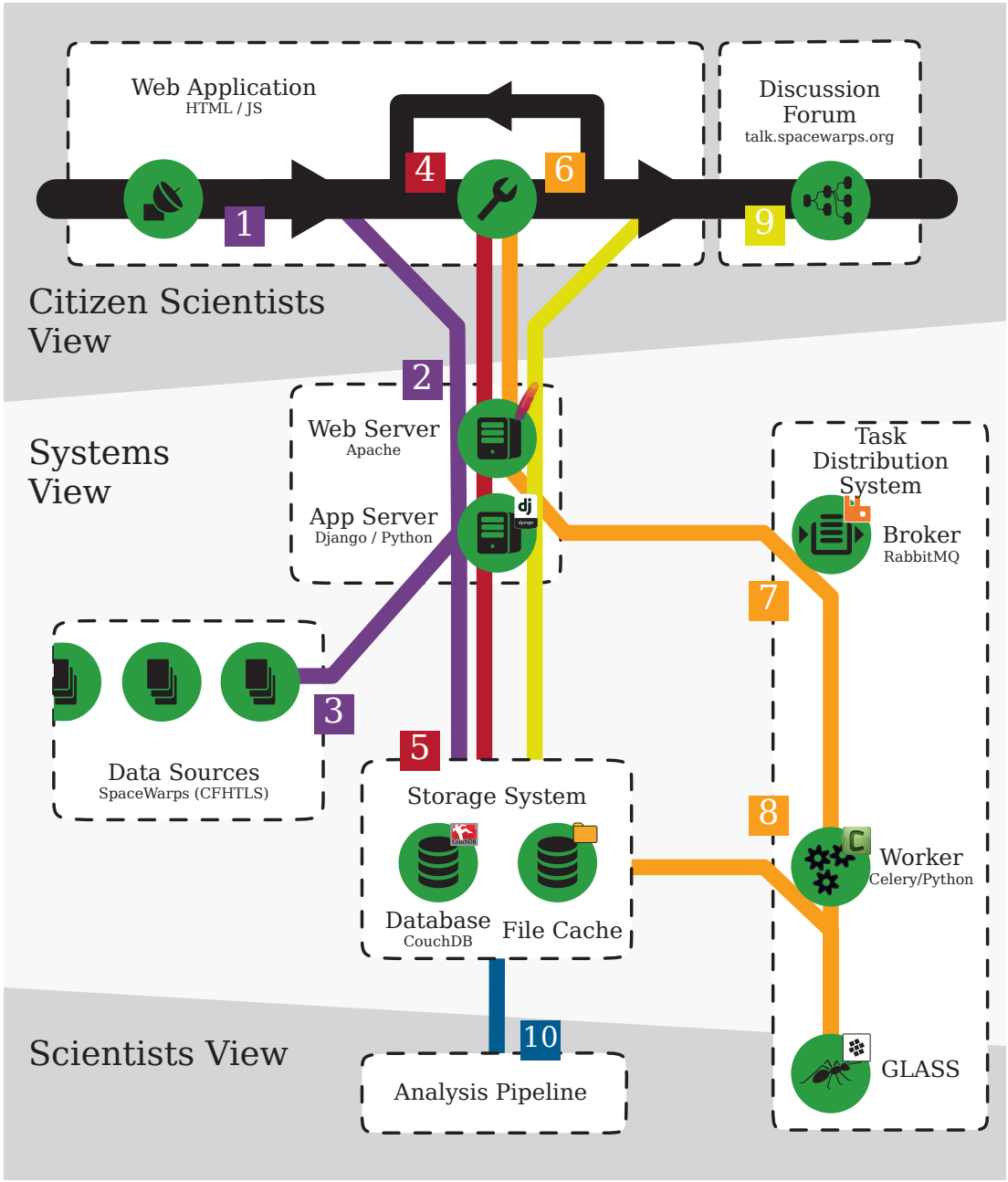

Figure 2.1: Overview SPAGHETTILENS system. Software components as green circles, grouped into logical units with dashed boxes and arranged vertically by user that interacts with them. Numbers show steps of model generation; grouped by colour into four tasks.

2.2 Overview of the modelling system

Figure 2.1 gives an overview over the complete setup of the software components that build the software stack SPAGHETTILENS. This figure shows three different views onto the system: The ones of a citizen scientist, a scientist and an internal system view. The software components are depicted as green circles, grouped into logical units with dashed boxes. These boxes are elaborated on in the following sections. This section gives an overview over all steps involved in creating a model. In Figure 2.1 these steps are annotated with numbers directly in the figure. They are grouped by colour into tasks, which reflect the following headings, each containing an enumeration of the assigned steps.

2.2.1 Loading of survey data (violet track)

1. The volunteer chooses an already identified lens candidate to work on by entering an ID from a supported data repository.
2. SPAGHETTILENS requests data from any available remote data repository if it is not already available locally.
3. SPAGHETTILENS saves metadata about the lens candidate in the database and caches the lens data. It delivers all data from the local cache.

2.2.2 Creation of model configuration markup (red track)

4. The citizen scientist adds markup to the lens candidate survey image, thus adding constraints to the lens mass distribution, based on an educated guess and experience.
5. The markup is encoded in a small text file, which is the model configuration file. It is stored in a document-oriented database.

2.2.3 Generation of lens model (orange track)

6. The web application asks for the model and visual representations for previously sent model config. If these data are available, they are sent back. If there is a task currently creating those data, its status is returned. Otherwise a new modelling task is created and added to the task queue.
7. The message broker manages the task queue. It mediates between the application server that creates tasks and a set of worker nodes that process them. The broker keeps track of the state of tasks.
8. A worker node receives a task and executes the actual modelling backend GLASS. It creates a model and graphical representations of the model as feedback for user.

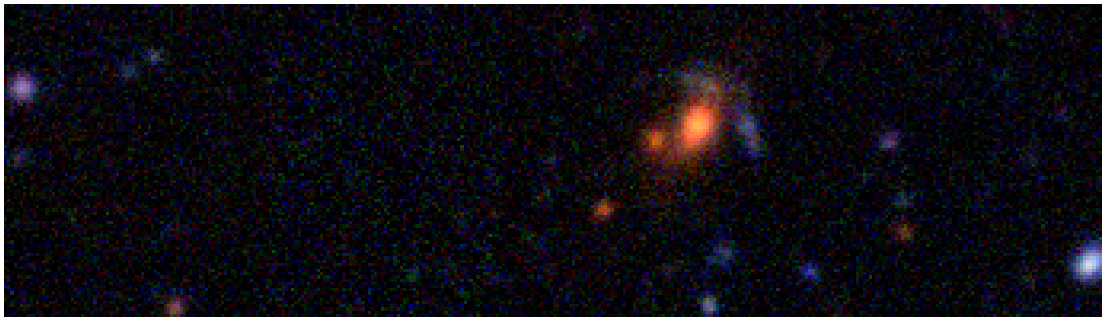

Figure 2.2: Example CFHT LS input image. Cutout of original input image of lens J021514.6−092440.

Once finished, usually after a few seconds to minutes, the worker node uploads the generated model and images into the cache of the storage system.

2.2.4 Generation and discussion of a version tree of models (yellow track)

9. The citizen scientist receives a link to their model for it to be shared and discussed with other volunteers. Others can use this link to revise a model and create a new child model. This branching version tree of models explores different possibilities. Discussion with scientist help prune the tree.

2.2.5 Analysis of models (blue track)

10. Scientists choose a collection of models. The models can be downloaded and analysed locally with a post processing pipeline as shown in Küng et al. (2015) and Küng et al. (2018). They prototype additional modules for SPAGHETTILENS like metrics and additional feedback images to be integrated into the main program.

2.3 Citizen scientist

Citizen scientists usually arrive with SPAGHETTILENS after they detected a lensing candidate in another tool like SPACEWARPS. After loading their candidate from the data source, the citizen scientist can start creating actual models. This task however is not straight forward, some basic knowledge about image classification is required.

2.3.1 Image classification

In the example Figure 2.2 one can see a lot of foreground objects like galaxies and other objects in all different colours. The colour schema has been chosen by the SPACEWARPS

team, based on Lupton et al. (2004), such that the contrast between faint extended objects and bright early type galaxies is optimized (Marshall, Verma, et al., 2016). This results in lensing galaxies being usually orange and lensed images being of blueish colour. The difficulty of this task is that what is seen is drastically different to what is asked for, both the image of the light source behind the lens and the mass distribution of the lensing galaxy.

The adopted strategy uses a topological classification for images in models, which is based on the concept of arrival time (Blandford and Narayan, 1986). The citizen scientist marks up the image with what in this work is called a *spaghetti diagram* of which examples are given in Figure 2.3. The diagrams themselves are well known and are sometimes used to characterise the output of models (e.g., Rusin et al., 2001; Keeton and Winn, 2003). What is novel in SPAGHETTILENS is that the spaghetti diagram serves as *input*. It provides the connection between the input image the citizen scientist sees and the mass distribution and it is easy to draw and input with computer graphics.

As usual in lensing, lens and source objects are assumed to lie on a plane each perpendicular to the line of sight. A light ray coming from (x_s, y_s) on the source plane, passing the lens plane at (x, y) and getting deflected will arrive an observer after the time t, its arrival time. Considering light rays though all points (x, y) of the lensing plane leads to an arrival time for each point – the arrival time surface $t(x, y)$. It is an abstract concept and not itself observable, but applying Fermat's principle to the arrival time surface shows where to expect the lensed images of the source: at stationary points of the arrival time surface.

The arrival time surface consists of two parts: First, there is a simple geometrical part t_{geom} due to the longer path. Second, photons traveling in the gravitational potential of a mass will experience a gravitational time delay t_{grav}. This results in the total travel time of a photon along this light ray as:

$$t(x, y) = t_{\mathrm{geom}} + t_{\mathrm{grav}} \tag{2.1}$$

The following is about the qualitative consequences of these components, the detailed expressions are given in Section 2.5. In the simplest situation, where there is no mass, only t_{geom} contributes to the arrival time surface. Since t_{geom} increases with growing distance from the source, it forms a paraboloid centered at the source, with one single minimum in the middle. By adding a lensing mass, t_{grav} distorts and locally increases the arrival time surface. The effect of the lensing mass on t_{grav} is the biggest in the centre of the lensing mass and falls off going out. In the process new maxima, minima and saddle points can be formed. Maxima and minima have contour lines circling around them, whereas at saddle points two contour lines cross each other, forming an X. These self intersecting saddle point contour lines are of special interest: they fix the overall topology, give us the exact location of saddle points and the regions where to find minima and maxima. The knowledge of these lines combined with the precise locations of the minima and maxima defines the arrival time surface.

Figure 2.3 illustrates these self intersecting contour lines. In Figure 2.3a there is no lensing mass and a single minimum. When mass is added, the former minimum can get expanded

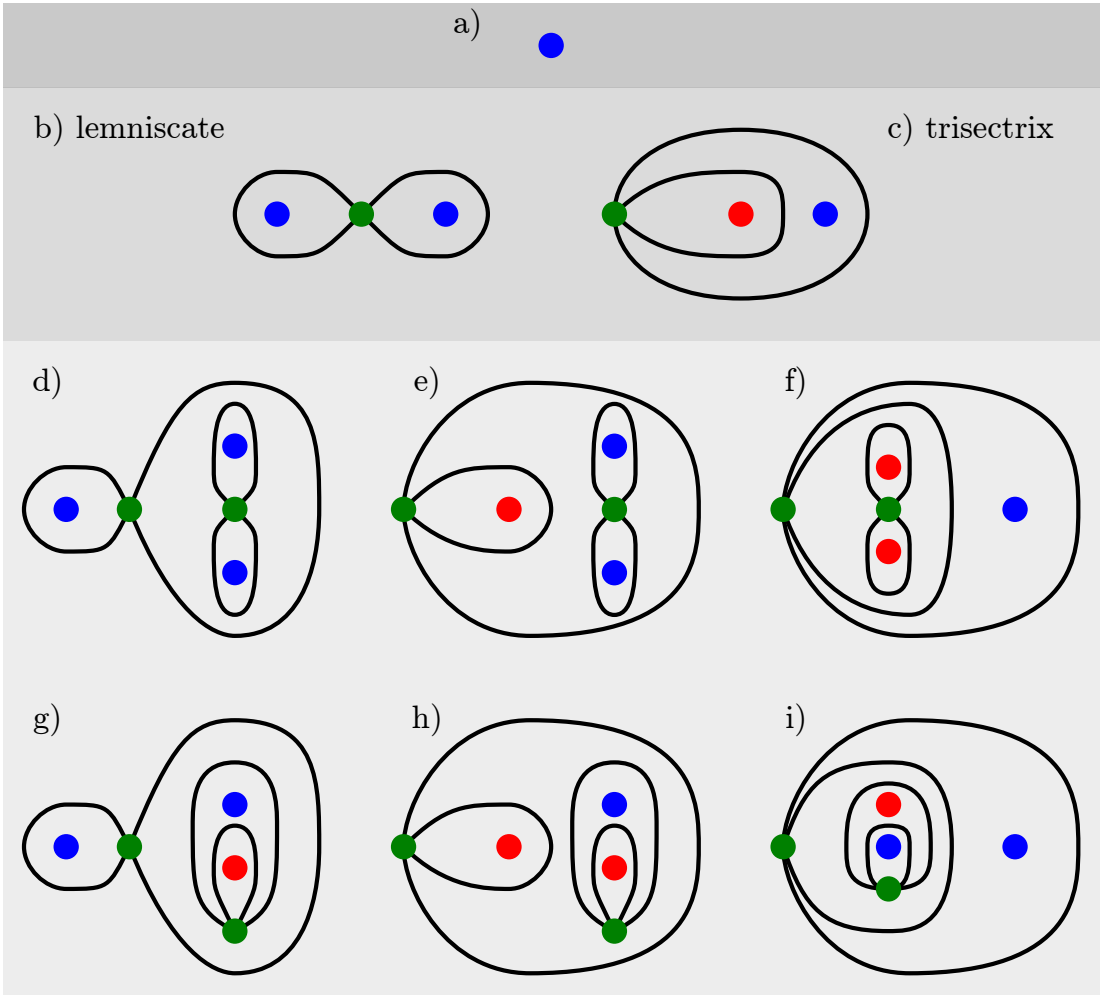

Figure 2.3: Abstractions of arrival time surfaces. Dots represent stationary points, minima in blue, maxima in red and saddle points in green and self intersecting contour lines are drawn in black. The first row shows the trivial single image setup with no lensing mass present. The second row shows the two possible three image configurations, the lemniscate on the left and the limaçon trisectrix on the right. The third row lists all theoretically possible five image configuration. (In the literature the maxima are sometimes excluded from the image count, because they are often too faint to be observed.)

into three stationary points. The former minimum can expand into a saddle point with two new minima nearby, the new figure is called a *lemniscate* and shown in Figure 2.3b – or it can expand into a saddle point with a minimum and a maximum nearby, the latter at the centre of the lensing mass. This is called a *limaçon trisectrix* and shown in Figure 2.3c.

If the geometry of the lensing mass is more complex, theoretically any of the six distinct image situations shown in Figures 2.3d to 2.3i are possible by again expanding one of the minima or maxima with a lemniscate or limaçon trisectrix. In practice however one predominantly sees Figure 2.3e for galaxy lenses.

2.3.2 Configuring the model

The general design of the user interface (UI) features three horizontal sections as depicted in Figure 2.4. On the top one can find the main toolbar, where the general workflow of the application is controlled – generating a model from the model config and submitting the model config and the resulting model. The bottom row shows an optional help section, that displays a short help text to the item the mouse is currently hovering and which can be disabled by advanced volunteers. Because the task at hand involves comparing input and output, the middle section of the UI was designed to reflect that by being split into an input area and an output area. The input area, where the model config is created, is placed on the left including all tools needed during the creation of the input. The output area on the right allows the user to select which output data to see once a model config was generated.

The input area in Figure 2.4 shows the two main elements of the user interface: stationary points of different kind and self intersection contour lines. The user interface is designed to only allow valid inputs to been drawn by following the idea of Figure 2.3: We start with the trivial case, a minimum, which then can be extended into the lemniscate three image case by clicking on it. The citizen scientist can change between a lemniscate and a trisectrix configuration by dragging one minimum and the according contour line inside the other, and vice versa. Additional foreground objects that might contribute to lensing may be marked up using an additional tool – the point mass.

2.3.3 Modelling

After a first stationary point assignment by the citizen scientist, the input model config can be modelled. This process starts with a button press and is otherwise automatic, but it takes a significant amount of computing time on the order of minutes. The markup is sent to the backend simulation software which creates the actual model and renderings of the mass distribution, the contour lines of the arrival time surface and a synthetic quasi image of the images produced by the model generated as a feedback to the citizen scientist. This data in turn allows them to reiterate their initial guess and getting a feeling for the modeling process.

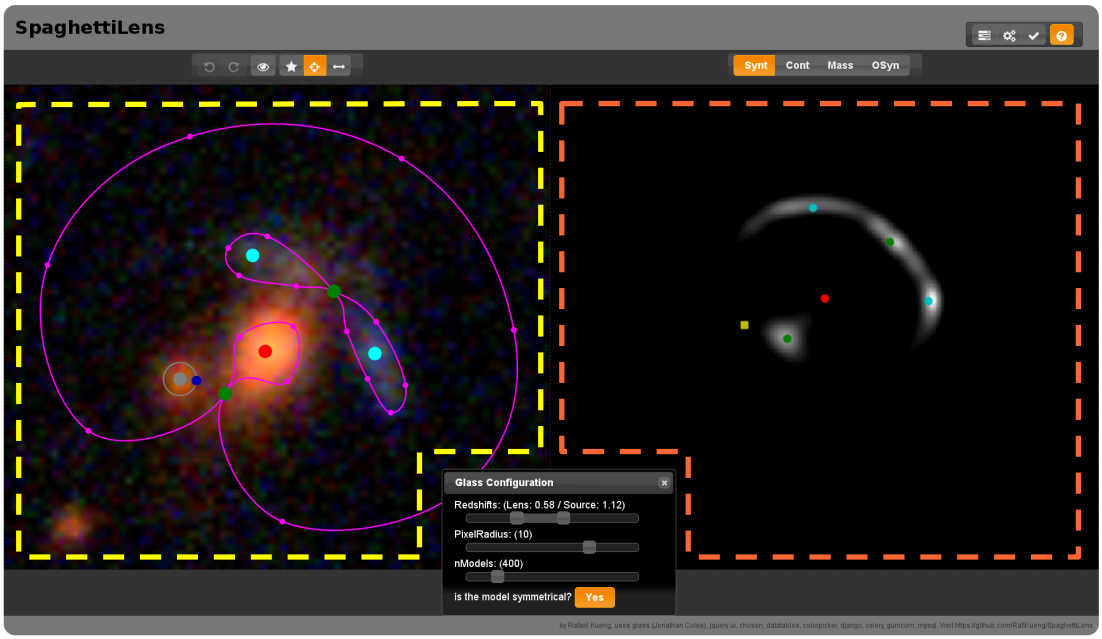

Figure 2.4: Screenshot of the user interface. The top area shows the controls: the top row shows the main controls on the right; the second row shows the controls for the input on the left and for the output on the right. Mid left (yellow dashed): input canvas with a survey image in the background and in the foreground: a) spaghetti markup in magenta, b) minima, maximum and saddle points of the arrival time surface as cyan, red, respectively green dots, and c) an external point mass in gray. Mid right (orange dashed): output area; showing a synthetic image rendered from the model created from the model config. On the bottom dark gray area context sensitive help is displayed (here empty). A pop-up placed bottom mid shows the simulation settings.

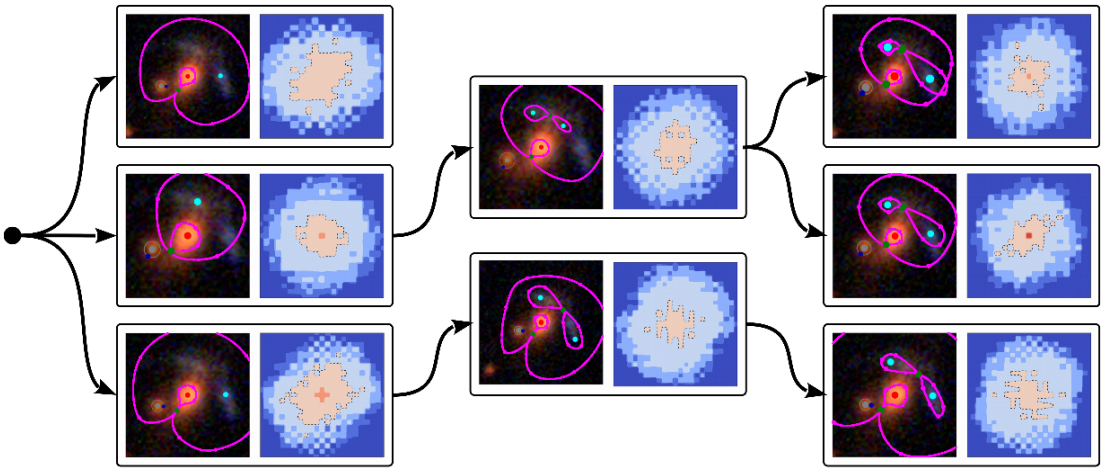

Figure 2.5: Example of a version tree of models for the lens candidate J021514.6−092440. For each model we show the marked-up image and the false colour map of the projected mass distribution. The mass map is not sufficient to determine a best model, but on the basis of diagnostics of how well the lensed image structure is reproduced the model at right in the middle is the most successful, see Küng et al. (2018). As we can see from the spaghetti diagrams, early versions interpret the system as three image system, but later the five image interpretation is favored.

2.3.4 Discussion

Once the volunteer is happy about the result they can save their model in the archive. It gets an unique URL by which it can referred. The volunteers are then encouraged to post their resulting model onto the forum and discuss, evaluate and compare different models – their second and equally important task. The system allows to continue working on one model using the resulting link. This leads to a version tree of models, which explores the different possibilities of modeling a particular lensing system. An example tree is shown in Figure 2.5. The discussion among citizen scientists and with scientists is crucial, it prunes the tree and leads to a smaller selection of models to further investigate.

2.4 System components

This section gives detailed technical insight into all the components of the SPAGHETTILENS system. The corresponding entities are labeled in Figure 2.1 and depicted with green circles. They represent software daemons and services running on one or multiple server systems, either physical or cloud based virtual machines.

To reduce the risk of obsolescence, all the software used is open source and emphasis was put on selecting only well established technology and complying with standards. Components which are already widely used by big companies and organisations were preferred, to ensure

support and updates over an extended period of time. Effort was invested in employing only loosely coupled components that generally only do one task. Additional thought was given to ensure good horizontal scaling – each components capacity can be scaled up by adding more identical copies of it to the system on the fly. This can be achieved by either buying new hardware or by adding another, identical virtual server instance in case of a cloud installation. This has the advantage of allowing more natural growth of the project, which is especially important in a scientific environment and in the starting phase of a project with limited funding. For a small number of contributing citizen scientists it is sufficient to setup a desktop computer with all components on one system. Once the stress on the system grows with the user number, it is advised to move one component after another onto dedicated machines or into the cloud, dictated by performance measures, hopefully founded by the increasing publicity of the project.

The simulation backend creates the biggest load by orders of magnitudes, thus the initial setup consists of a dedicated computer[1] as the main server machine with two worker nodes and an additional two worker nodes running on a desktop computer[2] of the author. This allowed up to four concurrent simulation tasks, which in turn corresponds to about six concurrent citizen scientists at work before they start having to wait for their simulation to be executed. During predicted periods with higher user numbers, for example during demonstrations, additional worker nodes were started manually on idle machines at the authors institute.

2.4.1 Application server

The application server is build using DJANGO, a web framework that is written in PYTHON and allows one to setup the application using PYTHON as well. It has basically three tasks.

The first task is to make survey data which are false colour images from the sky available to the citizen scientists. Section 2.4.3 elaborates in more detail. A second task is to manage model configs generated by the volunteers, which are small text files that encode the markup provided by the citizen scientists. Once a volunteer marked up a lens in the UI, the resulting model config can be stored in the database. The design considerations of the database system are illustrated in Section 2.4.4. The third task is to deliver the actual model. If the data do not yet exist, the application server starts worker threads to create requested data. See Section 2.4.5 for details.

To deploy the application server an APACHE web server with `mod_wsgi` module is employed. The APACHE web server also delivers static files, data and images that already have been created by the application server. This is a conservative and well tested strategy that is easy and quick to setup. For future scaling, DJANGO can be deployed using the `uWSGI` protocol and server as an individual process decoupled from APACHE, possibly on its own machine.

[1] `swlabs`: Intel(R) Core(TM) i5-4670; 4 cores, 3.5 GHz, 8 GB RAM
[2] `taurus`: Intel(R) Xeon(R) E5-1603; 4 cores, 2.8 GHz, 8 GB RAM

2.4.2 Web application

The client side web application and the UI are implemented using standard compliant web techniques like HyperText Markup Language 5 (HTML5), JavaScript (JS) and Scalable Vector Graphics (SVG). A traditional design theme was chosen to respect the wide range of age of all citizen scientists participating.

The input area is the centre piece of the application. It renders the survey data it gets from the server on a JS canvas, where the rendering could be customized. On top of the JS canvas lies a SVG canvas that is used to draw all the UI elements described in Section 2.3. The self intersecting loops are implemented as connected Bézier curves, and the hierarchy of loops forms a tree.

At any time while the citizen scientist is working the SVG layer has a certain state which represent a certain model config. Every edit in the UI creates a new state. The states can be directly sent to the application server to be saved and modelled, but also easily loaded back into the web application. This allows for a simple implementation of an undo–redo functionality, as well as the loading of a model config created by other citizen scientists back into the application.

2.4.3 Data sources

The SPAGHETTILENS system does not itself offer data to be analysed, it relies on external data sources. They provide images of one or multiple spectral bands per object either in several image files, as premixed regular image file or as a Flexible Image Transport System (FITS) file. The volunteers will have the possibility to modify the colour scaling for future data sources that offer FITS files, however the system currently only implements the already composed images from the SPACEWARPS project[3]. These data can be passed on to the web application, which can create its own false colour image locally. Data sources are usually publicly available archives of past surveys and thus are expected to be available during the lifetime of SPAGHETTILENS. New data sources can be added in the form of modules.

Due to Cross-Origin Resource Sharing (CORS) restrictions, the client side web application cannot easily download data and images from a third party site. For security reasons, CORS is restricted in most current browsers and has to be allowed by a third party site especially for a specific origin, like SPAGHETTILENS. To prevent possible problems with CORS, the server gets the images from the survey archives, caches it locally in the cache file system and delivers it to the web application. This has the additional advantage, that special access to non public archives for SPAGHETTILENS could be negotiated and kept server-side, without the need of handing out the credentials to the citizen scientists.

[3] See section 3.2 of Marshall, Verma, et al., 2016 for details

2.4.4 Data storage – cache and database

During the process of creating a model for a lens, there are several kinds of data that need to be handled by the system. First, the image data from the source survey and metadata about these images. Second, the model config created by the citizen scientists. Third, the model that is created by the system using the model config and fourth, the images for the model.

As previously stated, there are currently hundreds of known lenses and this number is likely to increase one hundred fold. The goal was that SPAGHETTILENS could scale up to that number of possibly tens of thousands of lenses. On average, we expect for each lens tens to hundreds models, which leads to the requirement for SPAGHETTILENS to be able to handle in the order of a million models, as an upper limit.

Section 2.4.3 elaborated the need for a local cache of the original survey images. The image archives of the surveys are expected to be at least as stable and long-lived as this program, thus SPAGHETTILENS relies on those archives being available and only temporarily save the survey images locally in a cache when needed by a client. It does however keep track of the metadata for data sources and images in a database.

The most vital data of SPAGHETTILENS are the model configs created by the citizen scientists. They are of the order of tens of kilobytes and thus can be easily stored in a database as well. The models however are a factor thousand bigger and they might fill up available storage space at some point. For that reason, the models are saved in the cache file system as well, as are the analysis images, which are a factor hundred smaller than the models. If disk space is getting an issue, there can be clean up tasks that delete old models, which could be regenerated if requested using the model config.

The above considerations lead to the requirements of the database. The core functionality of the database is to manage the model configs, which are sent from the web application in JavaScript Object Notation (JSON) form. So the database is actually simply an object or document store, where objects are written once, hardly ever changed but read many times. The database will only save three different kinds of entries: information about different data sources, information about survey images, and model configs. Data analysis will mostly be done locally by the scientists, hence there are no advanced database functionalities like the ones offered by relational databases needed. Future scientific development might lead to additional data that need to be saved in the database, thus the database schema might need to be modified several times.

The database application is supposed to scale horizontally like the rest of the system, thus Brewers Theorem (Brewer, 2000; Brewer, 2012) has to been taken into consideration. It states that it is impossible for a distributed system to have all of the three properties consistency, availability and partition tolerance. Traditional relational databases are said to be “AC”, they guarantee consistency and availability, but are not partition tolerant. Since the distributed system is connected over a regular, unreliable network – possibly in a cloud service – partition tolerance has to be guaranteed. Since SPAGHETTILENS won’t have to handle concurrent writes to the same data, it can neglect consistency in favour of availability.

This considerations lead to the choice of the document store software CouchDB, a database application with "AP" characteristics, i.e.it features both partition tolerance and availability, with the trade-off of only being consistent eventually.

2.4.5 Task distribution system

The actual process of turning a model config into a model is done by a modified version of Glass (Coles, Read, and Saha, 2014). A short scientific introduction follows in Section 2.5. The modeling is a time consuming and computationally intensive task – it takes on the order of minutes at full processor load. On average one can expect that three concurrent volunteers will in total run two concurrent modeling processes – with one simulation process optimally being run on two to four CPU cores. Thus in this project this component will be the the limiting factor for the amount of concurrent users the system allows – by at least two to three orders of magnitude, and will always be the first that has to scale up. Follow up analysis and imaging to create visual representations of a model are relatively lightweight. This leads to the conclusion that the modeling and analysis pipeline has to be decoupled from the application server, to not block all the other operations during the creation of models.

This is the reasoning why this pipeline has been implemented with a task distribution system. Once the server gets a request for a resource – a model or a visual representation – that is not available in the cache file system, the server starts a task to create the resource. It is up to the client to try again later to see if the resources have been created in the meantime ("pulling"). The tasks are distributed to connected worker instances, where the actual computation takes place. Once finished, the worker uploads its result back into the cache file system using an established file transfer protocol, Secure Copy (SCP).

For the distributed task queue Celery was selected, due to also being programmed in Python and its good integration with the application server Django. Celery allows one to convert Django functions into tasks simply by adding a decorator. If such a function is called, it is sent to the message broker, which keeps track of the worker instances and distributes tasks to those instances. The message brokering is achieved by RabbitMQ, implementing the industry standard Advanced Message Queuing Protocol (AMPQ).

The worker instances can be started quickly on any computer that has a network connection to the message broker. This allows us to quickly integrate more worker machines in times of high system load, for example when the system is demonstrated during a presentation. This is currently a manual process, but can be easily automated for a cloud-based installation.

2.4.6 Discussion system

For the discussion system SpaghettiLens relies on the forum system deployed for Space-Warps, hosted on the Zooniverse servers. It is already established and offers all required features – for example the easy referencing of lensing candidates in discussion.

2.5 Scientific view

2.5.1 The modeling backend

There are many software packages around to do mass modeling of lenses. Lefor, Futamase, and Akhlaghi (2013) reviews thirteen of them, some being educational, some research oriented – some using parametric forms for the mass distribution, whereas in others the surface density is free form. We chose a more recently developed program GLASS, which is related to the older code PIXELENS (Saha and Williams, 2004). The reason for this choice is that the arrival time surface plays an integral role in GLASS which interfaces naturally with the concept of spaghetti diagrams.

As already mentioned before, the arrival time surface has two terms, $t_{\rm geom}$ and $t_{\rm grav}$ (Blandford and Narayan, 1986). The gravitational time delay is given by a two dimensional Poisson equation:

$$\nabla^2 t_{\rm grav} = -(1+z_{\rm L})\frac{8\pi G}{c^3}\,\Sigma \tag{2.2}$$

where $z_{\rm L}$ is the redshift of the lens and $\Sigma \geqslant 0$ is the surface density which needs to be recovered. The geometrical part is given by:

$$t_{\rm geom} = \frac{(1+z_{\rm L})}{2c}\frac{D_{\rm OS}}{D_{\rm OL}D_{\rm LS}}\left[(x-x_s)^2+(y-y_s)^2\right] \tag{2.3}$$

with the position of the source x_s and y_s unknown. $D_{\rm OL}$, $D_{\rm OS}$ and $D_{\rm LS}$ are angular diameter distances from observer to lens, observer to source and lens to source respectively.

A citizen scientist identifies point-like features of the image, which are conjectured multiple images from the same source point, in a survey image as minima, maxima or saddle points of the arrival time surface $t(x,y)$. Each image (x_i, y_i) gives a constraint on the first derivative of the arrival time surface $\nabla t(x_i, y_i) = 0$ and constrains the second derivative. Prior information like Σnon negative and centrally concentrated provides further constraints. As a result $\Sigma$is not determined uniquely but it is confined into a high dimensional simplex. The interior of this simplex is sampled (Lubini and Coles, 2012) and usually two hundred mass distributions make one ensemble of mass distributions, which in this work is called *a model*.

2.5.2 Post processing

There are several strategies possible for selecting a collection of models to be post processed. Simple strategies like evaluating all generated models or selecting the most recently-generated ones might be promising for some simple analysis. This can be done either manually or by implementing map/reduce functions that can run directly on the database and return a subset of the models. The strength of this setup however is the collaboration between the citizen scientists and the scientists. In discussion, citizen scientist determine a consensus selection of the best models for further analysis.

The first application of SPAGHETTILENS tested the system and the performance of citizen scientists in a test case (Küng et al., 2015) with simulated lenses. In (Küng et al., 2018) lensing mass and the stellar mass for lens candidates discovered by the SPACEWARPS project (More, Verma, et al., 2016) are compared. For this analysis, volunteers created models for 58 of the 59 lens candidates detected.

2.6 Scaling discussion

The metrics obtained while testing SPAGHETTILENS (Küng et al., 2015) and while generating a first set of models (Küng et al., 2018) let us calculate some rough estimates on the scaling requirements of the system. The latter work presents 377 generated models for 58 candidate lenses, generated by eight users over a period of more than two years. During regular operation, the system run on two machines with four worker nodes in total, but successful scaling tests were done with up to twelve machines running 24 worker nodes. Additionally, the experience gained in the first run of SPACEWARPS (Marshall, Verma, et al., 2016) gives a rough estimate on the numbers of volunteers.

The optimistic plan is for SPAGHETTILENS to create models for tens of thousands of lenses in five to ten years (Küng et al., 2015). Since some 10 models were generated per lens on average, we assume that hundreds of thousands of models are to be generated, by hundreds of users. Thus this citizen science project aims to have a comparably low user number, but with high amount of contribution per user, due to the rather steep learning curve.

This section discusses the requirements and the scaling needed for this scenario and potential upper limit for the costs. SPAGHETTILENS is currently being set up on the ScienceCloud[4] infrastructure of the University of Zurich (SCUZH). For this reason the estimates calculated below are based on this offer, commercial ones are comparable.

2.6.1 Storage space upper limit estimates

Each model generated takes up on the order of 20 MB per model. The storage space required in the database are a few 10 kB, thus neglectable in comparison. The total requirement for the storage space adds up to 20 TB. This would cost about 800 $/yr[5] given the prices at the time of writing.

2.6.2 Computing power upper limit estimates

The median run-time of the 58 selected models in Küng et al., 2018 was of the order of 250 s on a dual core worker node. Assuming ten minutes per model as a save average to

[4] `https://www.s3it.uzh.ch/en/scienceit/`

[5] 1 TB/yr costs 40 CHF at the time of writing; the “Basic” offer for 500 CHF includes 1 TB/yr; 1 CHF ≈ 1 $

create a model on a dual core worker node leads to the computing power required for 10^6 models:

$$10\,\text{min/model} \cdot 10^6\,\text{models} \cdot 2\,\text{CPU} \approx 40\,\text{CPU yr}$$

The other components of the system web server, app server, database, and broker combined experience at least one to two orders of magnitudes lower load compared to the worker nodes. A machine with four vCPU to host all other server components showed no significant load even under the 24 worker node test case and will most probably be sufficient even for higher loads. The required 44 CPU yr hours would add up to ∼880 $/yr[6].

2.6.3 Bandwidth upper limit estimates

The whole web application runs mostly on the client side browser and only communicates with the server to start the modeling process. Thus the task is not very IOPS (Input / output operations per second) heavy. We can safely assume that the load of one user will stay below one request per second. Given we expect hundreds of users, the IOPS load will be below 1000 IOPS, a magnitude easily manageable for current day web servers.

Usually a generated model will not be transferred to the client, but only the rendered images with sizes up to a few Megabytes, one order of magnitude below the size of the generated model. The actual external traffic volume needed is thus of the order of 2 TB.

For internal communication between the components gigabit networking equipment is common. Since read and write speed even to classical hard drives are above that value, this connection is most probably the bottle neck of the system. Gigabit ethernet would allow for up to:

$$\frac{125\,\text{MB/s}}{20\,\text{MB/model}} \approx 6\,\text{model/s}.$$

Given a model takes 10 min to generate, this system can theoretically handle up to 3600 concurrent worker nodes.

2.6.4 Recruitment and training of volunteers

The analysis in Marshall, Verma, et al., 2016 gives some upper limits for the amount of users to realistically expect. That work noted that 1 % of the ∼40 000 volunteers made 90 % of the contributions. The authors also noted that the skill factor was distributed more broadly than the contribution rate with 20 % of agents accumulating 80 % of the skill. SPAGHETTILENS plans to recruit volunteers from this pool of either highly active or highly skilled users, and hopes to motivate of the order of 1 % of the initial SPACEWARPS volunteers to commit to SPAGHETTILENS in the end phase if the project develops as expected.

The training of these volunteers will be the most critical aspect of the scaling, which is time intensive and cannot be done by online tutorials alone. The author expects that it will always

[6] 1 vCPU yr costs 20 CHF at the time of writing; “Basic” offer includes 10 CPU yr

involve manual training in video con, given the difficulty of the task. Since several runs to create sets of models are planned, with an increasing amount of lenses, it is expected that the volunteer community grows accordingly with each run. The author suggests to recruit expert modellers among the already participating volunteers to take over teaching tasks and train groups of new volunteers. This process can realistically be scaled up to teach hundreds of volunteers over a few iterations if it is possible to find enough passionate teachers in each run. Whether the percentage of passionate "community teachers" among the volunteers is high enough to allow for a natural growth needs further investigation and is outside the scope of this work. There are however also other, established solutions available to train hundreds of volunteers with just a few teachers which can support or replacement community teachers, for example online tutorials, combined with video chat based question and answer sessions. The established methods however have the drawback of being much more time consuming.

2.7 Conclusions

This work reports on the software stack SPAGHETTILENS that allows citizen scientists to create mass models of gravitational lens candidates. It offers a means to cope with the expected increase of detected lenses and the lack of human resources to create mass models for all of them. A novel way of input for gravitational lens modeling is introduced, called a *spaghetti diagram*, providing a visual connection between the survey image that serves as template and the required result, the mass distribution. This allows non professional citizen scientists to use this software to create lens models and become modeling experts. SPAGHETTILENS encourages collaboration by allowing to load and modify existing models, and thus creating a version tree of models.

On the technical side, SPAGHETTILENS solves the problem of handling compute intensive tasks. It implements a task queue on the server side. During times with high demand on the system, additional worker nodes can be simply plugged in. This principle holds true for all components of the software stack: they are designed to be modular and allow for horizontal scaling.

SPAGHETTILENS is implemented for lensing, but its modularity makes it easily adaptable to other problem cases that feature a resource intensive task to be done server side and that want to encourage citizen scientists to collaborate.

A test of the system with simulated lenses (Küng et al., 2015) and a first modeling effort (Küng et al., 2018) let us conclude that the novel input concept and the system works and that citizen scientists perform well.

In the current version the user interface still lacks a few advanced functions. Examples are custom colour mapping for data sources offering FITS files, that not all possible settings of the modelling software are exposed to the user, and the ability to modify the generated output images by changing brightness or contrast for example.

The next steps are to scale up the system for the next run of SPACEWARPS, finish the ongoing porting to the cloud environment SCUZH and invest time in recruiting more volunteers for the project. The scaling of the software should pose no problems and be easily manageable, especially in a cloud based environment. On the other hand, the project lacks good online training materials, so far all training is done on a personal level using videocon. Whether the recruitment and the teaching of new volunteers by 'community teachers' will work as proposed remains to been demonstrated.

2.8 Acknowledgments

I would like to show my gratitude to my supervisor Prasenjit Saha for his tremendous support, the scientific guidance and the discussions during all of this work. Additionally the valuable feedback and ideas of all the citizen scientists involved were essential for this work. I would like to thank especially Elisabeth Baeten, Claude Cornen, Christine Macmillan and Julianne K. Wilcox for their valuable input during the development of this project and their contributions afterwards.

This work was supported by the University of Zurich Candoc research grant (Forschungskredit Candoc; FK-14-081 and FK-15-087). The funding source had no involvement in study design; in the collection, analysis and interpretation of data; in the writing of the report; or in the decision to submit the article for publication.

Chapter 3

Testing Citizen Science Lens Modelling

Original title:
"Gravitational lens modelling in a citizen science context"

Rafael Küng[1], Prasenjit Saha[1], Anupreeta More[2], Elisabeth Baeten[3], Jonathan Coles[4], Claude Cornen[3], Christine Macmillan[3], Phil Marshall[5], Surhud More[2], Jonas Odermatt[6], Aprajita Verma[7], Julianne K. Wilcox[3]

[1] Physik-Institut, University of Zurich, Winterthurerstrasse 190, 8057 Zurich, Switzerland
[2] Kavli Institute for the Physics and Mathematics of the Universe, University of Tokyo, 5-1-5 Kashiwanoha, Kashiwa-shi 277-8583, Japan
[3] Zooniverse, c/o Astrophysics Department, University of Oxford, Oxford OX1 3RH, UK
[4] Exascale Research Computing Lab, Campus Teratec, 2 Rue de la Piquetterie, 91680 Bruyeres-le-Chatel, France
[5] Kavli Institute for Particle Astrophysics and Cosmology, Stanford University, 452 Lomita Mall, Stanford, CA 94035, USA
[6] Kantonsschule Zug, Lüssiweg 24, 6300 Zug, Switzerland
[7] Sub-department of Astrophysics, University of Oxford, Denys Wilkinson Building, Keble Road, Oxford, OX1 3RH, UK

Published in:
Monthly Notices of the Royal Astronomical Society, Vol. 447, Iss. 3, pp. 2170–2180 (03/2015)

Abstract

We develop a method to enable collaborative modelling of gravitational lenses and lens candidates, that could be used by non-professional lens enthusiasts. It uses an existing free-form modelling program (GLASS), but enables the input to this code to be provided in a novel way, via a user-generated diagram that is essentially a sketch of an arrival-time surface.

We report on an implementation of this method, SPAGHETTILENS, that has been tested in a modelling challenge using 29 simulated lenses drawn from a larger set created for the SPACEWARPS citizen science strong lens search. We find that volunteers from this online community asserted the image parities and time ordering consistently in some lenses, but made errors in other lenses depending on the image morphology. While errors in image parity and time ordering lead to large errors in the mass distribution, the enclosed mass was found to be more robust: the model-derived Einstein radii found by the volunteers were consistent with those produced by one of the professional team, suggesting that given the appropriate tools, gravitational lens modelling is a data analysis activity that can be crowd-sourced to good effect. Ideas for improvement are discussed; these include (a) overcoming the tendency of the models to be shallower than the correct answer in test cases, leading to systematic over-estimation of the Einstein radius by 10% at present, and (b) detailed modelling of arcs.

3.1 Introduction

The first work on lens modelling (Young, Deverill, et al., 1981; Young, Gunn, et al., 1981) was developed after the discovery of the first two gravitational lenses (Walsh, Carswell, and Weymann, 1979; Weymann et al., 1980), where a massive galaxy causes a background quasar to appear as two or four images. For the second lens to be discovered (PG1115+080), mass models scored an early success with the prediction that one of the lensed images seen would split further into two at higher resolution. That galaxies must sometimes cause multiple images had long been expected (Zwicky, 1937b), and it had even been argued that the phenomenon could help measure cosmological parameters (Refsdal, 1964, 1966), but apparently nobody was expecting that lenses would need detailed modelling. The first observations, however, immediately stimulated models. The reason for that lies in the image separation. Recall that image separations are of order of the angular Einstein radius

$$\Theta_{\mathrm{E}} \sim \left(\frac{4GM}{c^2 D_L}\right)^{1/2} \simeq 0.1'' \left(\frac{M}{\mathrm{M}_\odot}\right)^{1/2} \left(\frac{D_L}{\mathrm{pc}}\right)^{-1/2}, \tag{3.1}$$

where D_L is the distance to the lens, and M its mass. A lensing galaxy with $M \sim 10^{11}\,\mathrm{M}_\odot$ at $\sim 1\,\mathrm{Gpc}$ would cause image separations of $\sim 1''$, which is comparable to the size of the galaxy; typically the lensed images are seen through the galaxy halo. Hence, the lensed images depend on the detailed mass distribution of the lensing galaxy. Galaxy lenses therefore require models of their mass distributions.

Since those early discoveries, more than 400 secure lenses are now known. Modelling of the mass distribution is part of any research using lenses, but so far no modelling study has spanned all known lenses. The largest single one (Koopmans et al., 2009) models 58 separate lenses to infer the distribution of dark matter around galaxies. In other work, Leier, Ferreras, Saha, and Falco, 2011 combined lens models of 21 galaxies with models of their stellar populations, to find the relation between stars and dark matter, and Sereno and Paraficz, 2014 modelled 18 time-delay lenses together to infer cosmological parameters.

Imaging surveys now under way aim to increase the inventory of lenses another ten or a hundred fold (see, e.g., Marshall, Moustakas, et al., 2005; Oguri and Marshall, 2010), with both automated and visual search techniques proposed (e.g., Marshall, Hogg, et al., 2009; More, Cabanac, et al., 2012; Gavazzi et al., 2014). For example, SPACEWARPS (Marshall et al, in prep; More et al, in prep) is a citizen science project[1] in which volunteers are presented sky-survey images and are invited to identify lens candidates, by eye. Simulated lenses are mixed in with the data, both to help train volunteers on what to look for, and to provide measures of the effectiveness of the search. The motivation for SPACEWARPS is to enable volunteers, some of whom had previously serendipitously identified lens candidates on earlier citizen science surveys, either to make discoveries missed in automatic searches by software robots, or to perform the necessary inspection of an automatically-generated sample, for quality control. Robots can be built to be good at detecting lensing system in

[1] `http://www.spacewarps.org`

clean, uncrowded fields with high signal-to-noise, but in more general test situations, robots miss lenses (low completeness) or contaminate the results with non-lenses (low purity) (Marshall, Hogg, et al., 2009).

The encouraging early results from the first SPACEWARPS lens search, carried out on the $\simeq 172\,\mathrm{deg}^2$ Canada-France Hawaii Telescope Legacy Survey (CFHT LS) imaging by over 30 000 volunteers (Marshall, Verma, et al., 2016; More, Verma, et al., 2016) prompted the question: could the modelling of the lenses also be done by the volunteers? If so, modelling could help prioritise lens candidates at an early stage, which would be very useful with new wide-field and sensitive surveys, which will yield thousands of lens candidates. There are several software tools for lens modelling available, and work has been done on generic interfaces (e.g., Lefor, 2014). Some early designs for SPACEWARPS included a prototype lens modelling tool (Naudus, Wallin, and Marshall, 2010). Moreover, some SPACEWARPS volunteers are quite experienced from earlier projects, having individually spent a thousand hours or more with data, and are very interested in more demanding projects. The interests of citizen science communities are just beginning to be studied (e.g., Raddick et al., 2013), but it is clear that some volunteers welcome open-ended challenges, and sometimes these have led to new scientific results: one example is the discovery of an exceptional extra-solar planet (Schwamb et al., 2013); another is the development of new algorithms for protein folding (Khatib et al., 2011). All these are grounds for optimism. There is, however, a basic difficulty in strong gravitational lensing. Lensed images do not look much like their source, and still less do they resemble the lensing-mass distribution. To model a lens, one needs either to do a lot of random guessing, or to have a good intuition for what works.

In this paper, we propose a way around the difficulty, and report on a modelling test on SPACEWARPS using simulated lenses. The three following sections are devoted to the concept, the implementation, and tests respectively.

In Section 3.2 we introduce a markup system for lensed images, which we call a "spaghetti diagram." A spaghetti diagram resembles the visible image system, in a cartoon-like way, and at the same time it encodes the basis of a mass model. This supplies an intuitive link between the image system and the mass distribution, which look frustratingly different from each other. Spaghetti diagrams are essentially the saddle-point contours originally introduced to gravitational lensing by Blandford and Narayan, 1986 as a way of classifying lensed images. They are sometimes shown as part of the output of lens models (for example Rusin et al., 2001; Keeton and Winn, 2003; Lubini and Coles, 2012). In the present work, however, spaghetti diagrams are the *input* through which the modeller tells the SPAGHETTILENS program what to do.

In Section 3.3 we describe the SPAGHETTILENS program, which implements the above scheme. SPAGHETTILENS is an interface to and extension of the GLASS framework for modelling lenses (Coles, Read, and Saha, 2014). We will not go into software details in this paper, instead concentrate on lens modelling per se, but we remark that SPAGHETTILENS is designed to be friendly to the forum style of citizen science projects, and enables incremental collaborative model refinement by different people, without sacrificing any of the technical features of GLASS.

In Section 3.4 we describe a modelling challenge where a diverse sample of 29 simulated lenses was modelled multiple times by a small number of SPACEWARPS volunteers using SPAGHETTILENS. The models were then examined in two ways. One was whether the spaghetti diagram was correct. The other was the recovery of the Einstein radius of the lens. In addition, we show some visual comparisons of the actual and recovered lens shape and radial profile, and identify some areas to improve. Profile and shape recovery with GLASS has been studied in more detail in (Coles, Read, and Saha, 2014).

Section 3.5 gives the general outlook and next steps.

3.2 Fermat's principle and spaghetti diagrams

We first explain the lensing theory relevant to SPAGHETTILENS, following the formulation of gravitational lensing in terms of Fermat's principle by Blandford and Narayan, 1986.

3.2.1 Geometrical and gravitational time delays

Consider a lens at some redshift z_L and let (x, y) be planar coordinates at the lens, transverse to the line of sight. Let $\Sigma(x, y)$ be the mass distribution. It is a mass per unit area, i.e.density projected along the line of sight. The mass distribution is often given in a dimensionless form

$$\kappa(x, y) \propto \Sigma(x, y) \tag{3.2}$$

called the convergence. Let there be light, in the form of a more distant source, at redshift z_S, behind point (x_s, y_s) on the lens.

We now imagine a virtual photon flying from the source to some (x, y) on the lens, then changing direction and coming to the observer. Such a direction change would increase the light travel time compared to coming through (x_s, y_s). The increased light travel time from the geometry of deflection would be

$$t_{\text{geom}}(x, y) \propto (x - x_s)^2 + (y - y_s)^2, \tag{3.3}$$

assuming the delay is small compared to the total light travel time.

An additional delay of the photon comes from travelling through the curved spacetime at the lens. This gravitational time delay t_{grav} is related to the mass distribution of the lens. The relation is generally written as a two-dimensional Poisson equation, but an alternative expression, avoiding calculus, is as follows. The value of t_{grav} through (x, y) equals its average value on the circumference of a small circle centred at (x, y), plus a constant times the mass within that circle. The constant is $2G/c^3$ times the cosmological expansion factor $(1 + z_L)$. Thus

$$t_{\text{grav}}(x, y) = \left\langle t_{\text{grav}}(x_\circ, y_\circ) \right\rangle + (1 + z_L)\frac{2G}{c^3} M(x_\bullet, y_\bullet). \tag{3.4}$$

We have used $(x_\circ, y_\circ)$ to denote the circumference of a circle, and $(x_\bullet, y_\bullet)$ to indicate the integrated mass within the circle. Section 3.7 relates this expression to the better-known explicit form for the gravitational time delay.

The light travel time of a virtual photon is therefore longer by

$$t(x, y) = t_{\text{geom}} + t_{\text{grav}} \tag{3.5}$$

than it would have been with no lens present. Real photons take paths that make $t(x, y)$ extremal, that is, having a minimum, maximum or saddle point (Fermat's principle).

The proportionality factors in (3.2) and (3.3) depend on the redshifts and cosmological parameters, and are given in Section 3.7.

3.2.2 Arrival-time contours

The full function $t(x, y)$, also known as the arrival-time surface, applies to virtual photons. In other words, it is an abstract construct and not itself observable. But observable image positions can be derived from the arrival-time surface, so visualising the surface is useful. Figure 3.1 does so. In this figure, a maximum, if present, is easy to see. To locate mimima and saddle-points, however, one needs to examine the contours of equal arrival time. A saddle point is characterised by a contour crossing itself, forming an X. Mimima, on the other hand, have contours looping around them, as do maxima.

The saddle-point contours which form an X are especially interesting, because they set the overall topography of the arrival-time surface. They obviously give the locations of the saddle points, and roughly localise the minima and maxima as well. If more precise locations of the minima and maxima are added, the whole arrival-time surface is already approximately known. Since the arrival-time surface has an exact relation to the lens-mass distribution and the source position, in effect the mass distribution is also automatically approximately specified. In other words, a simple sketch of saddle-point contours along with locations of minima and maxima —which we call a "spaghetti diagram"— is implicitly already an approximation to a lens-mass distribution.

The preceding assumes a point source. To get an idea of what an extended source would do, let us imagine moving the original source slightly. The contours of constant arrival time will naturally move slightly, and so will the images. The movement of the contours will be most noticeable where the contours are far apart, that is where the arrival-time surface is nearly flat. As is evident from Figure 3.1, this is the region where the minimum and saddle points lie, or near the images. In this region, points on the source that are close together produce images that are comparatively far apart. In other words, the image is highly magnified. In summary, lower curvature in the arrival-time surface for a point source implies larger magnification of an extended source. Conversely, where the arrival-time surface is strongly curved, the image will be demagnified. We see from Figure 3.1 that the arrival-time surface tends to be highly curved near the maximum. Hence maximum tend to be demagnified. In practice, maxima of the arrival time are nearly always too faint to see. The minima and saddle points dominate.

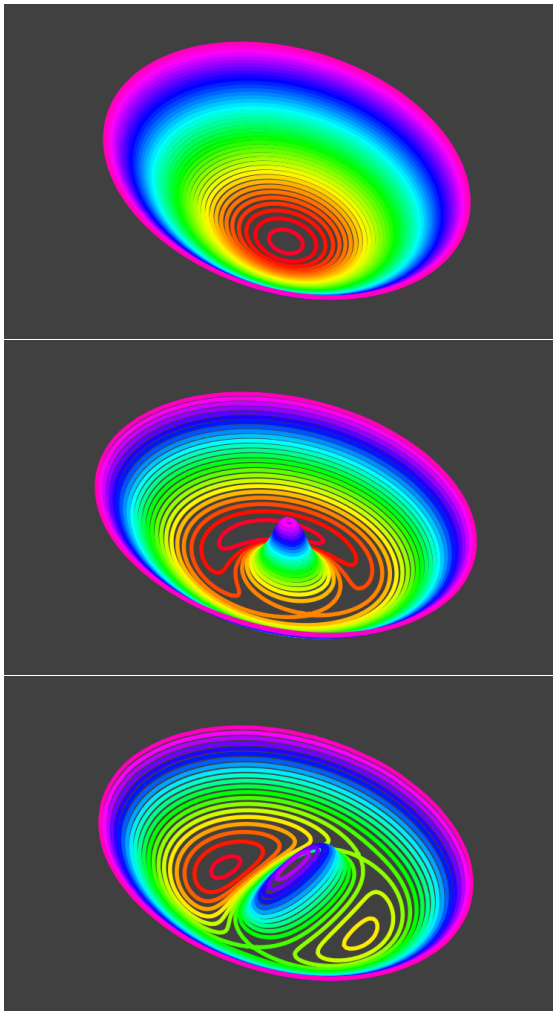

Figure 3.1: Perspective views and contour maps of example arrival time surfaces. Contours are coloured in rainbow order (red: least delay, violet: highest delay). The special contours that self-cross at saddle points are the basis of spaphetti diagrams. *Upper panel:* No lens, hence showing the parabolic shape of the geometrical time delay. The image would be at the bottom, coinciding with the source. *Middle panel:* A circular lensing mass (offset from the source) has been added, which has pushed the minimum to one side and introduced a maximum and saddle point, each corresponding to an image. The saddle-point is characterized by a self-crossing "spaghetti" contour. *Lower panel:* An elongated lensing mass has been added. There are now two minima, two saddle points, and a maximum, each corresponding to an image.

3.3 A lens modelling program

SPAGHETTILENS is a mass modelling program that makes use of the SPACEWARPS infrastructure, in particular, the image database and the discussion forum.[2] The forum is essential for establishing contact between interested members of the SPACEWARPS community and the project science team, and then for enabling collaboration between them. We were able to collaborate together on modelling objects from SPACEWARPS in the usual style of medium-sized astronomical collaborations, with video-conferencing and in-person meetings where possible. Preliminary results were immediately summarized on modelling threads on the forum, and anyone interested was made welcome to join at any time.

Modelling with SPAGHETTILENS involves three stages, (1) markup of the image, followed by (2) intensive numerical computation carried out on a server in the background, followed by (3) review of diagnostics and possible discussion. Human interaction is essential to the first and third stages, while stage 2 is completely automated. We now describe the three stages.

3.3.1 Image markup

One begins by going to the SPAGHETTILENS web application[3] and entering the number of a SPACEWARPS image tile. SPAGHETTILENS then presents the image, along with zoom and pan options and a markup tool to construct a spaghetti diagram. The human modeller now has to make an educated guess for the topography of the arrival-time surface, and input the locations time-ordering of the maxima, minima, and saddle-points. The markup tool (which is inspired by Figure 6 of Blandford and Narayan, 1986, and is like that figure made interactive and overlaid on data) lets the modeller enter the information by sketching saddle-point contours. Examples can be seen in Figure 3.2 and the upper-left panels of Figures 3.3 to 3.10. The loops in the markup tool were the origin of the "spaghetti" metaphor.

The markup tool allows only valid lensing configurations to be entered. The user does not need to think explicitly about the image parities (though the markup tool provides this information using colour codes) or about time-ordering, or worry about the odd-image theorem. The exact placement of the loops in a spaghetti diagram has no significance. Only the hierarchy of which loop is inside which is relevant. The loops are there simply to help modeller's intuition.

As implemented so far, SPAGHETTILENS assumes that the lens is dominated by a single galaxy. Accordingly, only one maximum in the arrival-time surface is permitted, and it is taken to be the centre of the main lensing galaxy. The user can, however, mark additional minor galaxies: these are modelled as point masses, the mass being fitted by the program along with the rest of the mass distribution.

[2] `http://talk.spacewarps.org`
[3] `http://mite.physik.uzh.ch`

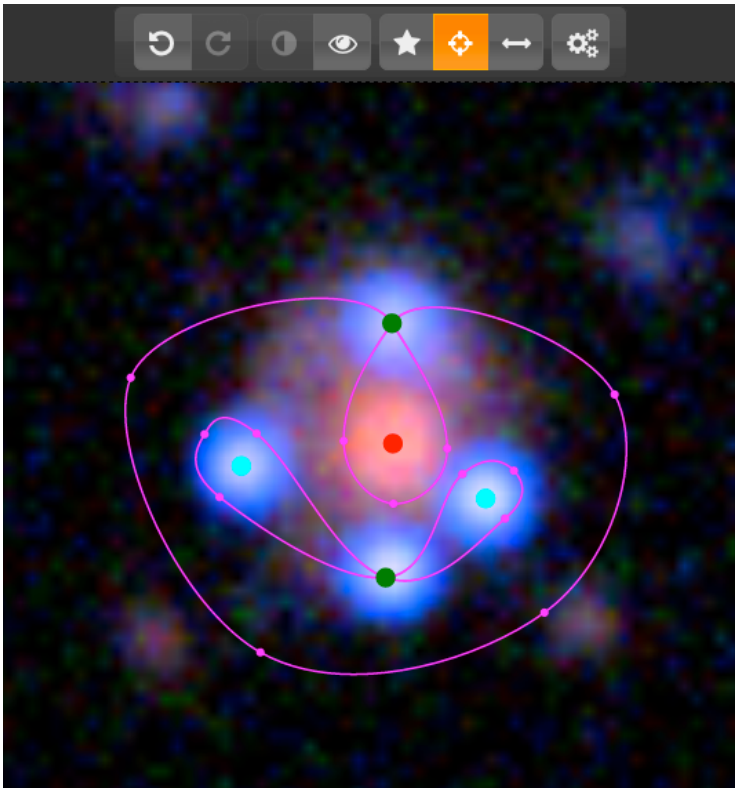

Figure 3.2: Screen grab of SPAGHETTILENS in action. A SPACEWARPS image has been loaded in, re-centred and zoomed. Five images and the associated "spaghetti" contours have then been suggested, using the marking tools associated with the buttons along the top of the panel. The mass model is generated server-side when the right-most button is pressed.

3.3.2 Numerics

Having sketched a spaghetti diagram, the user presses a button to initiate the next stage. SPAGHETTILENS then translates the spaghetti diagram into input for GLASS, and forwards this input. The task of GLASS, which runs server-side as it is compute-intensive, is to find a mass distribution $\kappa(x, y)$ that exactly reproduces the given locations of the maximum, minima and saddle points. This criterion by itself is extremely under-determined – there are infinitely many mass distributions that will reproduce a given set of maxima, minima and saddle points, but typically they (a) produce lots of extra images, and (b) look very unlike galaxies. Additional assumptions (a prior) are necessary. GLASS uses the following priors (cf. Saha and Williams, 1997; Coles, 2008).

1. The mass distribution is built out of non-negative tiles of mass. (Sometimes these tiles are called mass pixels, but we should emphasise that they are unrelated to image pixels, and are much larger.)

2. There is a notional lens centre, say (x_0, y_0) which is identified with the maximum of the arrival time. The source can have an arbitrary offset with respect to the lens centre.

3. The mass distribution must be centrally concentrated, in two respects. First, the circularly averaged density must fall away like

$$\left[(x-x_0)^2+(y-y_0)^2\right]^{-1/2} \tag{3.6}$$

   or more steeply. Second, the direction of increasing density at any (x, y) can point at most 45° away from (x_0, y_0).

4. The lens must be symmetrical with respect to 180° rotations about (x_0, y_0). This symmetry assumption can be relaxed if the user wishes.

There are still infinitely many models that satisfy both data and prior constraints, but now they are more credible as galaxy lenses. It is then possible to generate an ensemble of models. The sampling technique used by GLASS is described in (Lubini and Coles, 2012). Typically, ensembles of 200 models are used. That is to say, what we call a SPAGHETTILENS model is really the mean of an ensemble of 200 models, and its estimated uncertainty is the range covered by the whole ensemble.

3.3.3 Diagnostics

After the model ensemble has been generated, SPAGHETTILENS post-processes it to present results and diagnostics to the user for inspection. This takes the form of three figures.

1. A synthetic image of the lensed features.

2. A contour map of the arrival-time surface $t(x, y)$.

3. A gray scale plus contour map of the mass distribution.

The synthetic image generated by SPAGHETTILENS assumes a simple circularly symmetric source with linearly decreasing surface brightness profile. The user can change the contrast level on the image, which (though it is not saved) amounts to adjusting the size of the source. These synthetic images are still very crude, and not always useful for assessing models. The best indicator, in practice, of whether the modelling was successful is contour map of $t(x, y)$, with saddle-point contours highlighted. It is, in effect, the computer's refinement of the spaghetti diagram input by the user. If the arrival-time surface looks qualitatively similar to the spaghetti diagram, that generally indicates a successful model. The mass distribution also provides indications; successful models generally lead to smooth-looking mass distribution, whereas an irregular or checkboard pattern in the mass map signals a bad model.

After examining this feedback, the user can choose to save the model to the SPAGHETTILENS archive, at which point it is assigned an unique URL. They can also modify the input and try again, or discard the attempt altogether. After archiving, there can be discussion among modellers, through the SPACEWARPS forum or by any other means, and revision of the model. This is achieved simply by sharing the model's URL; following its hyperlink takes one to the SPAGHETTILENS app, pre-loaded with the correct data image and input spaghetti. Any archived model can be revised by any user: they can modify the spaghetti configuration slightly or drastically, or change options like the size of the mass tiles. Particularly interesting lens candidates lead to trees of models in this way. Discussion among modellers tends to prune a model tree, focusing attention on the most interesting models.[4]

3.4 A lens modelling challenge

We now describe a test of the lens-modelling system, under conditions that mimic as closely as possible the modelling of real lens discoveries. The lenses to be modelled were the simulated lenses (known as "sims") already sprinkled onto the SPACEWARPS field. Once a small user base had grown around SPAGHETTILENS, a modelling challenge was announced through the SPACEWARPS forum. The challenge set consisted of 29 sims, chosen to represent the different visual morphologies of SPACEWARPS sims. Modellers then contributed 119 models for these sims (at least two for each sim). Models were reported on the same forum used to model real candidate lenses. Modellers were free to consult and refine each other's models, but had no information on how the sims were generated.

Once the modelling was complete, the models were compared with the originals. There were two main tests: a check of whether the spaghetti diagrams were correct for the lens in question, and a comparison of the effective Einstein radii of the sims and the models.

[4] See "Collaborative gravitational lens modelling..." in `http://letters.zooniverse.org` for an example.

3.4.1 The simulated lenses

The SPACEWARPS sims are described in detail in More et al (in prep), but relevant here is that the sims were of three kinds, as follows.

1. Lensed quasars: The lens is modelled as a singular isothermal ellipsoid (SIE) and a constant external shear whereas the quasar is represented with a circular Gaussian source whose size is given by the point spread function (PSF) in each imaging band.
2. Galaxy-scale lenses: The lens model is the same as above whereas the background galaxy is modelled as an elliptical de Vaucouleurs.
3. Group-scale lenses: The lens model includes SIE models for the central galaxy and the inner group members, plus a circular NFW (Navarro, Frenk, and White, 1996, 1997) to represent the underlying dark matter distribution and the background galaxy model stays the same as galaxy-scale lenses.

The `gravlens` program (Keeton, 2001b) was used. Formulas for the lenses appear in Keeton, 2001a. The SIE lenses follow Equations (33–35) of that work, with core radius set to zero. The NFW lens is in Equations (48) and (50), while shear is the γ term in Equation (76).

The information in this section was not revealed to the main developer of SPAGHETTILENS (RK, who also chose the challenge set) or to the modellers (EB, CC, CM, JO, PS and JW) while modelling was in progress. That is, the modellers had no advance knowledge of what kind of parameterisation had been used to make the sims. After the modelling stage, AM released the details of the sims for post-modelling analysis. Results from the latter now follow.

3.4.2 Some example models

Of the 119 models proposed, we now discuss eight examples in some detail. Results from these are shown in Figures 3.3 to 3.10. The first four of these show the most common image morphologies, the other four explain some problem cases.

Each of Figures 3.3 to 3.10has the following layout.

marked-up CFHT LS image	model synthetic image
$t(x, y)$	model $t(x, y)$
$\kappa(x, y)$	model $\kappa(x, y)$

The model synthetic image presented in this paper is not the original one, but an interpolated version generated by an updated version of SPAGHETTILENS. The image presented during the original experiment was of lower resolution. The two plots in the middle showing $t(x, y)$ have uniform, but arbitrary spaced contour lines. The $\kappa(x, y)$ plots in the bottom row show

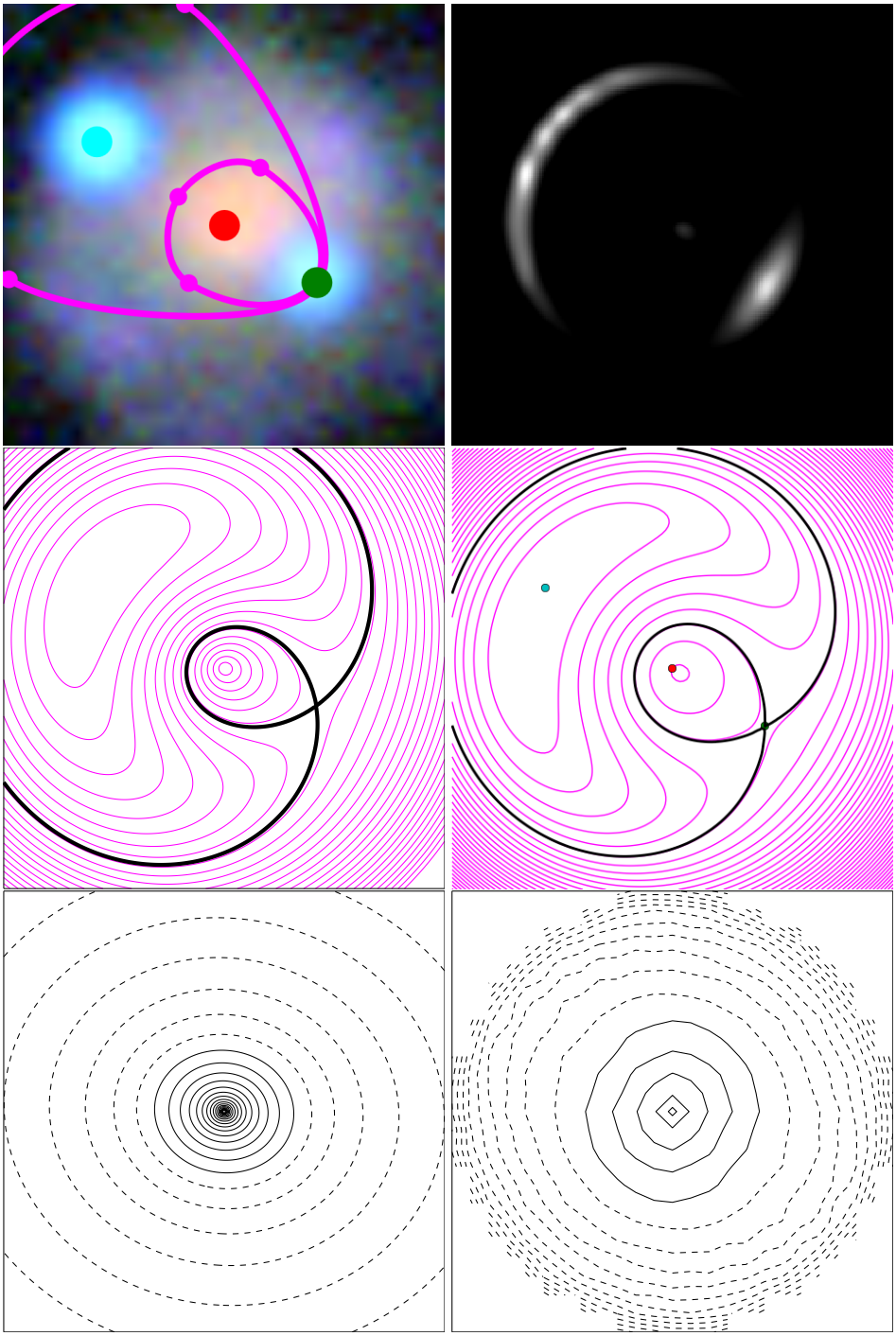

Figure 3.3: A simulated lens that mimics a lensed quasar, and model results. The left panels derive from the simulation, and the right panels are SPAGHETTILENS output. Details of individual panels are in Section 3.4.2.

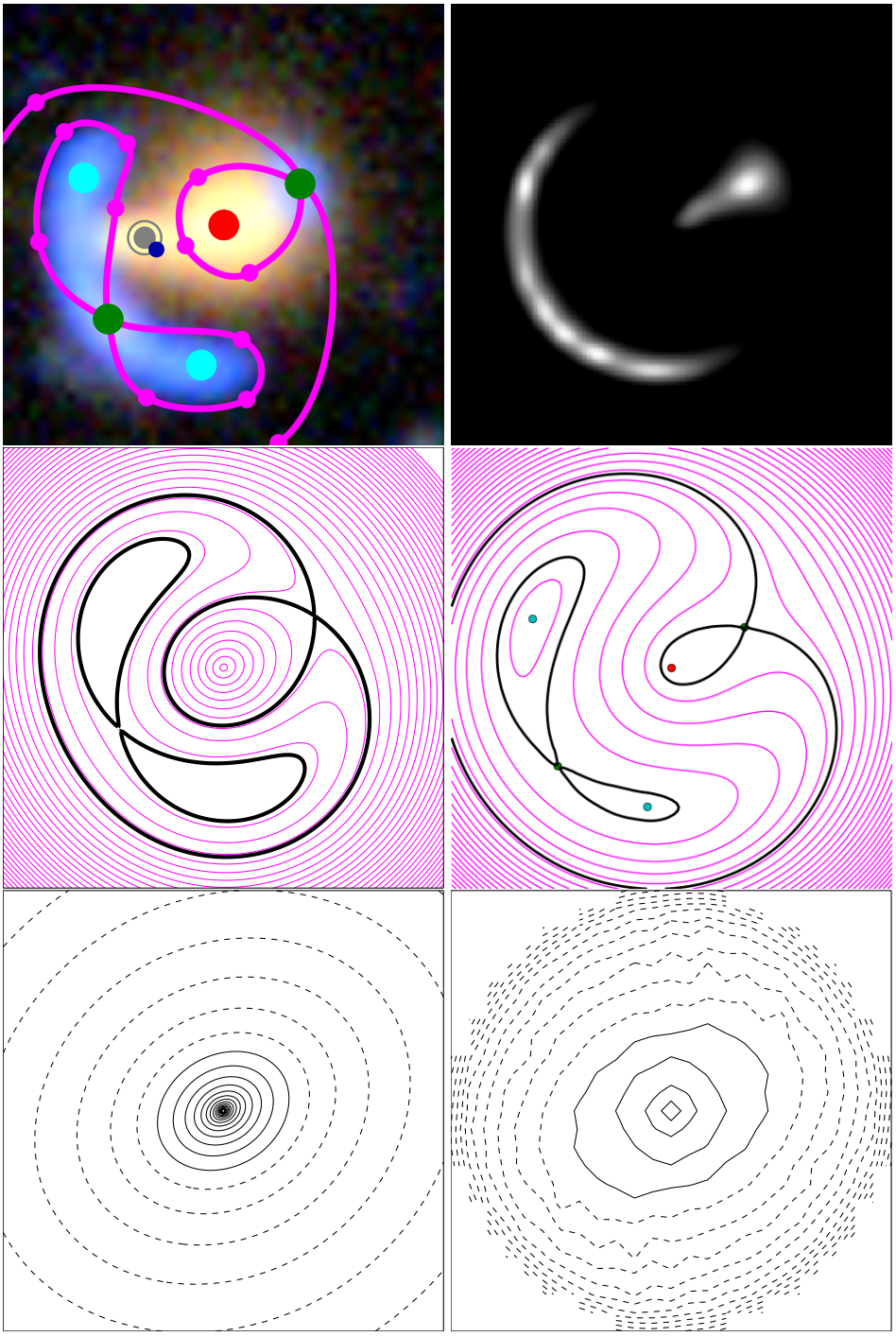

Figure 3.4: Results from a system with an arc plus a counter-image, typical of lensed galaxies. (See Section 3.4.2 for details.)

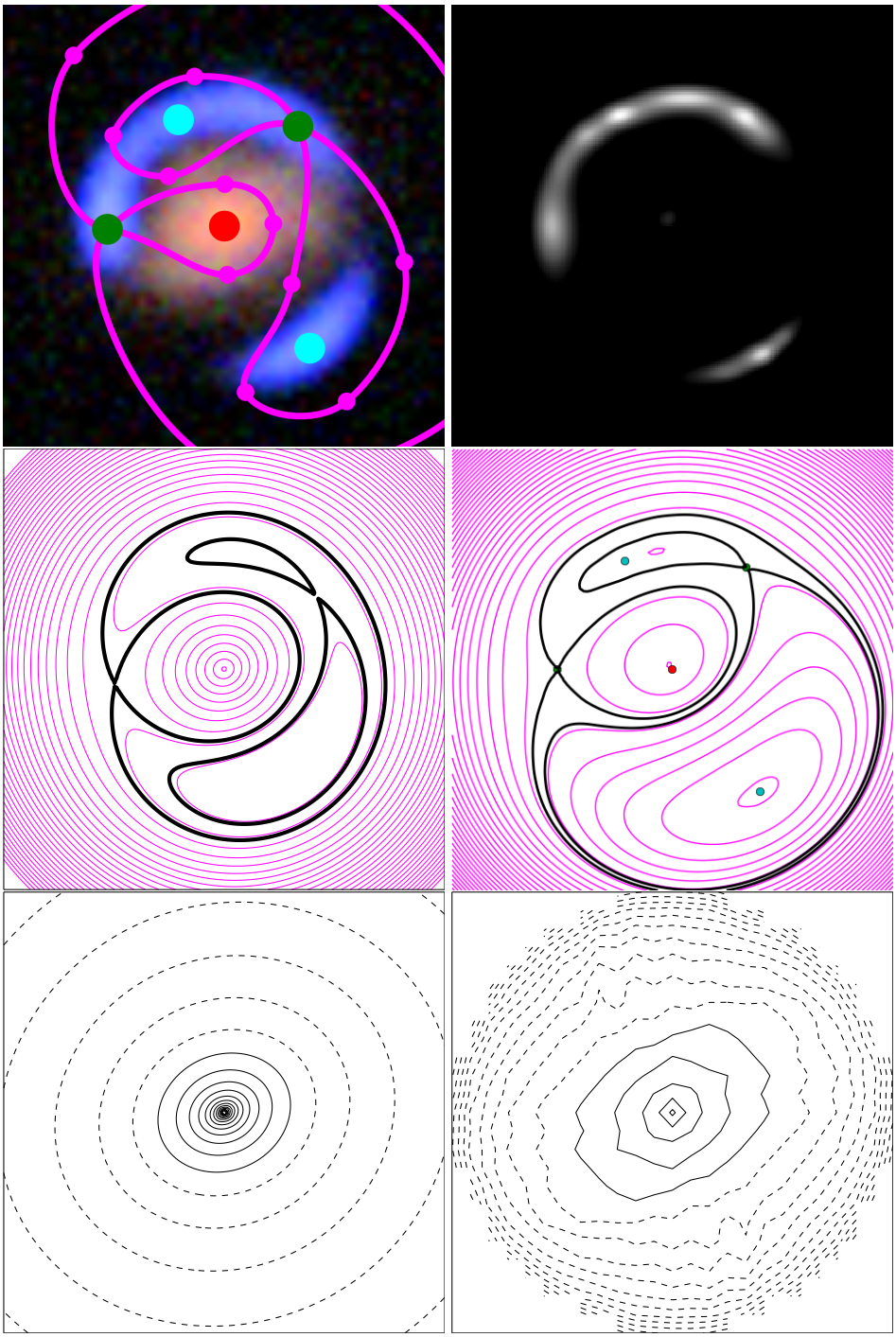

Figure 3.5: Another configuration of arc plus counter-image: an arc and counter image where the arc is closer to the lensing galaxy than the counter image. (See Section 3.4.2 for details.)

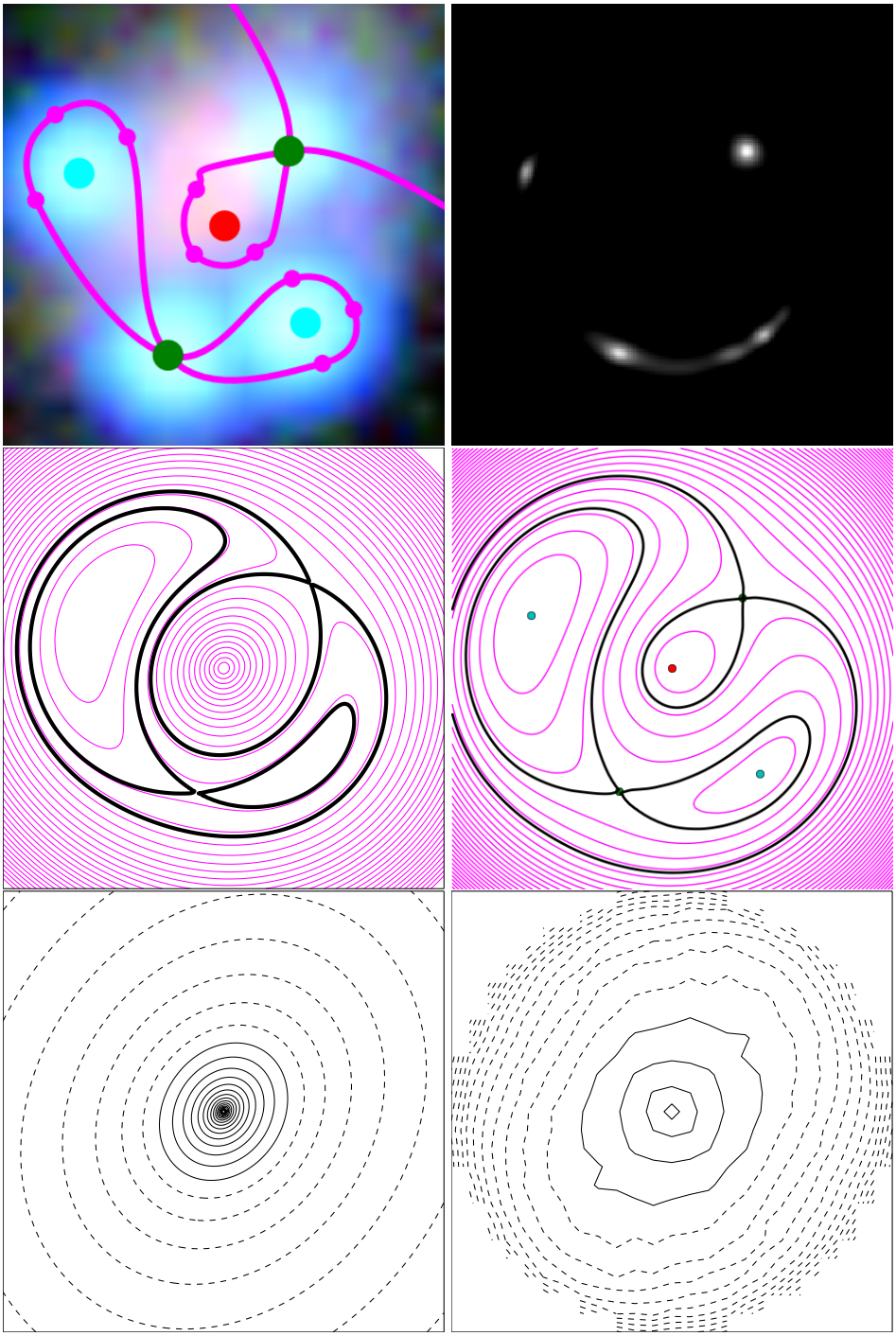

Figure 3.6: A four-image configuration typical of lensed quasars. (See Section 3.4.2 for details.)

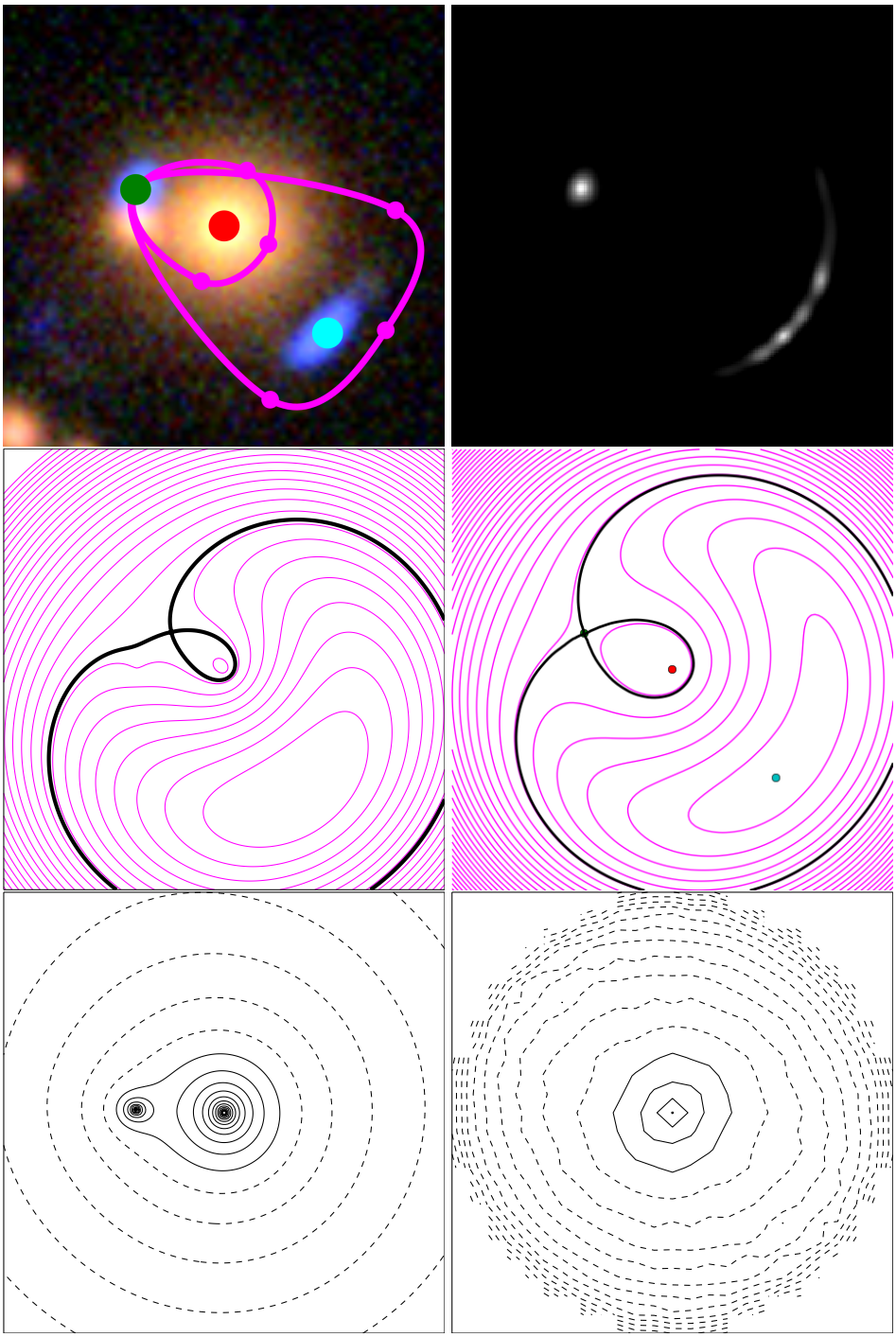

Figure 3.7: A lens with unrecovered mass substructure. (See Section 3.4.2 for details.)

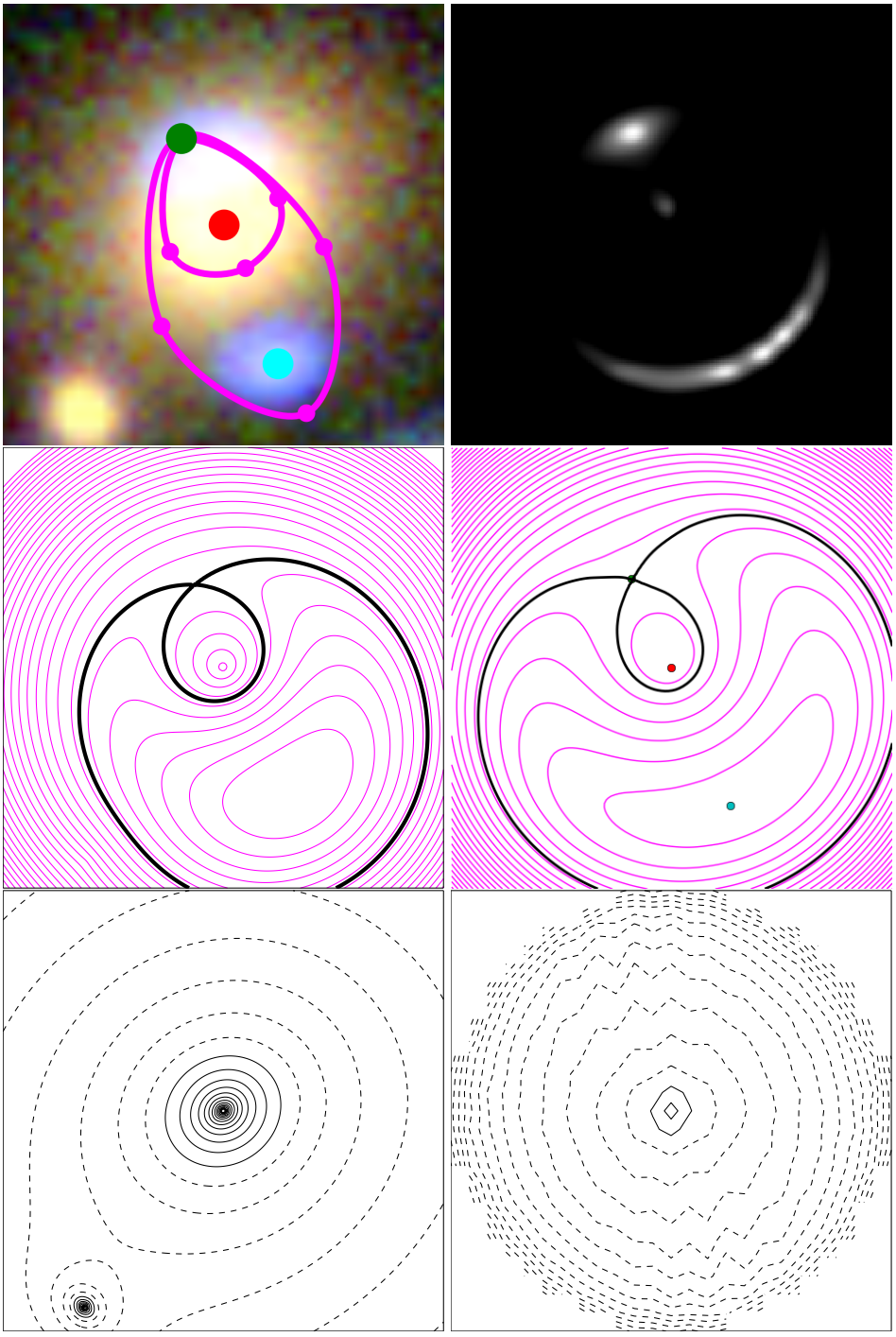

Figure 3.8: A sim with unrecovered substructure, resulting in a poor mass model. (See Section 3.4.2 for details.)

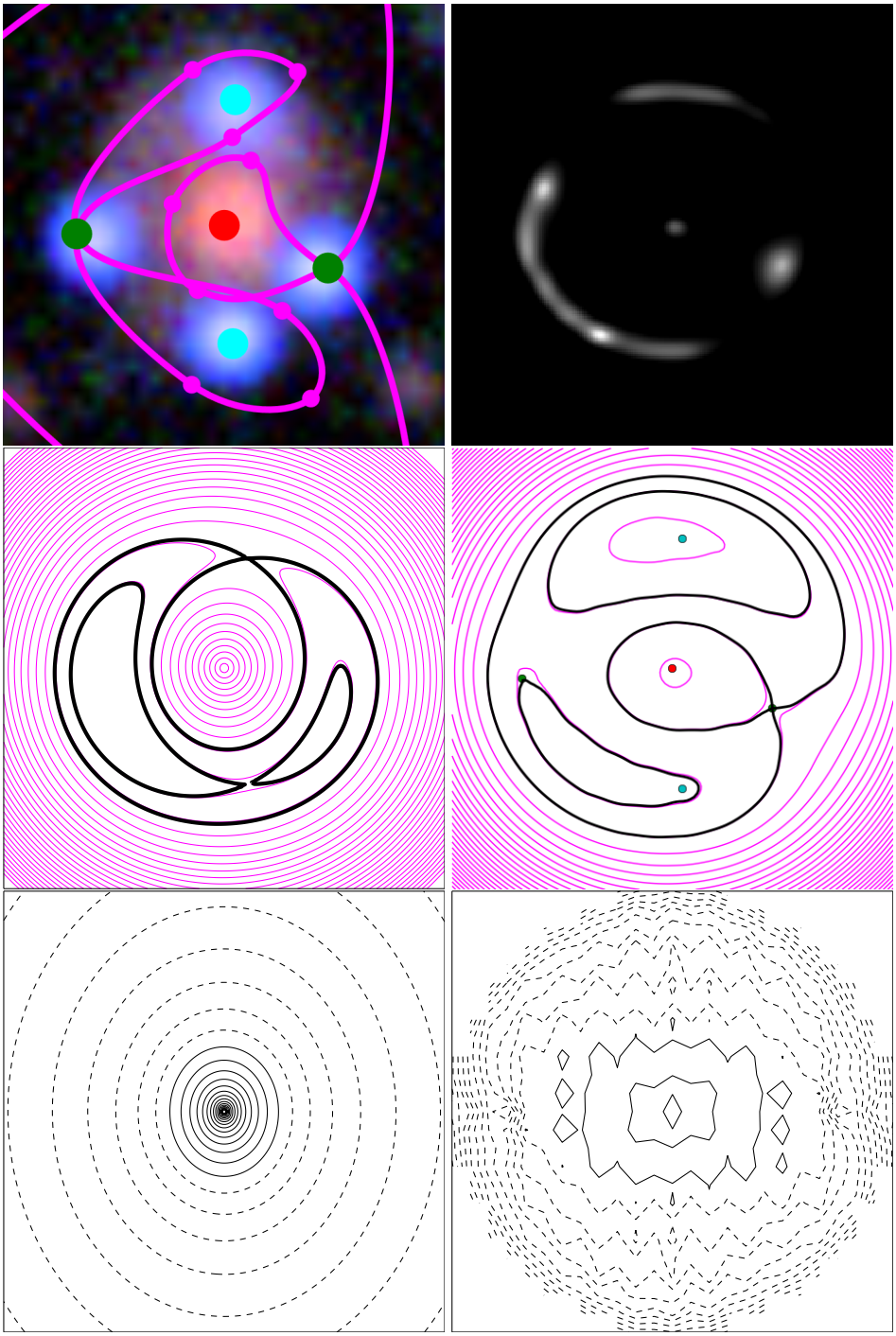

Figure 3.9: A four-image system with image parities incorrectly identified. The model is poor, but the estimated Einstein radius is not bad. (See Section 3.4.2 for details.)

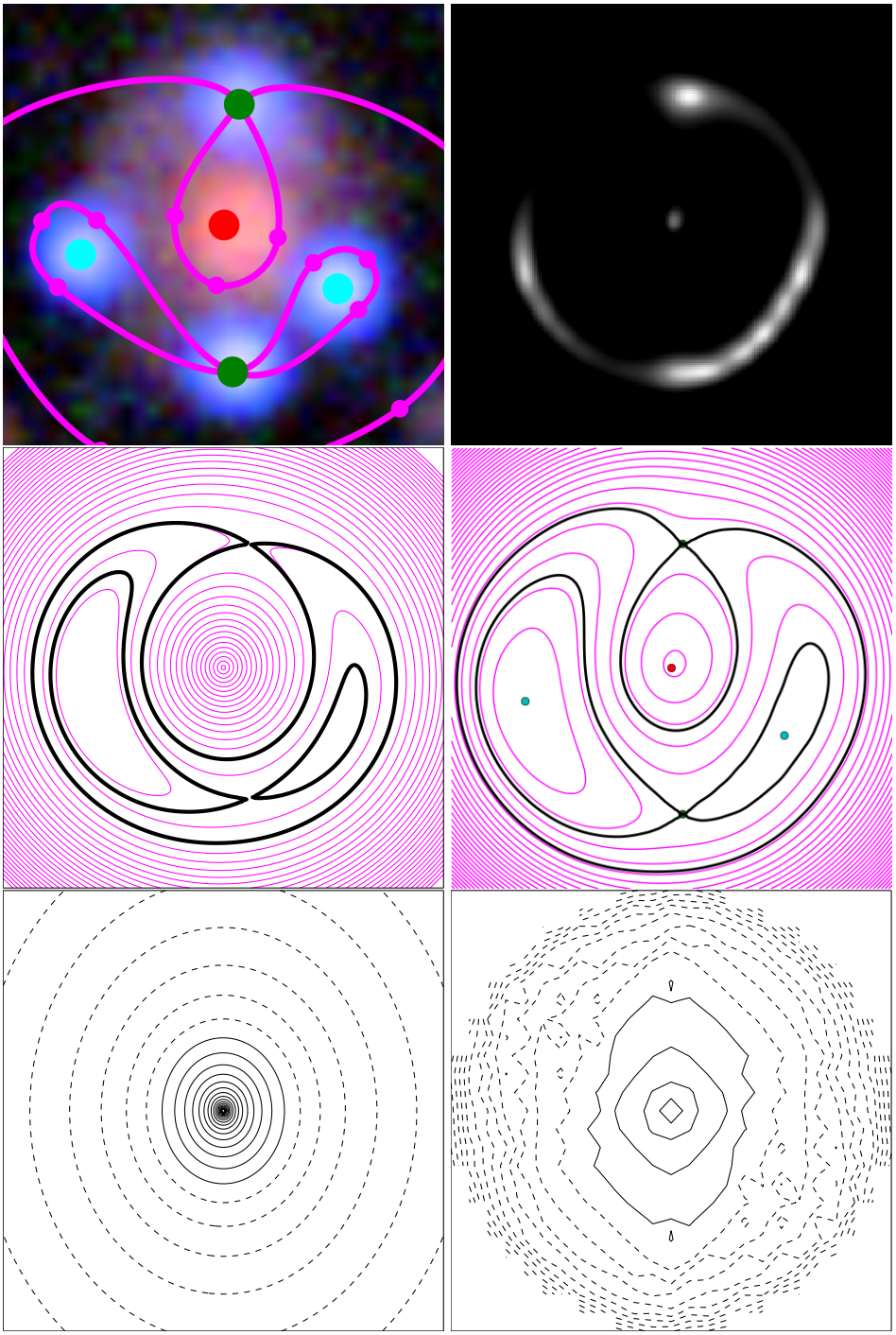

Figure 3.10: The same system as in Figure 3.9, this time with image parities correctly identified. (See Section 3.4.2 for details.)

solid lines for $\kappa > 1$ and dashed lines for $\kappa < 1$. The spacing is logarithmic, with 10 contours for every decade – that means contour spacing is a quarter magnitude in optical terms.

Let us now consider these cases in turn.

- Figure 3.3 shows the simplest case, with two clear images produced by a nearly-circular lens. The centre of the lensing galaxy is a maximum, the image nearer to the galaxy is a saddle point, and the image further away is a minimum. All these were correctly identified. As note above, in Section 3.3, the precise shape of the loops in the spaghetti diagrams is unimportant, only the implied image locations, parities and time-ordering matters. $\kappa(x, y)$ shows, that the model has a more shallow mass distribution than the simulation. This is a persistent issue throughout all models and is discussed in Section 3.4.4.

- Figure 3.4 shows an example of an arc that has split into three images. This kind of configuration, with a counter-image close to the lensing galaxy and a more distant arc/triplet on the other side, generically arises from an elongated mass distribution when the source is displaced along the elongated direction. The spaghetti diagram in this case has another markup element, a grey point and circle overlaid on a probable secondary lensing galaxy. This is an instruction to SPAGHETTILENS to allow a point mass at that location, distinct from the main mass map.

- Figure 3.5 shows another example of an arc plus counter-image, but (in contrast to Figure 3.4) the arc is closer to the lens than the counter-image. This configuration arises if the source displacement is perpendicular to the long axis of the lensing mass. Comparing the two panels in the middle row, we see that the modeller interpreted arc as consisting of three images, whereas the sim shows a single saddle point associated with the arc. But the identification is not really erroneous – we just need to take into account that the source is extended. In fact, in the sim the brightest part of the source is only doubly imaged, but the source extends into a region that produces four images. In the $t(x, y)$ of the sim, the hairpin-bending contours are typical of double on the verge of splitting into a quad.

- Figure 3.6 shows another quad. This kind of configuration arises when the mass is elongated and the source is displaced at an angle to the elongation. The minima and saddle points are correctly identified, and the orientation of the ellipticity of the mass distribution is correctly reproduced.

- Figure 3.7 shows a lens with substructure in the form of a smaller secondary galaxy. The galaxies in such group or cluster sims were based on galaxies visible in the images, but the modellers were not told in advance whether this was the case. The minimum and saddle point are correctly identified. The mass distribution misses the substructure, but overall appears reasonable.

- Figure 3.8 shows a sim with substructre, like Figure 3.8. In comparison to the above, the resulting mass model is poor.

- Figure 3.9 shows a quad. In this one, the identification of the minima and saddle points was incorrect, and mass distribution comes out elongated East-West instead of North-South. The mass distribution also appears somewhat jagged and the saddle-point contours are not as clean as in the previous examples; these are often indicators of a problem with the model. The enclosed mass is, however, none the worse – the reason is probably that in a relatively symmetrical image configuration, the Einstein radius is quite well constrained by the images in a fairly model-independent way.
- Figure 3.10 shows another model of the same system, the only one done by an expert in this sample. The image parities are correct. The elongation has the right orientation, but is too shallow.

3.4.3 Test of image identification

The first post-modelling test was a qualitative comparison of the original arrival-time surfaces and the input spaghetti diagrams given by the modeller. This tested first, for correct identification and location of the lensed images, and second, for the correct parities and ordering of the lensed images in respect of the arrival time.

While we expected the identification of lensed images to be trivial, given the generally clean appearance of the sims in the test, we expected the parities and time-ordering to be more difficult. While the SPAGHETTILENS tutorials had provided general guidelines, to be consistently correct with the time-ordering, a modeller needs to develop some intuition for arrival time surfaces. This is an area where experience and tutorials training could improve results at a later stage, and correspondingly, feedback on the difficulties modellers encounter can help improve the tutorial materials.

Table 3.1 presents a summary of the test. The evaluation was done manually, comparing the input to SPAGHETTILENS with the actual arrival-time surface of the sim. This amounts to comparing the middle-left and middle-right panels in each of Figures 3.3 to 3.10, and similarly for the other 111 models.

The images of the system were considered to have been located correctly, if all the images were identified and were approximated within about 5% of SPAGHETTILENS frame used to draw the spaghetti diagram. That frame size is adjustable by the user, but in practice it is somewhat larger than the spaghetti diagram. Such image-placement errors were found in only 9 models. That does not include inaccurate image placement over an arc, which was considered a separate category of error.

In addition to simple image-placement errors, ten types of errors were recognised and are listed in Table 3.1. Most of the problems were due to unclear arc-like structures. Critical errors like the failure to identify all five images in a five images system, or to include too many images, were rare.

The assignment of the parity of the images was a more difficult task, and was successful in only about 60% of the cases. The most common error was swapping of minima and

Table 3.1: Table of image-identification errors and the number of models containing each. A model can contain more than one type of error.

Total	119	100%
errors in image locations	9	8%
errors in image parities or time ordering	49	41%
inaccurate image placement over an arc	21	18%
identified two images of four	5	4%
identified two nearby images as one	3	3%
missed faint images	1	1%
proposed too many images	1	1%
modelled a three-image arc as one image	4	3%
modelled one image as a three-image arc	5	4%
swapped minimum and saddle in double	2	2%
swapped minima and saddles in quad	38	32%
swapped early and late saddles in a quad	7	6%

saddle-points in a quad; Figure 3.9 shows an example. Another, less common, error was flipping the spaghetti diagram, thus swapping the time-ordering of the two saddle points.

Incorrect image parities and time orderings tended to produce poorer-looking models, such as the checker board patterns in the mass map in Figure 3.9. Interestingly, however, the enclosed-mass profiles were quite robust. We will consider this aspect in the next section.

3.4.4 Test of mass-profile recovery

The second test was to compare the mass distributions $\kappa(x, y)$ of the sims and of the SPAGHETTILENS models. A visual comparison is presented for the eight models in Figures 3.3 to 3.10, in the lower-left versus lower-right panels. We will summarise the mass distributions drastically in a single number, the effective Einstein radius. Other measures for comparison of free-form lensing mass distributions appear in Coles, Read, and Saha, 2014, but comparing Einstein radii is already useful.

There is no standard way of defining the Einstein radius of a general non-circular lens. We adopt the simple definition

$$\langle \kappa \rangle_{\Theta_E} = 1, \tag{3.7}$$

that is, the effective Einstein radius Θ_E is such that the mean κ is unity inside a circle of radius Θ_E centered at the lens center.

To illustrate, Figure 3.11 compares the circularly averaged mass profiles of three different models of one particular lens; two of the models are shown in Figures 3.9 and 3.10. Each panel in Figure 3.11 shows the mean κ within a circle of given radius. The red curve is the correct profile for the sim. The two blue curves are the minimal and maximal mean enclosed κ from the internal ensemble in SPAGHETTILENS. Radial locations of the images are marked,

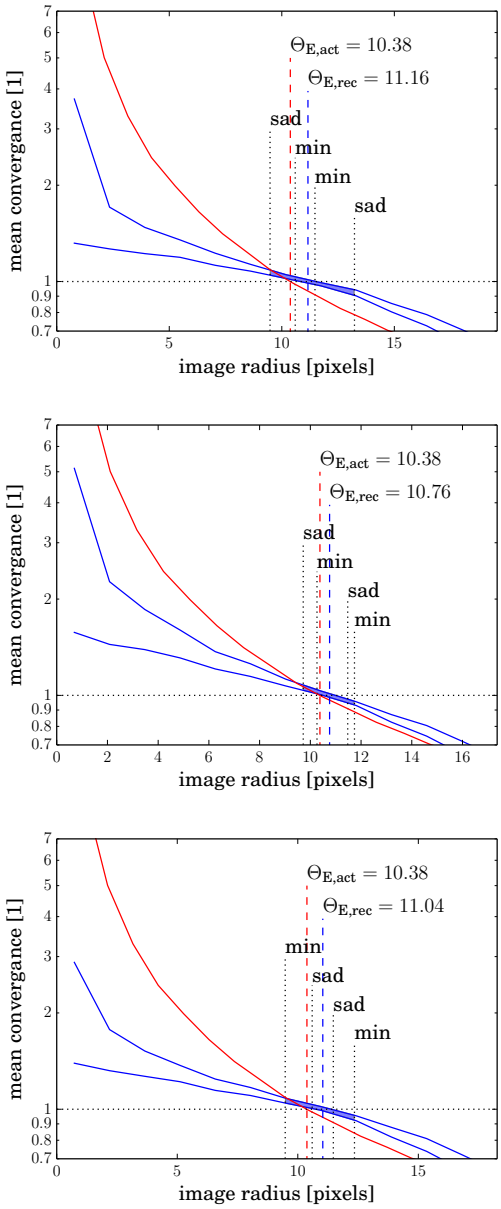

Figure 3.11: Mean κ inside a circle around the lens centre, as a function of the radius of the circle. (See Section 3.4.4 for details.) The upper panel corresponds to the model shown in Figure 3.9, in which the minima and saddle-points have been incorrectly swapped. The middle corresponds to Figure 3.10, where the image parities were correct. The lower panel corresponds to another model, where the image parities were correct but the time-ordering was incorrect.

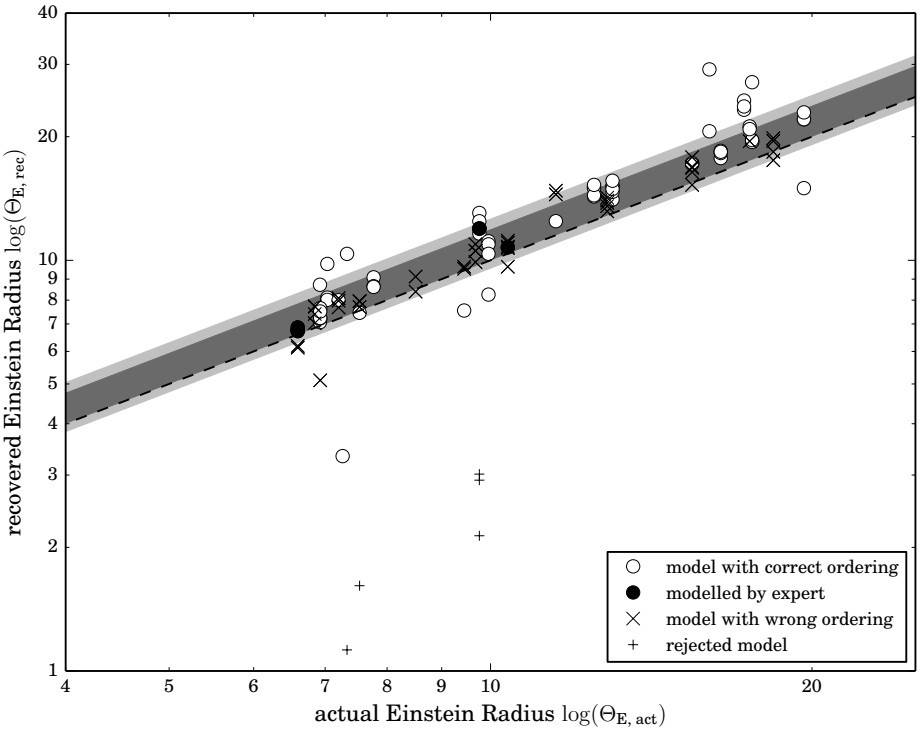

Figure 3.12: Model-recovered versus actual Einstein radii $\Theta_{\rm E,rec}$ and $\Theta_{\rm E,act}$. Plus signs indicate models flagged by the modeller as failures by commenting negatively about it in the forum. Light and dark grey bands show standard deviation of volunteers (15%) and expert (10%).

along with the image parities. The region between the blue curves is shaded between the radii of the innermost and the outermost images: this is the confidence region from the modelling. The definition (3.7) for Θ_E corresponds to crossing the dashed horizontal line at 1: the red curve crosses the dashed line at the actual Einstein radius $\Theta_{E,act}$; the recovered Einstein radius $\Theta_{E,rec}$ and its uncertainty are given by the blue curves crossing the dashed line. We see that in all three panels, the blue curves are shallower than the red curve and $\Theta_{E,rec}$ is more than $\Theta_{E,act}$, by more than the model uncertainties. Now, steeper mass profiles tend to give wider image separations – recall that the image separation for a circular isothermal lens is $2\Theta_E$, whereas for a point mass it is more (see, e.g., Courbin, Saha, and Schechter, 2002) – so $\Theta_{E,rec}$ being too high is really a consequence of the GLASS models being too shallow for the sims.

Figure 3.12 shows that $\Theta_{E,rec}$ of the models tend to be too high. However, this is entirely due to the GLASS model density profiles being too shallow, as illustrated above. We can separate out the performance of the SPAGHETTILENS interface and its users by comparing their results with the Einstein radii of SPAGHETTILENS models made by an expert (PS). Discounting the models which were flagged by the volunteers as poor, the mean Einstein radius overestimate was 10%, with a 15% standard deviation (shown by the light grey band in Figure 3.12). The expert models show a similar bias, with standard deviation 10% (the dark grey band in Figure 3.12). One source of this systematic error is that it is difficult to centre the lens accurately: an offset leads to a flatter mass profile for the model compared to the simulation.

3.5 Outlook

This work has developed the concept of saddle-point contours in the travel time of virtual photons, originally introduced by Blandford and Narayan, 1986 for understanding image structure in strong gravitational lenses, into a technique for mass-mapping lenses. Despite being highly abstract, saddle-point contours look like schematic arcs, and hence lend themselves to an intuitive markup tool for lenses or lens candidates, which we call a spaghetti diagram. At the same time, saddle-point contours encode information about possible mass distributions, which can be translated into input for an existing lens-modelling engine (GLASS, by Coles, Read, and Saha, 2014).

SPAGHETTILENS is an implementation of these ideas, enabling experienced but non professional lens enthusiasts to model newly-discovered lens candidates from the SPACEWARPS citizen science platform. The tests in this paper indicate that such modelling would be both feasible and scientifically interesting: given a suitable modelling tool, and appropriate guidance, a small team of non-professional volunteers was able to model a sample of 29 test lenses, and measure their Einstein radii with comparable accuracy to a professional expert.

There is, however, plenty of room for improvement:

1. SPAGHETTILENS tends to overestimate the Einstein radius (evident from Figure 3.12), and the model density profiles tend to be shallower than the SIE model used for

generating the sims. The likely explanation is that while the sims are steeply peaked at the centre, the pixellated mass model fixes a comparatively large area near the central at constant density. Allowing smaller pixels in the centre region, thus enabling a steeper centre (similar to the "high resolution" feature implemented in Coles, Read, and Saha, 2014) may remove this bias. The use of simply parameterised, appropriately steeply-profiled models would also avoid the problem.

2. Currently, SPAGHETTILENS does not attempt to model the source shape; the user identifies the brightest points on the image, and these are taken as images of a point-like source, whose positions must be reproduced exactly. For generating a synthetic image, a conical source profile is assumed. Fitting for the source profile to optimise resemblance to the observed lensed image after the lens model has been generated, is algorithmically straightforward (cf. Warren and Dye, 2003; Suyu et al., 2006) and planned to be implemented. This would alleviate another problem with SPAGHETTILENS, which is that there is as yet no quantitative figure of merit for any given model: assessment of each model is a judgment call based on the synthetic image, and on whether the mass distribution and the arrival-time surface show suspicious features. Another possibility would be use the SPAGHETTILENS models as a feeder to a different lens-modelling program that already implements source-profile fitting.

3. Another limitation so far in SPAGHETTILENS is that the lens is assumed to be dominated by one galaxy, which puts most galaxy-group lenses beyond the reach of the modeller. Since complicated group lenses are some of the most interesting candidates present, removing this limitation is most desirable. From the users' point of view, it would mean that spaghetti contours with more than one maximum can be allowed. For examples, see Figure 5c in (Rusin et al., 2001) and Figure 4b in Keeton and Winn, 2003.

4. At present, a single false-colour composite is used as the data. An option could be added to use all available filters, individually or in combination, at the user wishes.

5. As mentioned above, the option of revising an already-archived model is already available. Desired now are tools for comparing different models of a given system, both visually and through different statistical measures. As evidenced by a current collaborative modelling effort, a particularly interesting candidate can lead to an extended discussion and dozens of models, that in some way sample the high likelihood region of model parameter space.

6. Better tutorial materials are also needed, and this would address some of the problem areas found in the modelling challenge. For example, we saw in Section 3.4.3 that volunteers are most prone to making errors in two situations: when in identifying an arc- like structure while placing the points, and in identifying the correct ordering of the points in nearly-symmetric configurations. Better and more detailed introductory materials would also allow the community of modellers to grow faster and without individual instructions by experts or experienced volunteers.

The SPAGHETTILENS program was developed by Küng, with design suggestions from Coles, Cornen and Saha, and feedback from all co-authors. The simulations were created by A. More, in consultation with Marshall, S. More and Verma. Modelling was done by Baeten, Cornen, Macmillan, Odermatt, Saha and Wilcox, with post-modelling analysis by Küng and Saha. All authors participated in writing and editing the manuscript.

3.6 Acknowledgments

We thank the Swiss Society for Astrophysics and Astronomy and the Swiss Academy of Sciences. The work of AM and SM was supported by World Premier International Research Center Initiative (WPI Initiative), MEXT, Japan. AV is supported by a research fellowship from the Leverhulme Trust. RK is supported by the Swiss National Science Foundation. This work was supported in part by the U.S. Department of Energy under contract number DE-AC02-76SF00515.

3.7 Appendix: Relation to standard lensing formalism

The description of the arrival-time surface in Sections 3.2 and 3.2.2 omitted some details for the sake of a more intuitive explanation. The convergence κ and the geometric time delay $t_{\rm geom}$ were left as proportionalities (Equations (3.2) and (3.3)), and the gravitational time delay $t_{\rm grav}$ was given in an implicit form (Equation (3.4)). Here we fill in the details.

The original formulation of the arrival-time surface appears in equations (2.1) to (2.6) of Blandford and Narayan, 1986. Their equations can be rearranged as follows.

$$\begin{aligned} t_{\rm geom} &= \frac{(1+z_L)}{2c}\frac{d_S}{d_L d_{LS}}\left[(x-x_s)^2+(y-y_s)^2\right] \\ \nabla^2 t_{\rm grav} &= -(1+z_L)\frac{8\pi G}{c^3}\,\Sigma(x,y) \\ \kappa(x,y) &= \frac{4\pi G}{c^2}\frac{d_L d_{LS}}{d_S}\times\Sigma(x,y) \end{aligned} \tag{3.8}$$

The symbols d_L, d_S and d_{LS} are angular-diameter distances, respectively from observer to lens, observer to source, and lens to source. We have replaced angular positions on the sky with positions on the lens plane as

$$(x,y) = d_L(\theta_x,\theta_y)\,. \tag{3.9}$$

In the concordance cosmology

$$d_{LS} = \frac{c}{H_0}\,\frac{1}{1+z_S}\int_{z_L}^{z_S}\frac{dz}{\sqrt{\Omega_m(1+z)^3+\Omega_\Lambda}} \tag{3.10}$$

and similarly d_L and d_S.

The first line of Equation (3.8) is t_{geom} from Equation (3.3) with the proportionality filled in, and with the source offset at (x_s, y_s) rather than at the origin.

The last line of Equation (3.8) fills in the proportionality factor in Equation (3.2) for the convergence (or dimensionless surface density) κ.

The middle line of Equation (3.8) is a Poisson equation for the gravitational time delay, and is equivalent to the implicit expression (3.4). One way to verify the equivalence is to consider the small circle in Equation (3.4) as a region where Σ is constant, and approximate t_{grav} by its Taylor expansion to $O(x^2, y^2)$. Substituting in Equation (3.8) gives the Taylor coefficients in terms of Σ, and result satisfies the expression (3.4). Alternatively, we can proceed with a discrete form of the Poission equation from Equation (3.8). Discretising on a grid with spacing Δ, we have

$$\begin{aligned} t_{\text{grav}}(x,y) = \frac{1}{4}\Big[& t_{\text{grav}}(x+\Delta, y) + t_{\text{grav}}(x-\Delta, y) + \\ & t_{\text{grav}}(x, y+\Delta) + t_{\text{grav}}(x, y-\Delta)\Big] \\ & + (1+z_L)\frac{2G}{c^3}\,\pi\Delta^2\,\Sigma(x,y)\,. \end{aligned} \tag{3.11}$$

This is recognisable as a formula for solving the two-dimensional Poisson equation from Equation (3.8) by relaxation. Let us now replace the average over four neighbouring points by the circular average $\left\langle t_{\text{grav}}(x_\circ, y_\circ)\right\rangle$ and replace $\pi\Delta^2\,\Sigma(x,y)$ by the enclosed mass $M(x_\bullet, y_\bullet)$. These replacements are valid in the limit of a small grid. The result is the implicit Equation (3.4).

Chapter 4

Models of Gravitational Lens Candidates from SpaceWarps Canada-France Hawaii Telescope Legacy Survey

Original title:
"Models of gravitational lens candidates from SpaceWarps CFHT LS"

Rafael Küng[1], Prasenjit Saha[1], Ignacio Ferreras[2], Elisabeth Baeten[3], Jonathan Coles[4], Claude Cornen[3], Christine Macmillan[3], Phil Marshall[5], Anupreeta More[6], Lucy Oswald[7], Aprajita Verma[8], Julianne K. Wilcox[3],

[1] Physik-Institut, University of Zurich, Winterthurerstrasse 190, 8057 Zurich, Switzerland
[2] Mullard Space Science Laboratory, University College London, Holmbury St Mary, Dorking, Surrey RH5 6NT, UK
[3] Zooniverse, c/o Astrophysics Department, University of Oxford, Oxford OX1 3RH, UK
[4] Physik-Department, Technische Universität München James-Franck-Str. 1, 85748 Garching, Germany
[5] Kavli Institute for Particle Astrophysics and Cosmology, Stanford University, 452 Lomita Mall, Stanford, CA 94035, USA
[6] Kavli IPMU (WPI), UTIAS, University of Tokyo, Kashiwa, Chiba 277-8583, Japan
[7] Murray Edwards College, University of Cambridge, Cambridge CB3 0DF, UK
[8] Sub-department of Astrophysics, University of Oxford, Denys Wilkinson Building, Keble Road, Oxford, OX1 3RH, UK

Published in:
Monthly Notices of the Royal Astronomical Society, Vol. 474, Iss. 3, pp. 3700–3713 (03/2018)

Abstract

We report modelling follow-up of recently discovered gravitational-lens candidates in the Canada France Hawaii Telescope Legacy Survey. Lens modelling was done by a small group of specially interested volunteers from the SPACEWARPS citizen science community who originally found the candidate lenses.

Models are categorized according to seven diagnostics indicating

(a) the image morphology and how clear or indistinct it is,
(b) whether the mass map and synthetic lensed image appear to be plausible, and
(c) how the lens-model mass compares with the stellar mass and the abundance-matched halo mass.

The lensing masses range from $\sim 10^{11}\,M_\odot$ to $> 10^{13}\,M_\odot$. Preliminary estimates of the stellar masses show a smaller spread in stellar mass (except for two lenses): a factor of a few below or above $\sim 10^{11}\,M_\odot$. Therefore, we expect the stellar-to-total mass fraction to decline sharply as lensing mass increases. The most massive system with a convincing model is J1434+522 (SW 05). The two low-mass outliers are J0206−095 (SW 19) and J2217+015 (SW 42); if these two are indeed lenses, they probe an interesting regime of very low star-formation efficiency. Some improvements to the modelling software (SPAGHETTILENS), and discussion of strategies regarding scaling to future surveys with more and frequent discoveries, are included.

4.1 Introduction

By a curious coincidence, the typical escape velocity of massive galaxies – of the order of a few hundred km/s – is such that $v_{\rm esc}^2/c^2$, expressed as an angular distance, is comparable to the apparent sizes of galaxies at cosmological distances. This coincidence is fortunate, because it makes the gravitational lensing deflection angle of distant galaxies ($\alpha \sim 2v_{\rm esc}^2/c^2$) comparable to their size on the sky. As a result, strong lensing by galaxies produces images that probe their host dark matter haloes, providing a useful tool to understand galaxy formation. While there is a general consensus about the basic mechanisms at play, involving gravitational collapse, fragmentation, and mergers of dark-matter clumps, into which gas fell, cooling through radiative processes to form dense clouds and eventually stars, there is much debate about the details (for a summary, see Silk and Mamon, 2012). In particular, the nature of dark matter remains mysterious: most researchers take it to be a collisionless non-relativistic fluid (cold dark matter or CDM) readily studied by simulations (for example, the influential Millennium simulation, Springel et al., 2005). However, alternative scenarios, where dark matter has exotic dynamical properties (Saxton and Ferreras, 2010; Schive et al., 2016), or is not really matter at all, but a modification of gravity (McGaugh, Lelli, and Schombert, 2016), have also been considered.

All this motivates the use of strong gravitational lensing over galaxy scales to study the mutual dynamics of dark matter, gas and stars. Several studies in recent years have done so (see, e.g., Koopmans et al., 2009; Leier, Ferreras, Saha, and Falco, 2011; Leier, Ferreras, and Saha, 2012; Leier, Ferreras, Saha, Charlot, et al., 2016; Bruderer et al., 2016) but it is desirable to enlarge the samples from tens of lensing galaxies to thousands. Doing so requires both finding more lenses and also modelling their mass distribution. Recent searches through the CFHT Lens Survey (CFHT LS; Heymans et al., 2012) using arc-finders (e.g., More, Cabanac, et al., 2012; Maturi, Mizera, and Seidel, 2014; Gavazzi et al., 2014; Sonnenfeld et al., 2017) by either machine learning methods (e.g., Paraficz et al., 2016; Lanusse et al., 2018) or visual inspection by citizen science volunteers through the SpaceWarps project (More, Verma, et al., 2016) have, between them, discovered an average of four lenses per square degree, so one can be optimistic about finding many thousands of lenses in the next generation of wide-field surveys, from ground-based surveys such as LSST in the optical window and SKA in radio, to space-based missions such as Euclid and WFIRST (Oguri and Marshall, 2010; Collett, 2015). The availability of the recently published year 1 result of the Dark Energy Survey (Drlica-Wagner et al., 2017), which covered 1800 deg^2, suggests that the number of lenses could grow by at least an order of magnitude within a very short time period.

The expected flood of new lens discoveries will need a similarly large modelling effort to reconstruct their mass distributions. Lens-modelling robots have started to be developed (Nightingale, Dye, and Massey, 2017; Hezaveh, Levasseur, and Marshall, 2017) but so far are able to handle only very clean systems. For typical lenses, human input is still needed. With that in mind Küng et al., 2015 developed a new modelling strategy, implemented as the SpaghettiLens[1] system. The idea is to collaborate with experienced members of the citizen

[1] `http://labs.spacewarps.org/spaghetti/`

science community who have already participated in lens discovery through SPACEWARPS, as well as several other projects involving astronomical data. The system was tested on a sample of simulated lenses, which were part of the training and testing set in SPACEWARPS.

This paper follows up that study by applying SPAGHETTILENS to candidates discovered through SPACEWARPS. We present results from the modelling of 58 of the 59 lens candidates reported by More, Verma, et al., 2016. Each lens candidate was modelled following a collaborative refinement process, where anyone interested could improve the analysis by modifying an existing model or creating a new one. Note the difference with respect to the main SPACEWARPS project, where volunteers from a group of $\gtrsim 10^4$ people make independent contributions. Each person is presented with a random selection of survey-patches and invited to (in effect) vote on each. The system estimates the skill level of each volunteer according to test-patches interspersed with the real data, and weights their votes accordingly (Marshall, Verma, et al., 2016). There is an active forum for volunteers, but since everyone is seeing different data samples with minimal overlap, the forum has little if any influence on the votes. In SPAGHETTILENS, the number of volunteers is significantly lower, but the level of interaction is higher. The resulting model represents a consensus among contributors, as to the best that could be achieved with the available data and software.

We emphasise that the interpretation of the results presented here is tentative, because the systems are lens candidates at this stage, not secure lenses. Moreover the candidate-lens redshifts have large uncertainties, while the candidate-source redshifts can only be guessed at present. Nevertheless it is interesting to explore the trends observed with the already available data, based on some 300 models created by eight volunteers for 58 candidate lenses found in the 150 deg^2 Canada-France Hawaii Telescope Legacy Survey (CFHT LS).

This paper is organized as follows. Section 4.2 introduces the candidate lenses, their models and the diagnostics applied to them. The following sections elaborate on the diagnostics. Image morphology diagnostics are explained in Section 4.3 and diagnostics based on the mass models are discussed in Section 4.4. Stellar masses are presented in Section 4.5, to compare stellar and lensing masses. Finally, Section 4.6 summarizes and tabulates the diagnostics in Table 4.1.

We include three appendices devoted to various technical issues relating to the modelling. The online supplement gives the results from all the modelled systems generated for all the lensing candidates.

4.2 The candidates and models

SPACEWARPS is a citizen science gravitational lens search (Marshall, Verma, et al., 2016). Its first run searched the CFHT LS, a survey carried out in five optical bands (u^*,g',r',i',z') covering a total area of 160 deg^2 divided up into four fields W1–W4. The MegaPrime camera, used for the survey, has a field of view of 1 deg^2, with 0.186″ pixels. The flux limit of the survey is $g' < 25.6$ AB (5σ) with a typical seeing FWHM $\sim 0.7''$ (Erben et al., 2013). The cutouts shown to the volunteers were colour composites of the g', r' and i'

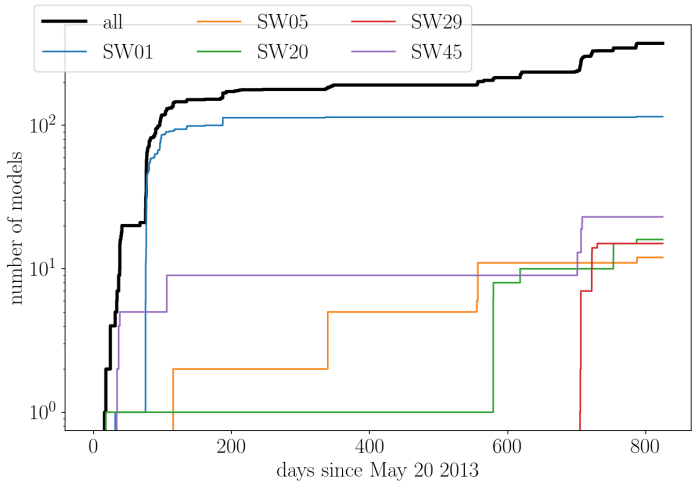

Figure 4.1: Number of models generated over time in days since the launch of SPAGHETTILENS; the black line shows all models, and the coloured lines show the five most active candidates. A total of 377 models were generated for 58 lens candidates, eight users contributed more than five models per person.

bands from randomly chosen regions. The programme resulted in 59 new lens candidates, of which 29 are considered high quality. Moreover, 82 previously known lens candidates were 'rediscovered'. The candidates have broadly similar redshifts ($0.2 < z < 1.0$), Einstein radii between 0.7 and 5″, and arc fluxes in g-band AB magnitudes between 22 and 26. These properties are similar to those found by previous robotic searches like ArcFinder and RingFinder (More, Verma, et al., 2016).

A first version of SPAGHETTILENS was launched in 2013 May, while the first run of SPACEWARPS was ongoing. Figure 4.1 shows the total number of models generated since launch for our lens candidates. A small number of volunteers started creating models of possible lens candidates from SPACEWARPS that were debated in the discussion forum. In the beginning of 2013 August (around day 70 since release), a modelling challenge for the candidate later to be identified as SW 01 was launched. A group of five volunteers presented their results in an online letter converging on a set of 30 models. In 2015 April (day 700), the first major version of SPAGHETTILENS was released. At the same time, the list of identified candidates was made available (as a preprint of More, Verma, et al., 2016). At this stage, the volunteers were asked to create models for all the lens candidates that were still missing. The work done for candidate SW 29 shows that the volunteers converged on a favourable model much faster, after 15 models, generated in 30 days. The total modelling effort resulted in a set of 377 SPAGHETTILENS models for all but one of the 59 SPACEWARPS lens candidates; candidate SW 39 was not modelled by any volunteer. Over its runtime, the system logged eight major contributors (defined as volunteers that generated, at least, five models).

In parallel, Küng et al. (2015) tested the system on simulated lenses and identified some

areas for improvement. In Section 4.8.1 we introduce fitting of the surface brightness profile of the source. This feature has not been included yet in SPAGHETTILENS, but we carried the analysis during post-processing for a few interesting cases. In Section 4.8.2 we show that fine-grained mass maps within the central region relieves a tendency in the earlier work for mass profiles to be too shallow. In Section 4.8.3 we consider the possibility of fitting a parametric lens model to the ensemble.

We characterise each model with seven diagnostics, grouped into three categories, whose purpose is to help identify the most likely cases of a gravitational lens, as well as flag the most interesting candidates for future follow-up observations. The diagnostics are as follows.

- First, we have diagnostics based on morphology. Section 4.3 and Figure 4.2 explain this diagnostic in more detail. We consider:
    1. Whether the images are unblended: Distinct, unblended images are an advantage in modelling, although not essential.
    2. Whether all images are discernible. The topography of an arrival-time surface, as encoded by a spaghetti diagram, may require more images than are visible, in which case the modeller has to insert conjectural image positions.
    3. Whether the lens is isolated.
    4. The image morphology concisely described: double or quads, further sub-categorized to indicate the elongation direction of the lensing mass.
- Secondly we have mass models, covered in Section 4.4. We assess the following points:
    5. Whether the mass map is reasonable (see Figure 4.5).
    6. Whether the arrival-time surface and synthetic image are plausible. In particular, an unsatisfactory model is flagged when additional images are implied in regions where they are not observed (see Figures 4.3, 4.4 and 4.6).
- Thirdly, whether the total implied lensing mass determined from the lens model is plausible, given the photometry of the lensing galaxy. In this work we define the lensing mass as the sum of all mass tiles in the model. These mass tiles reach out to typically twice the radius of the outermost image. Section 4.5 explains how we compare the lensing mass with the stellar mass. Galaxies may have haloes extending well beyond the mass maps in the models, so the calculated lensing mass is only a lower bound on the total galaxy mass. Hence, the lensing mass should be somewhere between the stellar mass (lower bound) and the total halo mass (upper bound). Extrapolation of the lens model to estimate the full virial mass may be possible (cf. Leier, Ferreras, and Saha, 2012), but is not attempted in this work.
    7. We then introduce a so-called halo index ($\mathscr{H}$), which quantifies how the lensing mass compares with these two constraints (see Figure 4.7).

4.3 Image morphology

The main input of a modeller to the process is a markup of the candidate lens system, which we call a spaghetti diagram. This is a sketch of the arrival-time surface from a point-like source, with proposed locations of maxima, minima and saddle points, and an implied time-ordering of the images. Such information encodes a starting proposal for the mass distribution. A spaghetti diagram is thus a completely abstract construction, and moreover it refers to a simplified system with a point source. However, spaghetti diagrams are intuitive because they tend to resemble the form of lensed arcs (see Figure 3 of Ferreras, Saha, and Burles, 2008), and of course they are simple to draw, and easy to vary and refine in an open collaborative environment. This makes them very practical for non-professional lens enthusiasts in the citizen science community. Details and tests are given in Küng et al. (2015).

We now discuss the diagnostics that can be taken from the process of drawing the spaghetti diagram, even before detailed mass-modelling takes place. Figure 4.2 shows nine examples, each consisting of a cutout of the SPACEWARPS image of a lens candidate, marked up with a spaghetti diagram. The volunteers are initially presented a square image with side $82''$ (440 pixels) in full size, but they have the ability to zoom in individually. The cutouts presented in Figures 4.2 to 4.5 are rescaled during post-processing, relative to the outermost image.

All the examples shown in Figure 4.2 identify five locations: the centre of the main lensing galaxy, which is also a maximum of the arrival time surface (red dots); two minima (blue dots); and two saddle points (green dots and also self-intersections of the curves). Only two (SW 05 and SW 42) of the nine systems, however, have five distinct features in plausible locations. In the other seven examples, an arc is interpreted as a blend of three or four images. This defines the 'unblended images' diagnostic. Note that this characterisation could be different if the spaghetti diagram were different. For example, SW 28 has also been modelled with the arc on the right interpreted as a single image, rather than as three images as shown in the figure; for such a model, the 'unblended images' diagnostic would be true.

The second diagnostic checks whether all images are visible. For example, we see in SW 58 at the top left of Figure 4.2 that an image at the second minimum is conjectural and does not correspond to any visible feature.

The third diagnostic tests whether the lens is isolated, or whether other galaxies could contribute to the lensing, based on visual inspection of the field. For this, we do not consider stars or other clearly foreground objects. Additional galaxies contributing to the lensing mass can be marked by the volunteer alongside the spaghetti diagrams. An example can be seen as the grey dot and circle in the cutout with SW 57 at the top right of Figure 4.2. Objects marked in this way are modelled as point masses. Other possible contributors to lensing are galaxies or groups that are not in the immediate vicinity of the lensed images, yet massive enough to exert an influence. These are accounted for by allowing a constant but adjustable external shear.

We remark that the lack of expected lensed images, or the presence of blended images or perturbing galaxies, does not imply that a given candidate is unlikely to be a lens. This means, rather, that the models are more uncertain and perhaps could be more easily improved by trying further variations in the markup.

The fourth diagnostic is based on the fact that the arrangement of lensed images of a point-like source through a non-circular gravitational lens depends on the location of the source relative to the long and short axes of the lens. This dependence is quite robust and independent of many other details of the lensing mass distribution. Sources close to being dead-centre behind a lens tend to produce quads; sources at larger transverse distance tend to produce doubles. We denote these as Q and D, respectively, and add a prefix to the Q systems as follows: we write LQ if the source is inferred as displaced along the long axis of the lens, SQ if displaced along the short axis, IQ if inclined to both axes, and CQ if only very little or no displacement is evident. Although the unlensed source and its location are obviously not seen, the LQ, SQ, IQ and CQ cases correspond to easily seen image morphologies (see, e.g., Saha and Williams, 2003).

- The simplest is the LQ case: this creates a saddle point and two minima in an arc, with the second saddle point on the other side of the lensing galaxy, closer to the galaxy than the arc. SW 58 and SW 28 in the upper row of Figure 4.2 are typical examples of LQ. If the source were moved outwards along the short axis, the minimum-saddle-minimum set would merge into a single minimum, leaving a D system; the transition is known as a cusp catastrophe.

- The middle row of Figure 4.2 shows three IQ systems: SW 05, SW 42 and SW 19. This type has a characteristic asymmetry, often with two images close together. If the source were moved outwards, the minimum-saddle pair would merge and mutually cancel, leaving again a D system. This transition is known as a fold catastrophe.

- The lower row of Figure 4.2 shows three SQ systems: SW 09, SW 29 and SW 02. The failed model, SW 57, at top right may also belong to this category. Here, the images have a fairly symmetric arrangement with an arc and a counter-image on the other side, but the spaghetti diagram is completely asymmetric. If the source were moved outwards along the long axis, the saddle-minimum-saddle set would merge into a single saddle – another form of cusp catastrophe. SQ can be visually distinguished from LQ by the relative distances of the arc and the counter-image. For SQ, the arc is closer, and for LQ the counter-image is closer.

CQ systems are often called ‘cross’ or ‘Einstein-cross’ systems; IQ systems are sometimes called ‘folds’, with ‘cusp’ commonly used for both SQ and LQ. The labels ‘short-axis quad’ and so on are not standard in the literature, but the morphological classification they express is familiar to experienced modellers. Hence, they can be useful to researchers wishing to apply other modelling methods to the same systems.

4.4 Mass models

Once a spaghetti diagram has been drawn on a web browser, it is forwarded to a server-side numerical framework, which searches for mass maps consistent with the image locations, parities and time ordering, given by the modeller. The mass maps are made up of mass tiles and are free-form, but are required to be concentrated around the identified lens centre (see Coles, Read, and Saha, 2014, for the precise formulation of the search problem). The modeller can also set various options for the search, such as the number of mass tiles and the extent of the mass map; all options have defaults. Typically, there are ~ 500 mass tiles arranged in a disc, centred on the lensing galaxy and extending to twice the radius of the outermost image. By default, the mass distributed is required to have a 180°-rotation symmetry, but this option can be unset. Assuming mass distributions can be found, which in practice is usually the case, a statistical ensemble of 200 two-dimensional mass maps is returned. From each mass map, further quantities such as lens potentials or enclosed masses can be derived. Thus, there are ensembles of 200 values for the surface density at any point, for the enclosed mass within a given radius and so on. In this paper, we present the averages and ranges of different quantities, but other quantities such as 90 % confidence ranges could also be computed. The whole ensemble of mass maps, along with derived quantities and uncertainties, makes up one SPAGHETTILENS model.

The mass will naturally depend on the lens and source redshifts, which are unknown when a lens candidate is first identified. However, this is not a problem, because a model can be trivially rescaled to use better redshift values, as they become available. The mass normalisation of the models is proportional, through the angular critical density, to the factor $d_L\, d_S\, d_{LS}^{-1}$, where d_L, d_S and d_{LS} are the usual angular-diameter distances. In the redshift ranges typical of galaxy lensing, the normalisation factor is roughly proportional to the lens redshift, and weakly dependent on the source redshift. This work applies photometric redshifts from the CFHT LS pipeline (Coupon et al., 2009) to the candidate lensing galaxies; the values range from $z = 0.2$ to 1 (see Table 4.1). The source redshifts are assumed as $z = 2$, unless an unambiguous photometric redshift is available. The lens redshifts entail rather big uncertainties, up to a few tens of percent (see Fig. 5 in Coupon et al., 2009). The lensing masses would be uncertain at the same level. On the other hand, the lensing masses in the sample range from $10^{11}\,\mathrm{M}_\odot$ to $10^{13}\,\mathrm{M}_\odot$; in comparison, the redshift uncertainty is not so important in this preliminary analysis.

The ensemble of mass maps can be post-processed in many different ways. Four different graphical quantities are particularly useful.

Figure 4.3 shows the arrival-time surfaces corresponding to the spaghetti diagrams of Figure 4.2. The arrival-time contours look like machine-made elaborations of the input spaghetti diagrams. If the saddle-point contours in the arrival time are qualitatively the same as the curves in the spaghetti diagram (the detailed shape of the spaghetti curves is unimportant), it immediately suggests a successful model. On the other hand, if the arrival-time surface has unexpected minima or saddle points, and especially if the unexpected features are far from identified lens images, that signals an improbable model. Figure 4.4

shows what we call synthetic images, meaning reconstructions of the extended lensed features by fitting for a source. These were generated by a new method, explained in Section 4.8.1, implemented during the offline post-processing after the modelling process was complete. The synthetic images provided by SPAGHETTILENS during the collaborative modelling and discussion were more crude; those are included in the online supplement.

The arrival-time surface and synthetic image are summarized by one diagnostic, the most important of all: are the lensed features satisfactorily reproduced? This diagnostic remains a judgment call by modellers. A useful quantitative criterion for whether the synthetic image is consistent with the data would need to allow for PSF dependence and unmodelled substructure – otherwise all models would be summarily rejected, something left for a future implementation in SPAGHETTILENS.

Figure 4.5 shows the projected mass maps of the sample. In fact, this figure only shows the ensemble-average mass maps, and not the variation within the ensemble, from which uncertainties can be inferred. The same applies to the arrival-time surfaces and synthetic images in the previous two figures. The uncertainties will be shown in a concise form in Figure 4.6. Figure 4.5 makes evident the tiled nature of the mass model. The tiles can be smoothed over by interpolation, and this was done in the mass maps during the modelling process, available in the online version. It is interesting, however, to note the tiling artefacts, if only as a reminder that the substructure in the mass distribution is very uncertain, even if some integrated quantities are well constrained. How the free-form mass maps relate to parametrized lens models is discussed in Section 4.8.3. Note that although the mass distribution can have discontinuous jumps, the lens equation and arrival-time surface are continuous.

Figure 4.6 shows the enclosed-mass profiles, expressed as the average convergence, κ, within circles of a given projected radius. Uncertainties are included (see the figure caption for details). Section 4.8.2 describes the improvements made since our earlier work (Küng et al., 2015), to allow for steeper profiles in the inner regions. The enclosed mass is typically best constrained at the notional Einstein radius, becoming more uncertain at larger and smaller radii.

The mass maps and mass profiles are the basis of a further diagnostic: are the mass distributions plausible? This is also a judgment call made by modellers, but it showed to be a powerful diagnostic, summarizing three aspects. The overall shape is forced to be 180°-rotation symmetric, usually a plausible assumption, but volunteers can deactivate this constraint. The profile slope turned out to be a good indicator of plausible models, as can seen by contrasting the model for SW 57 with the rest of the sample: The missing core in Figure 4.5 and the flat profile in Figure 4.6 disqualify this model. The clumpiness of the mass map is another useful indicator. Flat profile slopes can often be identified directly in the mass map, where the mass tiles form a checkerboard pattern.

More experienced volunteers applied these diagnostics already during the process of creating models as a criteria of a successful model, the evaluation presented in this work however was generated by the authors during post-processing.

4.5 Stellar and halo mass estimates

The stellar masses of the lens galaxies are derived by a comparison of the photometric data with stellar M/L estimates from population synthesis models. In principle, a detailed analysis of the spectral energy distribution is needed to derive accurate stellar masses (e.g., Gallazzi and Bell, 2009; Taylor et al., 2011). However, at the redshifts probed, the photometric data mainly constrain the information-rich 4000 Å break region, whose strength depends sensitively on age and metallicity, thereby providing a strong constraint on the stellar M/L. Hence, estimates to within ~ 0.3 dex in $\log(M_{\rm stel}/\mathrm{M}_\odot)$ can be derived with a single colour, preferably tracing a rest-frame colour similar to $U-V$ (see Figure 1 of Ferreras, Saha, and Burles, 2008), assuming a universal initial mass function (IMF). There is evidence from detailed absorption line strength analysis that massive galaxies can feature a non-standard IMF (e.g., Ferreras, La Barbera, et al., 2013). However, these variations, towards a bottom-heavy distribution, are typically found in the cores of massive early-type galaxies (La Barbera et al., 2016). The effect of these variations on the stellar M/L of lensing systems is still rather controversial (Smith, Lucey, and Conroy, 2015; Leier, Ferreras, Saha, Charlot, et al., 2016).

In this paper, we further simplify the analysis by assuming a relationship between the apparent total magnitude and stellar mass, at the redshift of the lens. For typical stellar-population parameters, the variation of this relation is at most $\Delta \log M_{\rm stel} \sim 1$ dex. A further potential systematic can arise from contamination of the light of the lensing galaxy by the lensed background source. Reducing or eliminating the latter would require detailed fitting of light distributions for each candidate (see Leier, Ferreras, Saha, and Falco, 2011), which we have not yet attempted. Nonetheless, because the lensing masses range over two orders of magnitude, it is still interesting to compare them with rough estimates of stellar mass.

We make use of the Bruzual and Charlot (2003) models to derive two functional forms of the stellar mass with respect to the i'-band magnitudes. The models have solar metallicity, with a Chabrier IMF, and assume two different age trends: a 'young' model, with a constant 500 Myr age at all redshifts, and an 'old' model where the age is the oldest one possible at each redshift, adopting a standard ΛCDM model with $H_0 = 70\,\mathrm{km\,s^{-1}\,Mpc^{-1}}$ and $\Omega_m = 0.3$.

Figure 4.7 shows a comparison of stellar and lensing mass in our sample. The comparatively large span of the error bars in stellar mass (horizontal axis) shows the range between the masses derived using the two age trends, respectively, and lies between 0.4 and 0.8 dex. It will be improved in future work by the use of available optical and NIR magnitudes to derive more accurate constraints on the stellar populations. In addition, we also derive halo masses for the lenses using an abundance-matching formula. This technique matches the distribution function of observed stellar mass in galaxies with that of dark-halo masses from N-body simulations, to define a simple relation between stellar mass and halo mass. We emphasise that a halo mass from abundance matching should be considered an 'average' estimate, and a significant scatter can be expected as galaxies with the same stellar mass can be found in different environments. We refer the reader to Leier, Ferreras, and Saha, 2012 for an assessment of the effect of abundance matching on the derivation of dark matter halo

properties in lensing galaxies. We follow the prescription of Moster et al. (2010), namely:

$$\frac{M_{\rm stel}}{M_{\rm halo}} = \frac{2C_0}{(M_{\rm halo}/M_1)^{-\beta} + (M_{\rm halo}/M_1)^{\gamma}} \tag{4.1}$$

$$C_0 = 0.02820, \qquad M_1 = 10^{11.884}\,{\rm M}_\odot$$
$$\beta = 1.057, \qquad \gamma = 0.556.$$

Figure 4.7 may be compared with Figure 4 in More, Jahnke, et al., 2011. The comparison of lensing and stellar mass produces the last of our model diagnostics, defined as a halo-matching index:

$$\mathscr{H} \equiv \frac{\ln(M/M_{\rm stel})}{\ln(M_{\rm halo}/M_{\rm stel})} \tag{4.2}$$

that relates the observed lensing to stellar mass, with the global ratio expected if the host halo corresponds to the average value derived by abundance matching. Several cases for $\mathscr{H}$ can be considered:

- $\mathscr{H} < 0$ is unphysical because $M < M_{\rm stel}$.
- $\mathscr{H} = 0$ means the stellar mass exactly accounts for the lensing mass (i.e.no dark matter affects the lensing model).
- $0 < \mathscr{H} < 1$ is the typical situation, where the lens includes stars and dark matter, but not the full halo.
- $\mathscr{H} = 1$ means that the lens consists of the entire halo.
- $\mathscr{H} > 1$ is in tension with abundance matching, because the lensing mass exceeds the expected halo mass.

The halo-matching index expresses whether the lensing mass is plausible given the flux received from the candidate lensing galaxy.

Figure 4.7 and Table 4.1 show that most of the candidates have stellar and lensing masses typical of massive ellipticals[2]. SW 05 is one of the most massive of all the candidates, corresponding to a galaxy-group mass scale. It is a particularly attractive system for follow-up observations at higher resolution, as it is a large system with clear multiple-image features. Modelling leaves little doubt that it is a lens. SW 04 seems to be even more massive, but the diagnostics leave some doubts about the validity of this model. The two lowest mass systems, SW 19 and SW 42, are important if they are indeed lenses, as they would be low-mass lenses dominated by dark matter. All the modelled systems have reasonable stellar-mass fractions, except for two cases where the stellar-mass fraction is too low ($\mathscr{H} > 1$): these are SW 42 and SW 57. In the case of SW 57, the model has poor diagnostics and should be discarded. The model for SW 42, on the other hand, is quite convincing – except for the high halo-matching index. If SW 42 turned out not to be a lens, that would support the halo-matching index as an effective criterion to discriminate models.

[2]The mass values themselves are given in the online version of Table 4.1

4.6 Summary and conclusions

We report on a first set of mass distributions and follow-up diagnostics for the SPACEWARPS lens candidates created with a novel approach that aims to be scalable by *orders of magnitude* to prepare for the many thousands of lenses the next generation of wide-field surveys will yield (e.g., Euclid and WFIRST).

Over the past few years, the way of discovering lenses has changed with the introduction of machine learning and citizen science methods, combined with the coverage of large areas of the sky by modern surveys. The way lensing mass models are constructed also needs to change, in order to be prepared for the increasing influx of lens candidates. The work in this paper represents a hybrid approach between the classical style, where a small team of experts invests many hours into the creation of a single model, and a citizen science project, where a crowd of amateur volunteers makes independent contributions. The authors of this paper are a collaboration of professionals and experienced citizen science volunteers, aiming to create early-stage lens models as soon as a lens candidate is found.

To assist volunteers in constraining lensing models, we introduce a set of diagnostics that helps us to assess the validity of the models. At a later stage, we encourage modellers to apply those diagnostics as feedback on the plausibility of their assumptions, and to suggest additional diagnostics.

The diagnostics (i)–(iv) (see Section 4.2) turned out to be useful measures of the difficulty in modelling a system, but they did not constitute necessary conditions for a promising model. They can help select systems to introduce novice volunteers to the modelling process. In contrast, diagnostics (v) and (vi) can be considered as necessary criteria for a good model. Volunteers employed those ones to evaluate their models, and turned out to be easy enough to grasp by new volunteers. The halo-matching index diagnostic (vii, $\mathscr{H}$) is an interesting criterion that might be useful for the modellers, but needs further investigation.

Table 4.1 is a summary of our results. It characterizes each modelled system with seven diagnostics, indicating (a) the image morphology and how clear or indistinct it is, (b) whether the mass map and synthetic lensed image appear to be plausible, and (c) how the model mass compares with the estimated stellar and full-halo masses. Missing entries are due unavailable imaging data, whereas missing rows are due to models that were not created for this particular candidate.

The trend in Figure 4.7, where higher-mass galaxies get progressively more dark-matter dominated, is expected (see, e.g., Ferreras, Saha, and Williams, 2005), as is the span of about one order of magnitude for the stellar mass and the two orders of magnitude in lensing mass. With future data, it will be interesting to compare the enclosed stellar and lensing mass as a function of radius, going from the star-dominated inner regions to the outer dark haloes. Leier, Ferreras, Saha, and Falco (2011) illustrate this behaviour in their Figure 5, but the present sample could go an order of magnitude higher in mass.

The quick creation of many models for the SPACEWARPS candidates successfully showed that a subset of citizen scientists is interested in being involved in more challenging tasks that

take some time to learn. The next step involves recruiting more lensing enthusiasts, as soon as the next round of SPACEWARPS is started. In the meantime, the improvements shown in the appendix will be integrated in the standard version of SPAGHETTILENS. Photometric fitting could also be integrated into SPAGHETTILENS. This would allow experienced citizen scientists to generate photometric redshifts and stellar masses, and thus generate preliminary dark-matter maps as soon as a lens candidate is identified.

4.7 Acknowledgements

This work was supported by the University of Zurich Candoc reseach grant (Forschungskredit Candoc; FK-14-081 and FK-15-087).

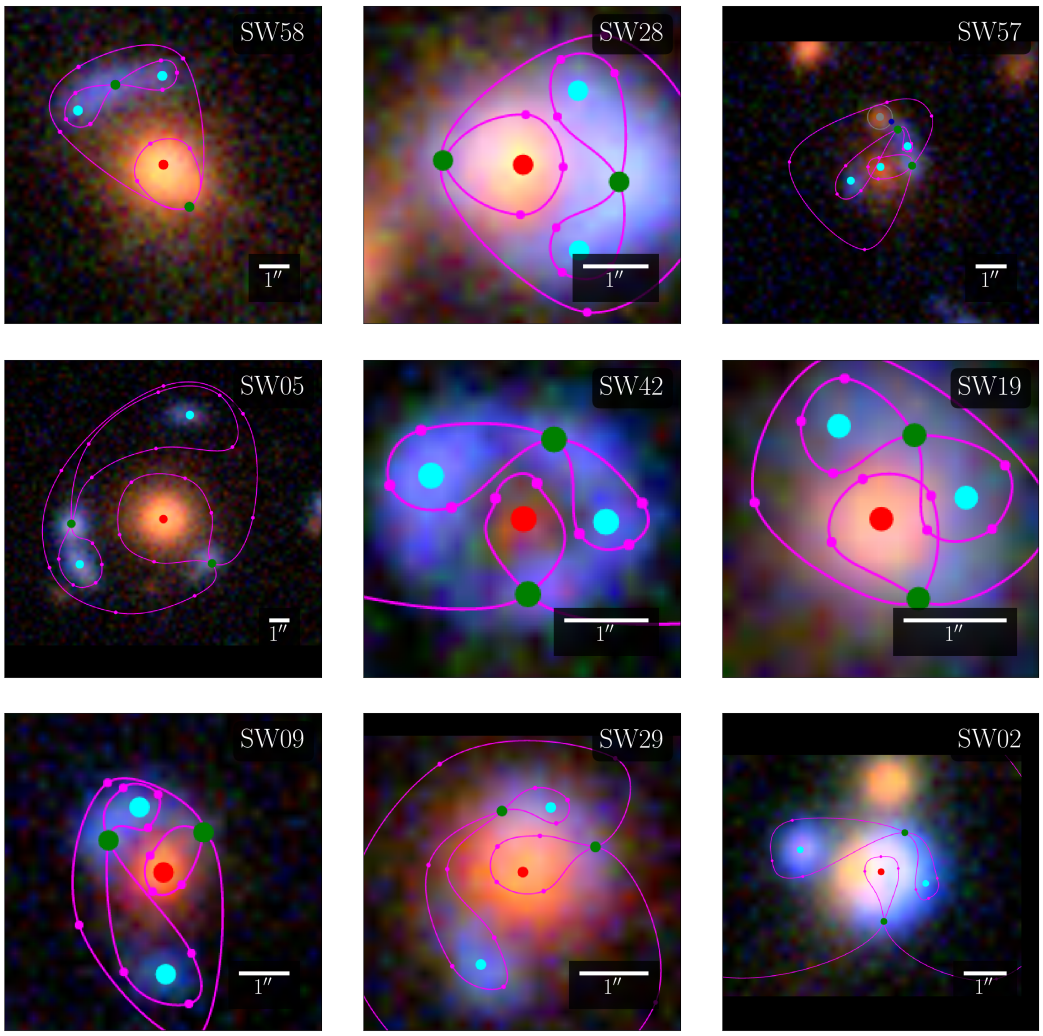

Figure 4.2: Nine of the lens candidates marked up with spaghetti diagrams. Red, blue and green dots are proposed locations for maxima, minima and saddle points of the arrival time respectively. The curves help guide the placement of the dots, but their precise appearance has no significance. These images are screenshots from the SPAGHETTILENS user interface, which applies interpolation to background images. The scaling is adjusted to fit the other images. This selection includes the best-modelled systems, but also one case (SW 57 at upper right) of unsuccessful modelling. Since the modelling process is collaborative among the volunteers, with anyone welcome to contribute new models or modify existing ones, there are variant spaghetti diagrams for all the modelled systems. The online supplement displays all the models presented for discussion during this work.

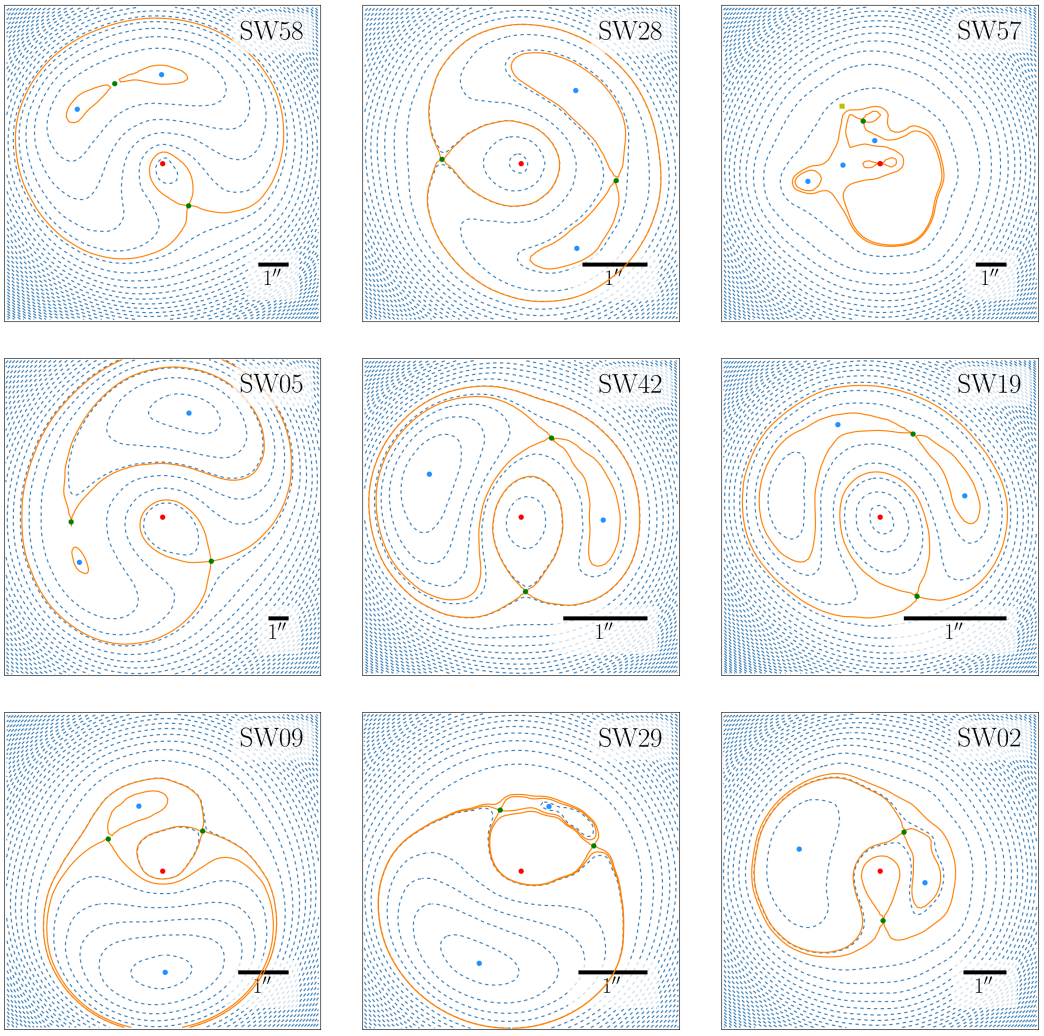

Figure 4.3: Arrival-time surfaces for models of the systems from Figure 4.2. The registration differs slightly from Figure 4.2, but the coloured dots represent exactly the sky positions specified in the earlier figure. The orange contours only qualitatively resemble the earlier pink curves, as they are now precise saddle-point contours from lens models.

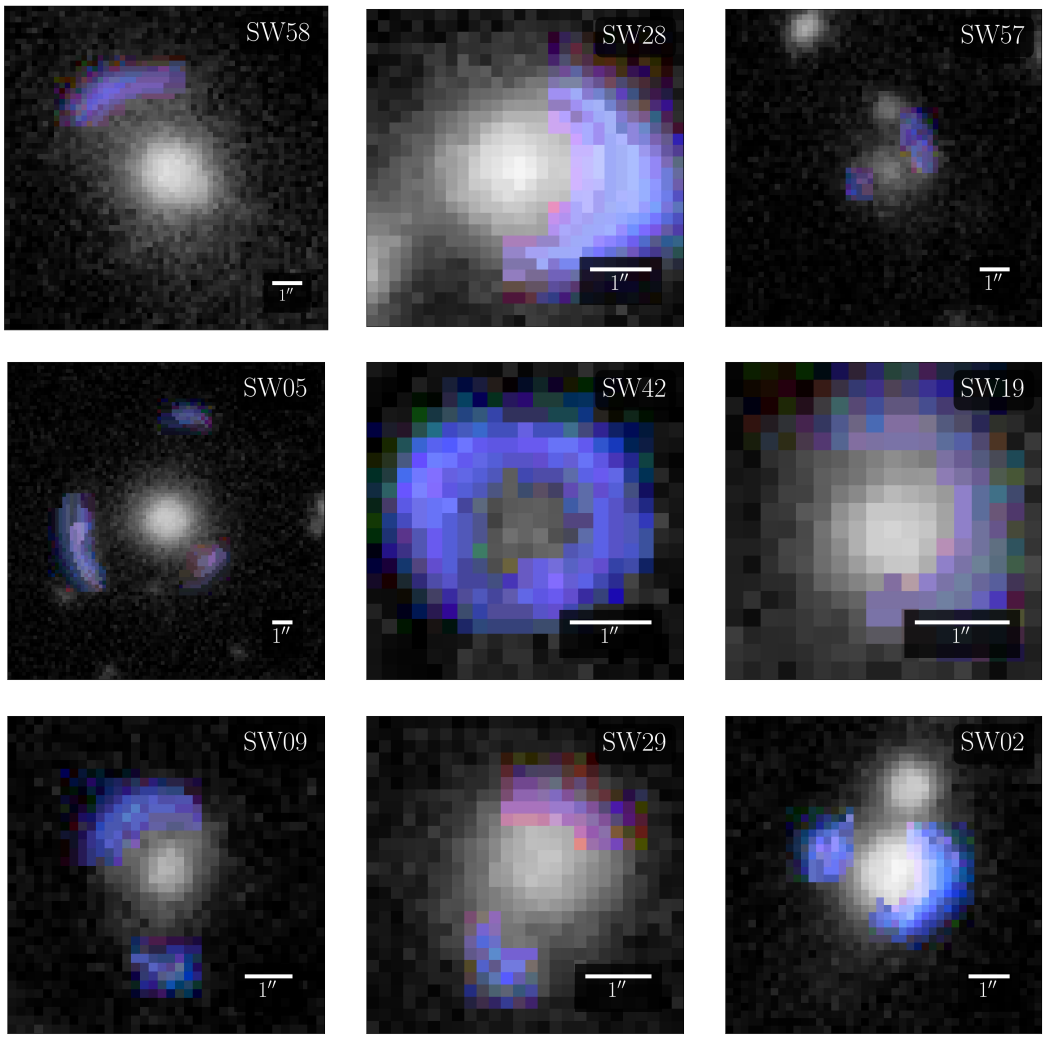

Figure 4.4: Synthetic images of the systems from Figure 4.2, derived from the lens models. The reconstructed lensed features keep the SPACEWARPS false-colour scheme from Figure 4.2. The rest has been changed to black and white.

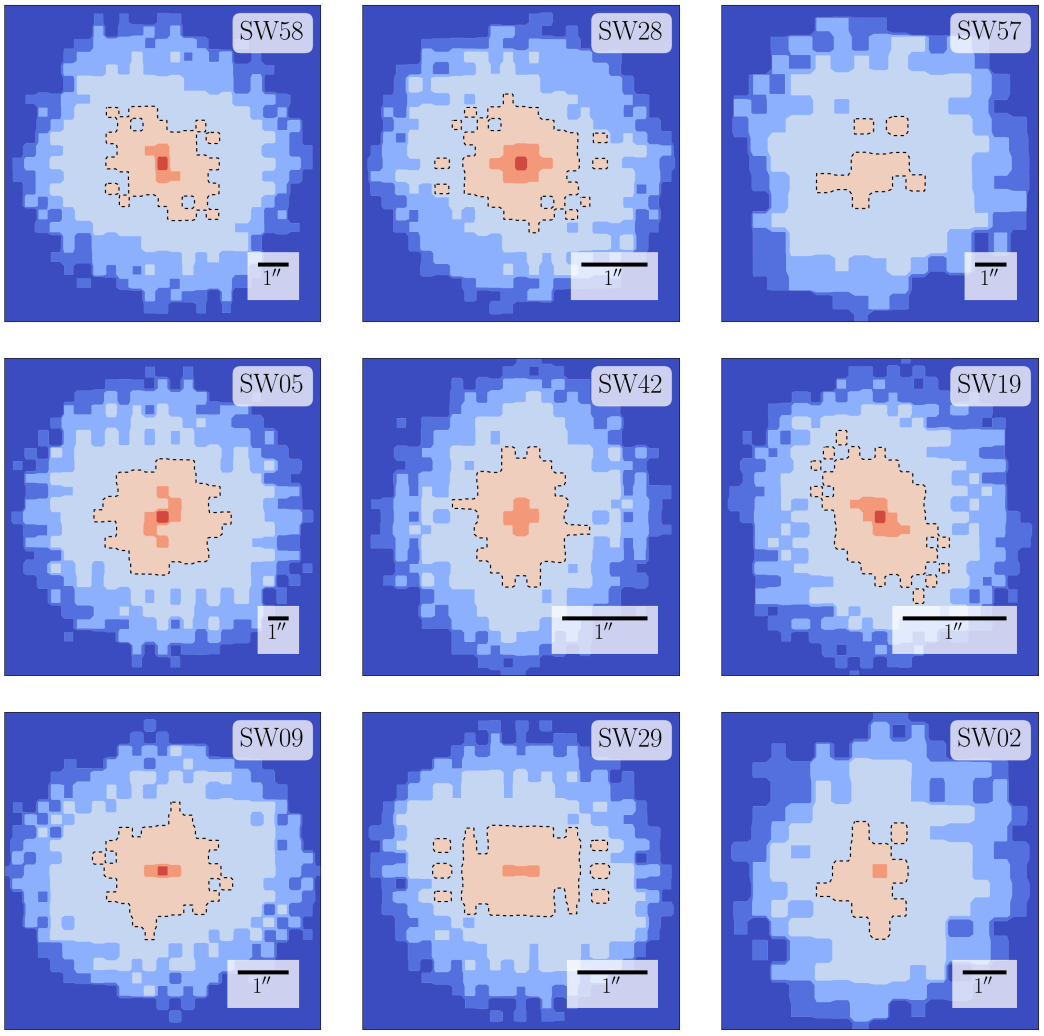

Figure 4.5: Ensemble-average mass distribution κ for which the results Figures 4.3 and 4.4 were derived. The dashed curves denote $\kappa = 1$. Most of the mass maps have a 180°-rotation symmetry, which is imposed by default. For SW 02 and SW 57, where the lensing mass is clearly asymmetric, the modeller chose to turn off the symmetry.

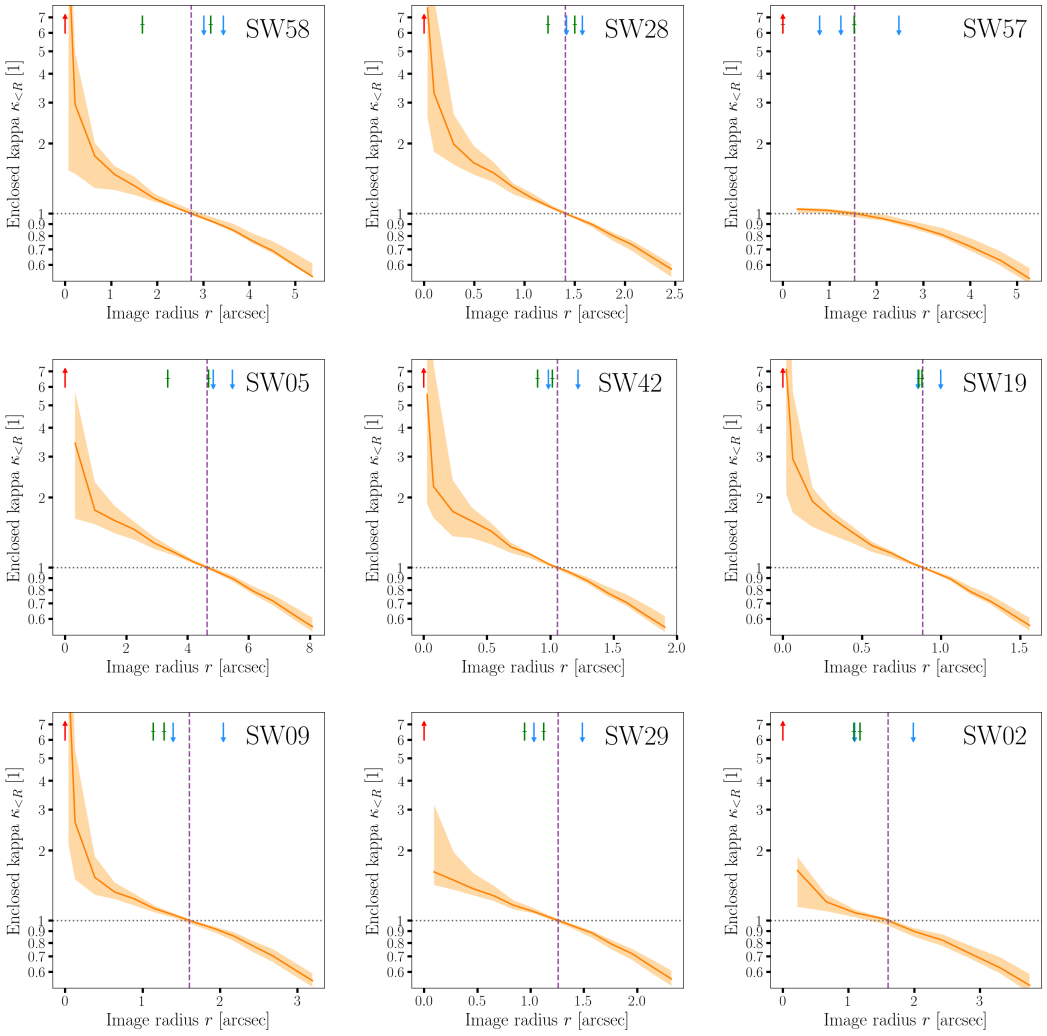

Figure 4.6: Cumulative circular-averages of the mass maps from Figure 4.5, with uncertainties. More precisely, we show the enclosed mass within a given projected radius, expressed as the mean κ with a given number of arcsec from the centre of the lensing galaxy. The orange bands refer to the full ensemble of mass maps for the models, while the red curves show the ensemble averages. The dashed vertical line indicates the notional Einstein radius, or where the mean enclosed κ is unity. The short vertical arrows mark the positions of the images (maxima, saddle points and minima).

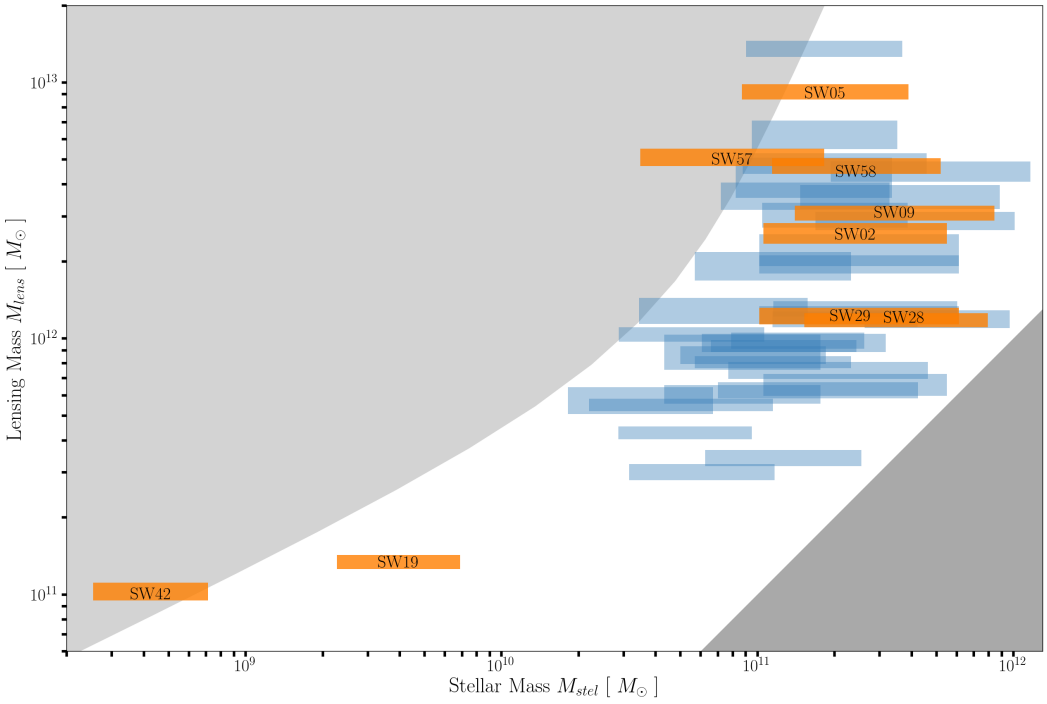

Figure 4.7: Total mass in the model against the estimated stellar mass, alongside the values for the whole sample. (The labelled orange bars are the systems shown in detail in Figures 4.2 to 4.6.) The horizontal extent of each bar indicates the extreme cases of a young (0.5 Gyr-old) stellar population and the oldest possible population at the given redshift. The vertical extent indicates the spread of masses in the lens-model ensemble. The lower-right shaded region is unphysical according to the stellar-population models, because it gives $M < M_{\rm stel}$. The upper-left shaded region is unphysical according to abundance matching (see Section 4.5) because it gives $M > M_{\rm halo}$. That is to say, the unshaded region is $0 < \mathscr{H} < 1$.

Table 4.1: Diagnostics of a selected model for each SPACEWARPS candidate (see Section 4.6).

SWID	ZooID	CFHT LS Name	$z_{\rm lens}$	unblended images	all images discernible	isolated lens	image morpho-logy	synthetic image reasonable	mass map reasonable	$\log_{10}\frac{M_{\rm stel}}{M_\odot}$	$\log_{10}\frac{M_{\rm lens}}{M_\odot}$	halo-matching index $\mathscr{H}$
SW 01	ASW 000 4dv8	J022409.5−105807	–	✗	✗	✗	LQ	✓	✓	–	–	–
SW 02	ASW 000 619d	J140522.2+574333	0.7	✗	✓	✗	SQ	✓	✓	11.4	12.4	0.47
SW 03	ASW 000 6mea	J142603.2+511421	–	✓	✗	✗	D	✓	✓	–	–	–
SW 04	ASW 000 9cjs	J142934.2+562541	0.5	✓	✗	✗	D	✗	✓	11.3	13.1	0.93
SW 05	ASW 000 7k4r	J143454.4+522850	0.58	✓	✓	✓	IQ	✓	✓	11.3	13.0	0.83
SW 06	ASW 000 8swn	J143627.9+563832	0.5	✗	✓	✓	SQ	✓	✗	11.1	11.9	0.46
SW 07	ASW 000 7e08	J220256.8+023432	–	✓	✓	✗	D	✓	✓	–	–	–
SW 08	ASW 000 99ed	J020648.0−065639	0.8	✓	✓	✗	D	✓	✓	11.4	12.3	0.40
SW 09	ASW 000 2asp	J020832.1−043315	1.0	✗	✓	✓	SQ	✓	✓	11.5	12.5	0.40
SW 10	ASW 000 2bmc	J020848.2−042427	0.8	✓	✗	✓	D	✗	✗	11.3	11.9	0.29
SW 11	ASW 000 2qtn	J020849.8−050429	0.8	✗	✓	✗	LQ	✓	✓	11.2	11.8	0.29
SW 12	ASW 000 3wsu	J022406.1−062846	0.4	✓	✓	✗	D	✓	✓	10.8	11.5	0.44
SW 13	ASW 000 47ae	J022805.6−051733	0.4	✗	✗	✗	SQ	✗	✗	11.1	11.9	0.46
SW 14	ASW 000 4xjk	J023123.2−082535	–	✗	✗	✗	SQ	✗	✓	–	–	–
SW 15	ASW 000 4nan	J084841.0−045237	0.3	✗	✓	✗	CQ	✓	✓	10.7	11.6	0.59
SW 16	ASW 000 9bp2	J140030.2+574437	0.4	✗	✗	✓	D	✗	✓	11.3	12.1	0.34
SW 17	ASW 000 5rnb	J140622.9+520942	0.7	✓	✗	✗	D	✗	✓	11.1	12.0	0.44
SW 18	ASW 000 7hu2	J143658.1+533807	0.7	✓	✗	✓	D	✗	✗	11.4	12.1	0.31
SW 19	ASW 000 1ld7	J020642.0−095157	0.2	✗	✓	✗	IQ	✗	✓	9.6	11.1	0.84
SW 20	ASW 000 2dx7	J021221.1−105251	0.3	✓	✓	✓	D	✗	✓	11.2	12.0	0.44
SW 21	ASW 000 4m3x	J022533.3−053204	0.5	✓	✗	✗	D	✗	✓	11.1	11.5	0.24
SW 22	ASW 000 9ab8	J022716.4−105602	0.4	✗	✗	✗	D	✗	✓	11.7	12.1	0.15
SW 23	ASW 000 3r61	J023008.6−054038	0.6	✗	✓	✗	LQ	✗	✓	11.2	12.6	0.71

SW 24	ASW 000 50sk	J023315.2−042243	0.7	✗	✓	✗	D	✓	✓	11.4	11.8	0.19
SW 25	ASW 000 07mq	J090308.2−043252	–	✗	✗	✓	D	✗	✓	–	–	–
SW 26	ASW 000 5ma2	J135755.8+571722	0.8	✓	✗	✓	D	✗	✗	11.4	12.3	0.43
SW 27	ASW 000 6jh5	J141432.9+534004	0.7	✗	✗	✗	LQ	✗	✓	10.7	11.7	0.67
SW 28	ASW 000 7xrs	J143055.9+572431	0.7	✗	✓	✗	LQ	✓	✓	11.5	12.1	0.23
SW 29	ASW 000 8qsm	J143838.1+572647	0.8	✗	✓	✓	SQ	✓	✓	11.4	12.1	0.31
SW 30	ASW 000 2p8y	J021057.9−084450	–	✓	✗	✗	IQ	✗	✗	–	–	–
SW 31	ASW 000 21r0	J021514.6−092440	0.7	✗	✓	✗	LQ	✓	✓	11.3	12.7	0.65
SW 32	ASW 000 4iye	J022359.8−083651	–	✗	✓	✗	IQ	✓	✓	–	–	–
SW 33	ASW 000 3s0m	J022745.2−062518	0.6	✓	✓	✗	D	✗	✓	10.9	12.1	0.77
SW 34	ASW 000 51ld	J023453.5−093032	0.5	✗	✗	✓	D	✗	✓	10.9	11.9	0.59
SW 35	ASW 000 4wgd	J084833.2−044051	0.8	✗	✓	✗	LQ	✓	✓	11.4	12.1	0.32
SW 36	ASW 000 096t	J090248.4−010232	0.4	✓	✓	✗	D	✗	✓	11.0	12.0	0.56
SW 37	ASW 000 86xq	J143100.2+564603	–	✗	✗	✓	SQ	✓	✓	–	–	–
SW 38	ASW 000 9cp0	J143353.6+542310	0.8	✗	✓	✓	LQ	✓	✓	11.6	12.6	0.42
SW 39	ASW 000 5qiz	J220215.2+012124	–	–	–	–	–	–	–	–	–	–
SW 40	ASW 000 8wmr	J221306.1+014708	–	✗	✓	✓	SQ	✓	✓	–	–	–
SW 41	ASW 000 8xbu	J221519.7+005758	0.4	✓	✗	✓	IQ	✓	✓	10.5	11.8	0.80
SW 42	ASW 000 96rm	J221716.5+015826	0.1	✓	✓	✗	IQ	✓	✓	8.6	11.0	1.04
SW 43	ASW 000 1c3j	J020810.7−040220	1.0	✗	✗	✗	SQ	✗	✓	11.6	12.4	0.34
SW 44	ASW 000 2k40	J021021.5−093415	0.4	✓	✓	✗	LQ	✓	✓	11.3	12.8	0.76
SW 45	ASW 000 24id	J021225.2−085211	0.8	✗	✓	✓	CQ	✗	✓	11.7	12.6	0.37
SW 46	ASW 000 24q6	J021317.6−084819	0.5	✓	✓	✗	D	✓	✓	10.9	11.8	0.49
SW 47	ASW 000 3r6c	J022843.0−063316	0.5	✓	✗	✓	D	✗	✓	11.2	12.6	0.71
SW 48	ASW 000 0g95	J090219.0−053923	–	✓	✗	✓	D	✓	✓	–	–	–
SW 49	ASW 000 07ls	J090319.4−040146	–	✗	✓	✓	D	✓	✓	–	–	–
SW 50	ASW 000 08a0	J090333.2−005829	–	✓	✗	✓	LQ	✓	✓	–	–	–
SW 51	ASW 000 6e0o	J135724.8+561614	–	✓	✓	✗	D	✗	✓	–	–	–
SW 52	ASW 000 6a07	J140027.9+541028	–	✓	✗	✓	SQ	✓	✓	–	–	–
SW 53	ASW 000 70vl	J141518.9+513915	0.4	✓	✗	✓	D	✗	✓	11.3	12.5	0.56

SW 54	ASW 000 7sez	J142620.8+561356	0.5	✗	✓	✗	CQ	✓	✓	11.1	12.3	0.68
SW 55	ASW 000 7t5y	J142652.8+560001	–	✗	✓	✓	CQ	✓	✗	–	–	–
SW 56	ASW 000 7pga	J142843.5+543713	0.4	✓	✗	✓	D	✗	✗	10.7	12.0	0.80
SW 57	ASW 000 8pag	J143631.5+571131	0.7	✗	✓	✗	SQ	✗	✗	10.9	12.7	1.08
SW 58	ASW 000 7iwp	J143651.6+530705	0.6	✗	✗	✓	LQ	✓	✓	11.4	12.6	0.58
SW 59	ASW 000 85cp	J143950.6+544606	–	✓	✗	✓	D	✓	✓	–	–	–

4.8 Appendix: Developments in SpaghettiLens

4.8.1 Improved synthetic images

The mass maps produced by the current implementation of SPAGHETTILENS are based on images of point-like features. No information about extended images is used, except in so far as they help the user identify images of point-like features. The synthetic images offered to users are rudimentary, corresponding to conical light profiles (i.e.circular light profiles with brightness decreasing linearly with radius).

We have now developed a prototype to improve the generation of synthetic images, as illustrated in Figure 4.8. Areas containing lensed images are selected (green frames in the figure). The selected areas should be as free as possible from other sources, including the lensing galaxy. Pixels within the selected areas are mapped to a grid on the source plane, using bending angles given by the mass model. The mapping from lens-plane pixels to source-plane grid cells is many-to-one, because of image multiplicity and magnification. The brightness of each source-plane pixel is set to the mean of all the lens-plane pixels mapped to it. Finally, the mapping is run back to the lens plane. The result is a synthetic image. In effect, one is reconstructing a source-plane brightness map by least squares.

The procedure is not yet implemented in SPAGHETTILENS but can be applied during post-processing. The new synthetic images could be used to improve the mass reconstruction, by weighing the ensemble of maps according to how good the synthetic images are.

4.8.2 Sub-sampling of the central region

The models of simulated lenses in Küng et al., 2015 showed a tendency to produce density profiles which were too shallow, resulting typically in overestimates of the Einstein radius. Allowing some extra mass tiles in central region, thus allowing the mass profile to rise more steeply near the centre, was suggested as a possible cure.

Figure 4.9 shows an experiment with smaller mass tiles in the inner region. Replacing the very central mass tile with nine smaller tiles allows for steeper central profiles. Doing the same for the 25 innermost mass tiles allows for even steeper central profiles, eliminating the systematic shallow profiles. However, it does not provide a completely satisfactory solution, because (a) it increases the number of mass tiles by 40 % and significantly increases the computational time, and (b) the square boundary between areas with different tile sizes is rather undesirable. The main modelling work in this paper was, however, done before the experiment with smaller mass tiles was complete. Some of the models presented in this paper apply the intermediate option (corresponding to the middle panel in Figure 4.9) while others use the old system. We note this paper mainly concerns the enclosed mass in the outer regions, so shallowness in the central region should not be an issue.

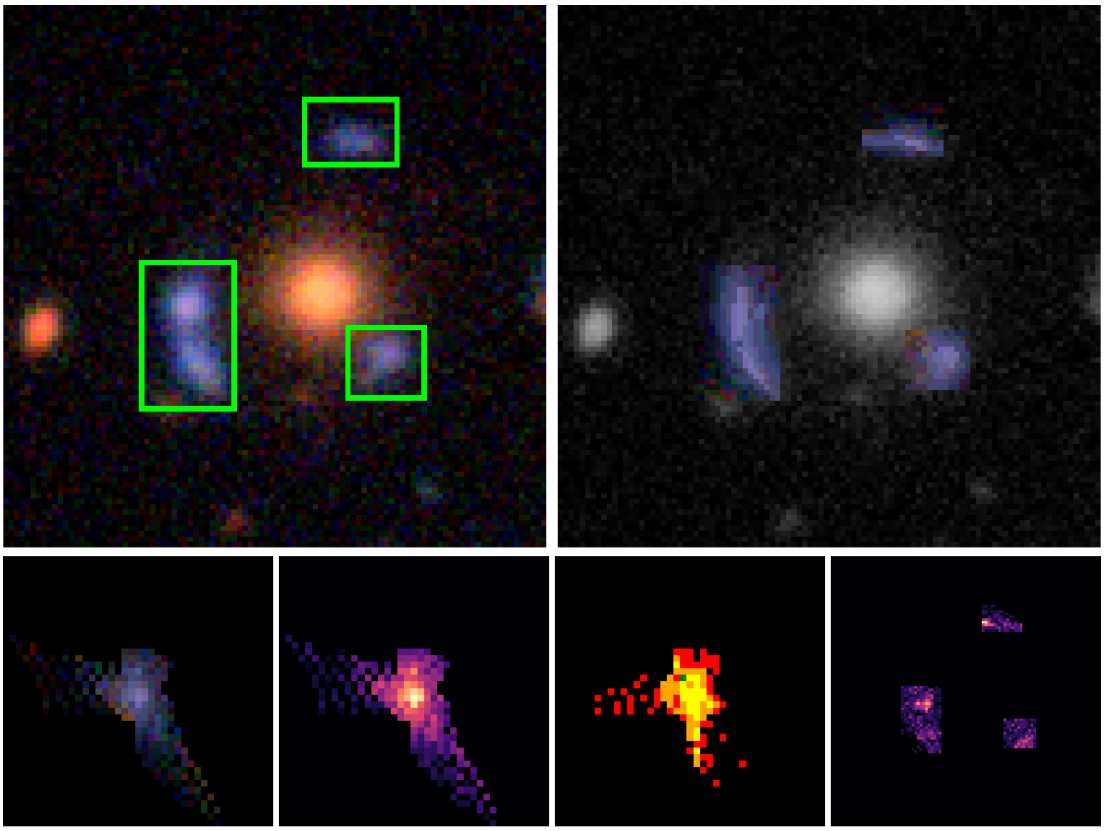

Figure 4.8: Synthetic lensed image with source-profile fitting for a model of candidate SW 05 (J143454.4+522850). Top-left: original image, with areas containing lensed images enclosed within green frames. Top-right: synthetic image (coloured arcs) with lensing galaxy and unrelated objects in grey-scale. Bottom from left to right: reconstructed source in colour, intensity (grey-scale), count of lens-plane pixels per source-plane pixel, and residual of original image to synthetic image.

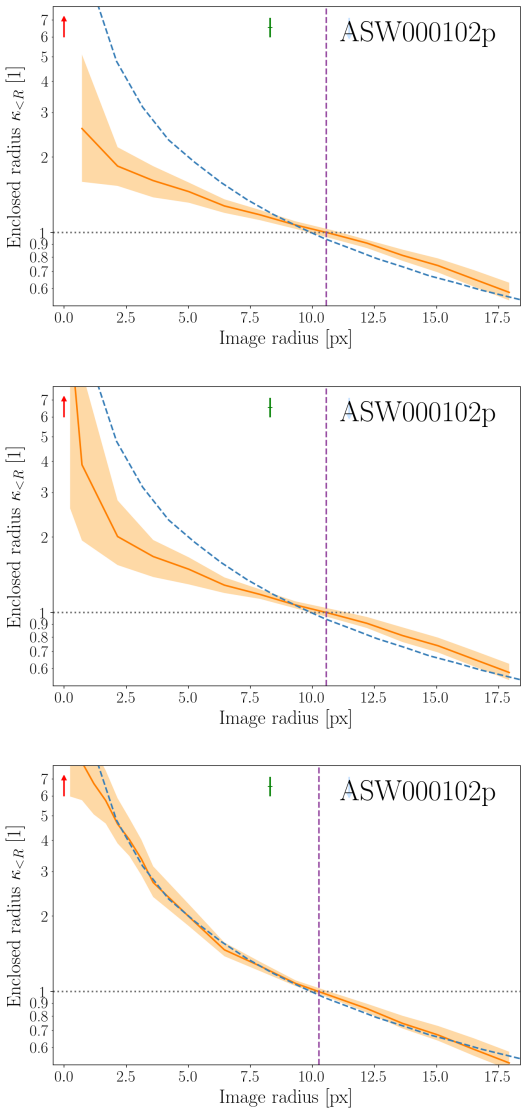

Figure 4.9: Model improvement resulting from the use of smaller mass tiles in the inner region of the mass model. Shown here are the average enclosed κ within a given projected radius, for three different reconstructions of a simulated lens (sim) from SpaceWarps. In each panel, the dashed blue curve is the correct answer. The orange band represents the statistical ensemble from SpaghettiLens, and the orange line shows the ensemble mean. Locations of images (maximum, saddle point, minimum) are marked with vertical arrows. The radial value at $\kappa = 1$ is the effective Einstein radius, r_{E}. The upper panel is taken from Küng et al. (2015), see Fig. 3 of that paper. The middle panel is the result when the innermost mass tile is replaced by nine smaller tiles. The lower panel results from replacing the innermost 5×5 tiles with nine smaller tiles each.

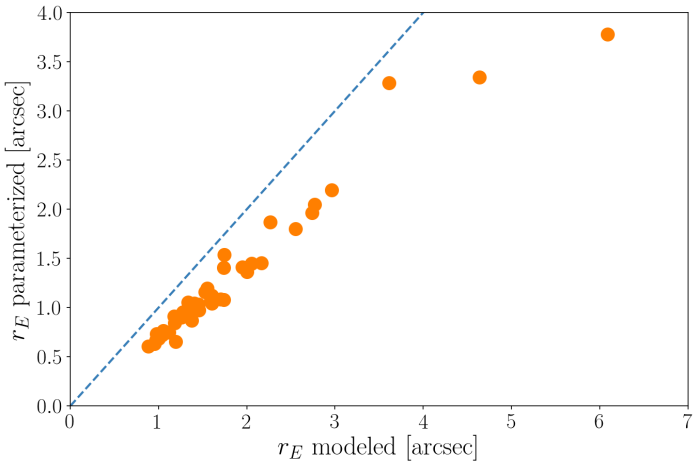

Figure 4.10: Comparison of Einstein radii $r_{\rm E}$ obtained from mass tiles to the results from a parametrized model to test the performance of the algorithm. The parametrized model was generated using principal component analysis on the ensemble of models. The blue dashed line represents a perfect recovery of $r_{\rm E}$.

4.8.3 Parametrisation of pixel models

In order to fit the set of pixelated models to a single parametrized model, a program was written that took a parametrized function and subtracted from it the mean and the principal components (PCs) of the data. This created the residual function. The number of PCs in the analysis was varied, to test how this affected the output. It was found that five PCs gave a reasonable approximation. A masking function was added, selecting only the data points that fell inside the image of the lens, and the PCs were clipped in order to keep the values inside the region of the ensemble. Any value higher than the clip was set to be the clip value. This was chosen to 2.5 because, assuming that the data follow a Gaussian error distribution, almost all the values for the variance should lie between 2 and 3 standard deviations from the mean. Minimizing the residuals function produces the set of parameters that fit the parametrized function to the original pixelated ensemble most closely. A least squares fit was used to perform this minimisation. The parametrised model function was obtained from the gravitational potential of an isothermal ellipsoid mass distribution (Keeton, 2001a). This model is frequently used to describe gravitational lenses, giving good fits to the observations. The isothermal ellipsoid model outputs three useful parameters: the radius of the Einstein ring, the ellipticity of the model and the angle of the ellipticity from the vertical, giving the orientation of the galaxy. By applying this model to simulated lenses for which the values of these parameters were already known, it was possible to assess the accuracy of the methodology, before applying the model to the candidate lensing galaxies. Preliminary results on the recovery of Einstein radii are shown in Figure 4.10.

Chapter 5

Outlook and Next Steps

Currently, the field of strong lensing is at a crucial turning point. First surveys, such as the CFHT LS, have been searched for strong lenses with several methods. This can be used to estimate how many lenses might be found in future surveys. Highly sophisticated next-generation surveys have already left the planning stages and are on the way to being realised. In Chapter 1, three future missions were named specifically. The first, the Dark Energy Survey (DES), is now operational and collecting data, and recently published the results of the first year of data collection. The second, the Large Synoptic Survey Telescope (LSST), is currently being built and on schedule, and engineering first light is anticipated in 2019. The last, the space telescope Euclid, passed the major milestone of the preliminary design review in 2015. In spring and summer 2017, the first scientific equipment (e.g., the NIR spectrometer and the photometer) were delivered, and launch is scheduled for 2020.

The scientific community is getting ready to handle orders of magnitude more data with possibly tens of thousands of lenses. One project is the Master Lens Database (Moustakas, 2012), launched to the public in autumn 2017, which aims to become an "exhaustive and current compilation of all discovered strong gravitational lenses"[1]. Robot lens detection is transitioning to methods of modern artificial research, such as deep learning (e.g., Lanusse et al., 2018) and neural network arc finder (Bom et al., 2017), that allow for large samples to be scanned without supervision, once trained. Additionally, the SPACEWARPS project is preparing for a second run on the DES observations.

This work presents a powerful and scaleable tool to possibly have tens of thousands of lenses modelled. The previous chapters discussed the tests and applications of this machinery on a small scale of 58 lenses with approximately eight users. It summarises the first steps to becoming an established tool to create a large number of models quickly. However, there remains much to do to achieve this goal.

[1] J. Brownstein, L. Moustakas; *The Master Lens Database and The Orphan Lenses Project*; `http://admin.masterlens.org/`; retrieved March 2017

Short term objectives include a possible transfer of the system from the dedicated local hardware to the cloud for easier maintenance, easier upscaling and for direct scaling of cost with the number of users. Regarding the software side, some of the improvements presented in Chapter 4 still need to be implemented in the user interface. A tool that allows for the determination of photometric redshifts could be integrated into the workflow, automating the manual analysis presented in Chapter 4. Scientifically, the significant uncertainties displayed in Figure 4.7 can be improved by using available optical and NIR magnitudes to get better constraints on the stellar populations. The results presented in that chapter are preliminary and should be compared with theory and simulations of galaxy formation models. The halo mass estimates can be improved by enhancing the modelling process of GLASS. The number of models generated for one ensemble model, sampling the solution space, could be increased and then be filtered by additional criteria post model creation. Lastly, training material, tutorials and introductions to allow new volunteers an easy entry into the field of gravitational lens modelling have to be created.

The longer-term goal to establish this work in the field of modelling is to acquire more volunteers for this project. The number of lens candidates is expected to increase by at least a hundredfold, and ideally so should the number of volunteers participating in this project. Finding the necessary few hundred dedicated, long-term volunteers is challenging, but doable. There are several ways to find people interested in modelling and to make this project more visible to the public.

The first strategy is the most conservative and promising – to continue the collaboration with SPACEWARPS and ZOONIVERSE and try to motivate a few very active volunteers to join the modelling community. The first run of SPACEWARPS attracted 37 000 citizen scientists. The analysis of the first run of SPACEWARPS presented by Marshall, Verma, et al. (2016) reported that there were approximately 10^4 volunteers; of which a few 10^3 gained considerable skill to potentially make a considerable contribution and a few 10^2 had enough time to scan through enough images to actually make a considerable contribution. There is a simple way to get into contact with these volunteers through the discussion forum of SPACEWARPS, where the SPAGHETTILENS project already is present and known. A next step could be the use of the SPACEWARPS or even the ZOONIVERSE mailing list for an invitational email to join the project.

A second strategy could involve a traditional outreach strategy in science, which would be collaborating with museums and exhibitions. Since in citizen science the volunteer is active, a special exhibition on a citizen science project that directly allows participation contrasts the default behaviour of a passive visitor, and thus might be desirable for museums. In Zurich[2], the Urania Observatory with its approximately 10 000 annual visitors could be a valuable partner. More general museums, such as the Zoological Museum Zurich, which attracts 140 000 visitors per year, might also merit consideration. On an international level, the American Museum of Natural History with its 5 000 000 visitors per year could be a valuable partner.

A third strategy would rely on social media. This strategy has the potential to reach the

[2] *Statistisches Jahrbuch der Stadt Zürich* 2017

Table 5.1: List of selected, physics-related YouTube channels. Number of *subscribers* and *total views* as per the status page of the corresponding channel. *Views per video* is the average number of views of the latest twenty uploaded, free videos. Retrieved Aug. 2017 from `http://youtube.com`

name	subscriber	total views	views per video
sixty symbols	660 000	66 000 000	130 000
Physics Girl	680 000	47 000 000	170 000
e-penser	900 000	64 000 000	550 000
minutephysics	4 000 000	330 000 000	760 000
Veritasium	4 300 000	370 000 000	1 270 000
SmarterEveryDay	5 000 000	390 000 000	1 950 000
Vsauce	12 300 000	1 250 000 000	5 740 000

most people, but is the least predictable. One approach could be trying to establish a presence on social media by creating regular content and promoting the project via Facebook, Twitter, Reddit and traditional media like free, daily newspapers. This is a task not to be underestimated and better organised and coordinated by the media and public relations departments of a faculty, or the university as a whole. Another, more promising approach is to try to be covered by already-established and well-known figures from the field of physics. Table 5.1 lists the leading YouTube channels that are famous for being physics-related. It might be challenging to reach out to one of the four professional, high-impact channels with more than one million subscribers. It is more reasonable to aim for one of the semi-professional, medium-range channels and invite the host over to present one's work in an appealing way.

This work might not only be applicable for strong lens modelling; the developed software stack may be useful for projects in other fields of science. There are many different possible applications of the form presented here. First, a data source is selected and information from and about this data source is presented. The volunteer sets up a process configuration that runs on the server and returns results. For example, in the field of big data and the analysis thereof, it might be favourable to allow users to set up a process configuration, to run it server-side where the data resides, and to only deliver the resulting data (instead of delivering all the data to the user for client-side analysis).

A similar design is currently being applied to the Gaia mission by ESA, respectively to its data archive currently under design. Due to the size of the data products, scientists no longer download the data for offline analysis, but upload their code to be run server-side (Arviset et al., 2016).

Another example from a different field is the project GAPMINDER[3]. It allows the visualisation and animation of open data sets with the aim of promoting a fact-based worldview. It presents a bubble chart and allows the selection of a data set for each of four variables, one for x- and y-axes respectively, one for the size and one for the colour of the bubble. The

[3] `http://gapminder.org`

animation then displays the evolution of these variables over time. This work could allow for something similar but would enable more complex kind of analyses than simply plotting.

Bibliography

Alard, C. (June 2006). „Automated detection of gravitational arcs“. In: *ArXiv: astro-ph/0606757*.

Applegate, D. E. et al. (Apr. 2016). „Cosmology and astrophysics from relaxed galaxy clusters - IV. Robustly calibrating hydrostatic masses with weak lensing“. In: *MNRAS* 457, pp. 1522–1534. DOI: 10.1093/mnras/stw005.

Arviset, C. et al. (June 2016). „The Gaia Archive: VO in Action in the Big Data Era“. In: *Astronomical Surveys and Big Data*. Ed. by A. Mickaelian, A. Lawrence, and T. Magakian. Vol. 505. Astronomical Society of the Pacific Conference Series, p. 218.

Baade, W. and F. Zwicky (May 1934). „On Super-novae“. In: *Proceedings of the National Academy of Science* 20, pp. 254–259. DOI: 10.1073/pnas.20.5.254.

Blandford, R. and R. Narayan (Nov. 1986). „Fermat's principle, caustics, and the classification of gravitational lens images“. In: *ApJ* 310, pp. 568–582. DOI: 10.1086/164709.

Bom, C. R. et al. (Jan. 2017). „A neural network gravitational arc finder based on the Mediatrix filamentation method“. In: *A&A* 597, A135, A135. DOI: 10.1051/0004-6361/201629159.

Bosma, A. (1978). „The distribution and kinematics of neutral hydrogen in spiral galaxies of various morphological types“. PhD thesis. PhD Thesis, Groningen Univ., (1978).

Brewer, Eric (Jan. 2012). „CAP twelve years later: How the "rules" have changed“. In: *Computer* 45.2, pp. 23–29. ISSN: 0018-9162. DOI: 10.1109/MC.2012.37.

Brewer, Eric A (2000). „Towards robust distributed systems“. In: *PODC*. Vol. 7, p. 7. DOI: 10.1145/343477.343502.

Bruderer, C. et al. (Feb. 2016). „Light versus dark in strong-lens galaxies: dark matter haloes that are rounder than their stars“. In: *MNRAS* 456, pp. 870–884. DOI: 10.1093/mnras/stv2582.

Bruzual, G. and S. Charlot (Oct. 2003). „Stellar population synthesis at the resolution of 2003“. In: *MNRAS* 344, pp. 1000–1028. DOI: 10.1046/j.1365-8711.2003.06897.x.

Butcher, Gregory S et al. (1990). „An evaluation of the Christmas Bird Count for monitoring population trends of selected species“. In: *Wildlife Society Bulletin (1973-2006)* 18.2, pp. 129–134.

Coles, J. (May 2008). „A New Estimate of the Hubble Time with Improved Modeling of Gravitational Lenses“. In: *ApJ* 679, pp. 17–24. DOI: 10.1086/587635.

Coles, J. P., J. I. Read, and P. Saha (Dec. 2014). „Gravitational lens recovery with GLASS: measuring the mass profile and shape of a lens“. In: *MNRAS* 445, pp. 2181–2197. DOI: 10.1093/mnras/stu1781.

Collett, T. E. (Sept. 2015). „The Population of Galaxy-Galaxy Strong Lenses in Forthcoming Optical Imaging Surveys“. In: *ApJ* 811, 20, p. 20. DOI: 10.1088/0004-637X/811/1/20.

Coupon, J. et al. (June 2009). „Photometric redshifts for the CFHTLS T0004 deep and wide fields“. In: *A&A* 500, pp. 981–998. DOI: 10.1051/0004-6361/200811413.

Courbin, F., P. Saha, and P. L. Schechter (2002). „Quasar Lensing“. In: *Gravitational Lensing: An Astrophysical Tool*. Ed. by F. Courbin and D. Minniti. Vol. 608. Lecture Notes in Physics, Berlin Springer Verlag, p. 1.

Crosta, M. et al. (Aug. 2015). „The ray tracing analytical solution within the RAMOD framework. The case of a Gaia-like observer“. In: *Classical and Quantum Gravity* 32.16, 165008, p. 165008. DOI: 10.1088/0264-9381/32/16/165008.

Cuillandre, J.-C. J. et al. (Sept. 2012). „Introduction to the CFHT Legacy Survey final release (CFHTLS T0007)“. In: *Observatory Operations: Strategies, Processes, and Systems IV*. Vol. 8448. procspie, p. 84480M. DOI: 10.1117/12.925584.

Cyburt, R. H. et al. (Jan. 2016). „Big bang nucleosynthesis: Present status“. In: *Reviews of Modern Physics* 88.1, 015004, p. 015004. DOI: 10.1103/RevModPhys.88.015004.

Dark Energy Survey Collaboration (Oct. 2005). „The Dark Energy Survey“. In: *ArXiv: astro-ph/0510346*.

Drlica-Wagner, A. et al. (Aug. 2017). „Dark Energy Survey Year 1 Results: Photometric Data Set for Cosmology“. In: *ArXiv: 1708.01531*.

Dyson, F. W., A. S. Eddington, and C. Davidson (1920). „A Determination of the Deflection of Light by the Sun's Gravitational Field, from Observations Made at the Total Eclipse of May 29, 1919“. In: *Philosophical Transactions of the Royal Society of London Series A* 220, pp. 291–333. DOI: 10.1098/rsta.1920.0009.

Einstein, A. (Dec. 1936). „Lens-Like Action of a Star by the Deviation of Light in the Gravitational Field“. In: *Science* 84, pp. 506–507. DOI: 10.1126/science.84.2188.506.

Eisenstein, D. J. (Nov. 2005). „Dark energy and cosmic sound [review article]“. In: *New A Rev.* 49, pp. 360–365. DOI: 10.1016/j.newar.2005.08.005.

Erben, T. et al. (Aug. 2013). „CFHTLenS: the Canada-France-Hawaii Telescope Lensing Survey - imaging data and catalogue products“. In: *MNRAS* 433, pp. 2545–2563. DOI: 10.1093/mnras/stt928.

Ferreras, I., F. La Barbera, et al. (Feb. 2013). „Systematic variation of the stellar initial mass function with velocity dispersion in early-type galaxies“. In: *MNRAS* 429, pp. L15–L19. DOI: 10.1093/mnrasl/sls014.

Ferreras, I., P. Saha, and S. Burles (Jan. 2008). „Unveiling dark haloes in lensing galaxies“. In: *MNRAS* 383, pp. 857–863. DOI: 10.1111/j.1365-2966.2007.12606.x.

Ferreras, I., P. Saha, and L. L. R. Williams (Apr. 2005). „Stellar and Total Mass in Early-Type Lensing Galaxies“. In: *ApJ* 623, pp. L5–L8. DOI: 10.1086/429995.

Gallazzi, A. and E. F. Bell (Dec. 2009). „Stellar Mass-to-Light Ratios from Galaxy Spectra: How Accurate Can They Be?“ In: *ApJS* 185, pp. 253–272. DOI: 10.1088/0067-0049/185/2/253.

Gavazzi, R. et al. (Apr. 2014). „RINGFINDER: Automated Detection of Galaxy-scale Gravitational Lenses in Ground-based Multi-filter Imaging Data“. In: *ApJ* 785, 144, p. 144. DOI: 10.1088/0004-637X/785/2/144.

Ghatak, A. K. (2010). *Optics*. Boston: McGraw-Hill Higher Education. ISBN: 0073380482.

Haklay, Muki (2013). „Citizen science and volunteered geographic information: Overview and typology of participation“. In: *Crowdsourcing geographic knowledge*. Springer, pp. 105–122. ISBN: 978-94-007-4586-5. DOI: 10.1007/978-94-007-4587-2.

Heymans, C. et al. (Nov. 2012). „CFHTLenS: the Canada-France-Hawaii Telescope Lensing Survey“. In: *MNRAS* 427, pp. 146–166. DOI: 10.1111/j.1365-2966.2012.21952.x.

Hezaveh, Y. D., L. P. Levasseur, and P. J. Marshall (Aug. 2017). „Fast automated analysis of strong gravitational lenses with convolutional neural networks“. In: *Nature* 548, pp. 555–557. DOI: 10.1038/nature23463.

Ivezic, Z. et al. (May 2008). „LSST: from Science Drivers to Reference Design and Anticipated Data Products“. In: *ArXiv: 0805.2366*.

Jong, J. T. A. de et al. (Jan. 2013). „The Kilo-Degree Survey“. In: *Experimental Astronomy* 35, pp. 25–44. DOI: 10.1007/s10686-012-9306-1.

Keeton, C. R. (Feb. 2001a). „A Catalog of Mass Models for Gravitational Lensing“. In: *ArXiv: astro-ph/0102341*.

Keeton, C. R. (Feb. 2001b). „Computational Methods for Gravitational Lensing“. In: *ArXiv: astro-ph/0102340*.

Keeton, C. R. and J. N. Winn (June 2003). „The Quintuple Quasar: Mass Models and Interpretation“. In: *ApJ* 590, pp. 39–51. DOI: 10.1086/374833.

Khatib, Firas et al. (2011). „Crystal structure of a monomeric retroviral protease solved by protein folding game players“. In: *Nature structural & molecular biology* 18.10, pp. 1175–1177.

Kilbinger, M. (July 2015). „Cosmology with cosmic shear observations: a review“. In: *Reports on Progress in Physics* 78.8, 086901, p. 086901. DOI: 10.1088/0034-4885/78/8/086901.

Koopmans, L. V. E. et al. (Sept. 2009). „The Structure and Dynamics of Massive Early-Type Galaxies: On Homology, Isothermality, and Isotropy Inside One Effective Radius“. In: *ApJ* 703, pp. L51–L54. DOI: 10.1088/0004-637X/703/1/L51.

Kullenberg, Christopher and Dick Kasperowski (Jan. 2016). „What is citizen science?–A scientometric meta-analysis“. In: *PloS one* 11.1, e0147152. DOI: 10.1371/journal.pone.0147152.

Küng, R. (Apr. 2018). „SPAGHETTILENS: A software stack for modeling gravitational lenses by citizen scientists“. In: *Astronomy and Computing* 23, pp. 115–123. DOI: 10.1016/j.ascom.2018.02.007.

Küng, R. et al. (Mar. 2015). „Gravitational lens modelling in a citizen science context“. In: *MNRAS* 447, pp. 2170–2180. DOI: 10.1093/mnras/stu2554.

Küng, R. et al. (Mar. 2018). „Models of gravitational lens candidates from Space Warps CFHTLS“. In: *MNRAS* 474, pp. 3700–3713. DOI: 10.1093/mnras/stx3012.

La Barbera, F. et al. (Apr. 2016). „Radial constraints on the initial mass function from TiO features and Wing-Ford band in early-type galaxies“. In: *MNRAS* 457, pp. 1468–1489. DOI: 10.1093/mnras/stv2996.

Landis, G. A. (Apr. 2016). „Mission to the Gravitational Focus of the Sun: A Critical Analysis“. In: *ArXiv: 1604.06351*.

Lanusse, F. et al. (Jan. 2018). „CMU DeepLens: deep learning for automatic image-based galaxy-galaxy strong lens finding“. In: *MNRAS* 473, pp. 3895–3906. DOI: 10.1093/mnras/stx1665.

Laureijs, R. et al. (Sept. 2012). „Euclid: ESA's mission to map the geometry of the dark universe“. In: *Space Telescopes and Instrumentation 2012: Optical, Infrared, and Millimeter Wave*. Vol. 8442. Proc. SPIE, 84420T. DOI: 10.1117/12.926496.

Lefor, A. T. (July 2014). „Comparison of strong gravitational lens model software II. HydraLens: Computer-assisted strong gravitational lens model generation and translation“. In: *Astronomy and Computing* 5, pp. 28–34. DOI: 10.1016/j.ascom.2014.04.002.

Lefor, A. T., T. Futamase, and M. Akhlaghi (July 2013). „A systematic review of strong gravitational lens modeling software“. In: *New A Rev.* 57, pp. 1–13. DOI: 10.1016/j.newar.2013.05.001.

Leier, D., I. Ferreras, and P. Saha (July 2012). „Diagnostics of baryonic cooling in lensing galaxies“. In: *MNRAS* 424, pp. 104–114. DOI: 10.1111/j.1365-2966.2012.21173.x.

Leier, D., I. Ferreras, P. Saha, S. Charlot, et al. (July 2016). „Strong gravitational lensing and the stellar IMF of early-type galaxies“. In: *MNRAS* 459, pp. 3677–3692. DOI: 10.1093/mnras/stw885.

Leier, D., I. Ferreras, P. Saha, and E. E. Falco (Oct. 2011). „Resolving the Baryon-fraction Profile in Lensing Galaxies“. In: *ApJ* 740, 97, p. 97. DOI: 10.1088/0004-637X/740/2/97.

Lenzen, F., S. Schindler, and O. Scherzer (Mar. 2004). „Automatic detection of arcs and arclets formed by gravitational lensing“. In: *A&A* 416, pp. 391–401. DOI: 10.1051/0004-6361:20034619.

Lintott, C. J. et al. (Sept. 2008). „Galaxy Zoo: morphologies derived from visual inspection of galaxies from the Sloan Digital Sky Survey“. In: *MNRAS* 389, pp. 1179–1189. DOI: 10.1111/j.1365-2966.2008.13689.x.

Lubini, M. and J. Coles (Oct. 2012). „A sampling strategy for high-dimensional spaces applied to free-form gravitational lensing“. In: *MNRAS* 425, pp. 3077–3084. DOI: 10.1111/j.1365-2966.2012.21673.x.

Lupton, R. et al. (Feb. 2004). „Preparing Red-Green-Blue Images from CCD Data“. In: *PASP* 116, pp. 133–137. DOI: 10.1086/382245.

Marshall, P. J., D. W. Hogg, et al. (Apr. 2009). „Automated Detection of Galaxy-Scale Gravitational Lenses in High-Resolution Imaging Data“. In: *ApJ* 694, pp. 924–942. DOI: 10.1088/0004-637X/694/2/924.

Marshall, P. J., L. A. Moustakas, et al. (Dec. 2005). „An Automated Search for Gravitational Lenses in the HST Imaging Archive“. In: *American Astronomical Society Meeting Abstracts*. Vol. 37. Bulletin of the American Astronomical Society, p. 20003.

Marshall, P. J., A. Verma, et al. (Jan. 2016). „SPACE WARPS - I. Crowdsourcing the discovery of gravitational lenses“. In: *MNRAS* 455, pp. 1171–1190. DOI: 10.1093/mnras/stv2009.

Maturi, M., S. Mizera, and G. Seidel (July 2014). „Multi-colour detection of gravitational arcs“. In: *A&A* 567, A111, A111. DOI: 10.1051/0004-6361/201321634.

McGaugh, S. S., F. Lelli, and J. M. Schombert (Nov. 2016). „Radial Acceleration Relation in Rotationally Supported Galaxies“. In: *Phys. Rev. Lett.* 117.20, 201101, p. 201101. DOI: 10.1103/PhysRevLett.117.201101.

Mohammed, I., P. Saha, and J. Liesenborgs (Apr. 2015). „Lensing time delays as a substructure constraint: a case study with the cluster SDSS J1004+4112“. In: *PASJ* 67, 21, p. 21. DOI: 10.1093/pasj/psu155.

Mohammed, I., P. Saha, L. L. R. Williams, et al. (June 2016). „Quantifying substructures in Hubble Frontier Field clusters: comparison with ΛCDM simulations“. In: *MNRAS* 459, pp. 1698–1709. DOI: 10.1093/mnras/stw727.

More, A., R. Cabanac, et al. (Apr. 2012). „The CFHTLS-Strong Lensing Legacy Survey (SL2S): Investigating the Group-scale Lenses with the SARCS Sample“. In: *ApJ* 749, 38, p. 38. DOI: 10.1088/0004-637X/749/1/38.

More, A., K. Jahnke, et al. (June 2011). „Gravitational Lens Candidates in the E-CDFS“. In: *ApJ* 734, 69, p. 69. DOI: 10.1088/0004-637X/734/1/69.

More, A., A. Verma, et al. (Jan. 2016). „SPACE WARPS - II. New gravitational lens candidates from the CFHTLS discovered through citizen science“. In: *MNRAS* 455, pp. 1191–1210. DOI: 10.1093/mnras/stv1965.

Morganti, R., C. N. Tadhunter, and T. A. Oosterloo (Dec. 2005). „Fast neutral outflows in powerful radio galaxies: a major source of feedback in massive galaxies“. In: *A&A* 444, pp. L9–L13. DOI: 10.1051/0004-6361:200500197.

Moster, B. P. et al. (Feb. 2010). „Constraints on the Relationship between Stellar Mass and Halo Mass at Low and High Redshift“. In: *ApJ* 710, pp. 903–923. DOI: 10.1088/0004-637X/710/2/903.

Moustakas, L. (Oct. 2012). *The Master Lens Database and The Orphan Lenses Project*. HST Proposal.

Naudus, P., J. Wallin, and P. Marshall (Jan. 2010). „Computer Modeling of Gravitational Lensing Systems“. In: *American Astronomical Society Meeting Abstracts 215*. Vol. 42. Bulletin of the American Astronomical Society, p. 43527.

Navarro, J. F., C. S. Frenk, and S. D. M. White (May 1996). „The Structure of Cold Dark Matter Halos“. In: *ApJ* 462, p. 563. DOI: 10.1086/177173.

Navarro, J. F., C. S. Frenk, and S. D. M. White (Dec. 1997). „A Universal Density Profile from Hierarchical Clustering“. In: *ApJ* 490, p. 493. DOI: 10.1086/304888.

Nightingale, J., S. Dye, and R. Massey (Aug. 2017). „AutoLens: Automated Modeling of a Strong Lens's Light, Mass and Source“. In: *ArXiv:1708.07377*.

Oguri, M. and P. J. Marshall (July 2010). „Gravitationally lensed quasars and supernovae in future wide-field optical imaging surveys“. In: *MNRAS* 405, pp. 2579–2593. DOI: 10.1111/j.1365-2966.2010.16639.x.

Paraficz, D. et al. (July 2016). „The PCA Lens-Finder: application to CFHTLS“. In: *A&A* 592, A75, A75. DOI: 10.1051/0004-6361/201527971.

Peebles, P. J. E. (July 1968). „Recombination of the Primeval Plasma“. In: *ApJ* 153, p. 1. DOI: 10.1086/149628.

Perlmutter, S. et al. (June 1999). „Measurements of Ω and Λ from 42 High-Redshift Supernovae“. In: *ApJ* 517, pp. 565–586. DOI: 10.1086/307221.

Planck Collaboration et al. (Sept. 2016). „Planck 2015 results. XIII. Cosmological parameters“. In: *A&A* 594, A13, A13. DOI: 10.1051/0004-6361/201525830.

Raddick, M. J. et al. (2013). „Galaxy Zoo: Motivations of Citizen Scientists“. In: *Astronomy Education Review* 12.1, p. 010106. DOI: 10.3847/AER2011021.

Rathna Kumar, S., C. S. Stalin, and T. P. Prabhu (Aug. 2015). „H_0 from ten well-measured time delay lenses“. In: *A&A* 580, A38, A38. DOI: 10.1051/0004-6361/201423977.

Refregier, A. et al. (Jan. 2010). „Euclid Imaging Consortium Science Book“. In: *ArXiv: 1001.0061*.

Refsdal, S. (1964). „On the possibility of determining Hubble's parameter and the masses of galaxies from the gravitational lens effect“. In: *MNRAS* 128, p. 307. DOI: 10.1093/mnras/128.4.307.

Refsdal, S. (1966). „On the possibility of testing cosmological theories from the gravitational lens effect“. In: *MNRAS* 132, p. 101. DOI: 10.1093/mnras/132.1.101.

Riess, A. G. et al. (Sept. 1998). „Observational Evidence from Supernovae for an Accelerating Universe and a Cosmological Constant“. In: *AJ* 116, pp. 1009–1038. DOI: 10.1086/300499.

Rusin, D. et al. (Aug. 2001). „B1359+154: A Six-Image Lens Produced by a z $\sim=$ 1 Compact Group of Galaxies“. In: *ApJ* 557, pp. 594–604. DOI: 10.1086/322251.

Saha, P. and L. L. R. Williams (Nov. 1997). „Non-parametric reconstruction of the galaxy lens in PG 1115+080“. In: *MNRAS* 292, p. 148. DOI: 10.1093/mnras/292.1.148.

Saha, P. and L. L. R. Williams (June 2003). „Qualitative Theory for Lensed QSOs“. In: *AJ* 125, pp. 2769–2782. DOI: 10.1086/375204.

Saha, P. and L. L. R. Williams (May 2004). „A Portable Modeler of Lensed Quasars“. In: *AJ* 127, pp. 2604–2616. DOI: 10.1086/383544.

Saxton, C. J. and I. Ferreras (June 2010). „Polytropic dark haloes of elliptical galaxies“. In: *MNRAS* 405, pp. 77–90. DOI: 10.1111/j.1365-2966.2010.16448.x.

Schive, H.-Y. et al. (Feb. 2016). „Contrasting Galaxy Formation from Quantum Wave Dark Matter, ψDM, with ΛCDM, using Planck and Hubble Data“. In: *ApJ* 818, 89, p. 89. DOI: 10.3847/0004-637X/818/1/89.

Schwamb, M. E. et al. (May 2013). „Planet Hunters: A Transiting Circumbinary Planet in a Quadruple Star System“. In: *ApJ* 768, 127, p. 127. DOI: 10.1088/0004-637X/768/2/127.

Seidel, G. and M. Bartelmann (Sept. 2007). „Arcfinder: an algorithm for the automatic detection of gravitational arcs“. In: *A&A* 472, pp. 341–352. DOI: 10.1051/0004-6361:20066097.

Sereno, M. and D. Paraficz (Jan. 2014). „Hubble constant and dark energy inferred from free-form determined time delay distances“. In: *MNRAS* 437, pp. 600–605. DOI: 10.1093/mnras/stt1938.

Silk, J. and G. A. Mamon (Aug. 2012). „The current status of galaxy formation“. In: *Research in Astronomy and Astrophysics* 12, pp. 917–946. DOI: 10.1088/1674-4527/12/8/004.

Silvertown, Jonathan (July 2009). „A new dawn for citizen science“. In: *Trends in Ecology & Evolution* 24.9, pp. 467–471. ISSN: 0169-5347. DOI: 10.1016/j.tree.2009.03.017.

Smith, R. J., J. R. Lucey, and C. Conroy (June 2015). „The SINFONI Nearby Elliptical Lens Locator Survey: discovery of two new low-redshift strong lenses and implications for the initial mass function in giant early-type galaxies“. In: *MNRAS* 449, pp. 3441–3457. DOI: 10.1093/mnras/stv518.

Sonnenfeld, Alessandro et al. (2017). „Survey of Gravitationally-lensed Objects in HSC Imaging (SuGOHI). I. Automatic search for galaxy-scale strong lenses“. In: *Publications of the Astronomical Society of Japan*, psx062. DOI: 10.1093/pasj/psx062.

Springel, V. et al. (June 2005). „Simulations of the formation, evolution and clustering of galaxies and quasars“. In: *Nature* 435, pp. 629–636. DOI: 10.1038/nature03597.

Suyu, S. H. et al. (Sept. 2006). „A Bayesian analysis of regularized source inversions in gravitational lensing“. In: *MNRAS* 371, pp. 983–998. DOI: 10.1111/j.1365-2966.2006.10733.x.

Taylor, E. N. et al. (Dec. 2011). „Galaxy And Mass Assembly (GAMA): stellar mass estimates“. In: *MNRAS* 418, pp. 1587–1620. DOI: 10.1111/j.1365-2966.2011.19536.x.

Udalski, A., M. K. Szymanski, and G. Szymanski (Mar. 2015). „OGLE-IV: Fourth Phase of the Optical Gravitational Lensing Experiment“. In: *Acta Astron.* 65, pp. 1–38.

Walsh, D., R. F. Carswell, and R. J. Weymann (May 1979). „0957 + 561 A, B - Twin quasistellar objects or gravitational lens“. In: *Nature* 279, pp. 381–384. DOI: 10.1038/279381a0.

Warren, S. J. and S. Dye (June 2003). „Semilinear Gravitational Lens Inversion“. In: *ApJ* 590, pp. 673–682. DOI: 10.1086/375132.

Werthimer, D. et al. (Aug. 2001). „Berkeley radio and optical SETI programs: SETI@home, SERENDIP, and SEVENDIP“. In: *The Search for Extraterrestrial Intelligence (SETI) in the Optical Spectrum III*. Ed. by S. A. Kingsley and R. Bhathal. Vol. 4273. Proc. SPIE, pp. 104–109. DOI: 10.1117/12.435384.

Westphal, A. J. et al. (Mar. 2005). „Stardust@home: A Massively Distributed Public Search for Interstellar Dust in the Stardust Interstellar Dust Collector“. In: *36th Annual Lunar and Planetary Science Conference*. Ed. by S. Mackwell and E. Stansbery. Vol. 36. Lunar and Planetary Inst. Technical Report.

Weymann, R. J. et al. (June 1980). „The triple QSO PG1115+08 - Another probable gravitational lens“. In: *Nature* 285, pp. 641–643. DOI: 10.1038/285641a0.

Young, P., R. S. Deverill, et al. (Mar. 1981). „The triple quasar Q1115+080A, B, C - A quintuple gravitational lens image“. In: *ApJ* 244, pp. 723–735. DOI: 10.1086/158750.

Young, P., J. E. Gunn, et al. (Mar. 1981). „Q0957+561 - Detailed models of the gravitational lens effect“. In: *ApJ* 244, pp. 736–755. DOI: 10.1086/158751.

Zaroubi, S. et al. (Oct. 2012). „Imaging neutral hydrogen on large scales during the Epoch of Reionization with LOFAR“. In: *MNRAS* 425, pp. 2964–2973. DOI: 10.1111/j.1365-2966.2012.21500.x.

Zwicky, F. (Feb. 1937a). „Nebulae as Gravitational Lenses“. In: *Physical Review* 51, pp. 290–290. DOI: 10.1103/PhysRev.51.290.

Zwicky, F. (Oct. 1937b). „On the Masses of Nebulae and of Clusters of Nebulae“. In: *ApJ* 86, p. 217. DOI: 10.1086/143864.

Curriculum Vitae

Personal Information

Name	Rafael KÜNG
Date of Birth	6 February 1984
Nationality	Swiss
Place of Origin	Beinwil (Freiamt) AG

Education

2014–2017 **Doctorate** (Dr sc. nat.)
Physik-Institut, Universität Zürich
Supervisor: Prof. Dr P. Saha *Chair:* Prof. Dr Ph. Jetzer
Title: Probing the Universe with Citizen Science and Gravitational Lensing

2011–2014 **Master** in Computational Science
Physik-Institut, Universität Zürich
Supervisor: Prof. Dr P. Saha
Title: SpaghettiLens – Lens Modelling Made Easy

2006–2011 **Bachelor** in Physics
Minors: Mathematics, Neuroinformatics, Special Informatics for Natural Sciences
Physik-Institut, Universität Zürich
Supervisors: Prof. Dr G. Lake, Dr Ch. Corbett Moran
Title: HaloViz – Fast Analysis and Visualisation of Halo Track Data

2000–2005 **Matura** with focus on Physics and Applied Mathematics
Kantonsschule Wohlen

Publications

2018 „SPAGHETTILENS: A software stack for modeling gravitational lenses by citizen scientists“
R. Küng
Astronomy and Computing **23** *pp. 115–123*

2018 „Models of gravitational lens candidates from Space Warps CFHTLS“
R. Küng, P. Saha, I. Ferreras, E. Baeten, J. Coles, C. Cornen, C. Macmillan, P. Marshall, A. More, L. Oswald, A. Verma, and J. K. Wilcox
MNRAS **474** *pp. 3700–3713*

2016 „SPACE WARPS - I. Crowdsourcing the discovery of gravitational lenses“
P. J. Marshall, A. Verma, A. More, C. P. Davis, S. More, A. Kapadia, M. Parrish, C. Snyder, J. Wilcox, E. Baeten, C. Macmillan, C. Cornen, M. Baumer, E. Simpson, C. J. Lintott, D. Miller, E. Paget, R. Simpson, A. M. Smith, R. Küng, P. Saha, and T. E. Collett
MNRAS **455** *pp. 1171–1190*

2016 „SPACE WARPS - II. New gravitational lens candidates from the CFHTLS discovered through citizen science“
A. More, A. Verma, P. J. Marshall, S. More, E. Baeten, J. Wilcox, C. Macmillan, C. Cornen, A. Kapadia, M. Parrish, C. Snyder, C. P. Davis, R. Gavazzi, C. J. Lintott, R. Simpson, D. Miller, A. M. Smith, E. Paget, P. Saha, R. Küng, and T. E. Collett
MNRAS **455** *pp. 1191–1210*

2015 „Gravitational lens modelling in a citizen science context“
R. Küng, P. Saha, A. More, E. Baeten, J. Coles, C. Cornen, C. Macmillan, P. Marshall, S. More, J. Odermatt, A. Verma, and J. K. Wilcox
MNRAS **447** *pp. 2170–2180*

Conferences, Schools and Talks

2017 “SpaghettiLens” (poster)
Jul 09–14 LERU Doctoral Summer School – Citizen Science: nexus between research and public engagement
Zurich, Switzerland

2017 ACES Workshop (LOC)
Jun 29–30 *Zurich, Switzerland*

2017 “Mapping dark matter with citizen science” (talk)
Feb 06–07 Swiss Cosmology Days 2017
Basel, Switzerland

2016 “SpaghettiLens – A citizen science powered distributed modelling software
Oct 16–20 stack written in Python” (poster)
Astronomical Data Analysis Software & Systems – ADASS XXVI
Trieste, Italy

2016 11th International LISA Symposium (LOC)
Sept 02–09 *Zurich, Switzerland*

2016 20th Microlensing Workshop
Jan 13–15 *Paris, France*

2015 “Lensing galaxies in the CFHT Legacy Survey” (talk)
Jul 12–18 Fourteenth Marcel Grossmann Meeting – MG14
Roma, Italy

2015 "Lensing galaxies in the CFHT Legacy Survey" (poster)
Jun 22–26 European Week of Astronomy and Space Science – EWASS 2015
Teneriffe, Spain

2015 "Modelling gravitational lenses in SpaceWarps" (talk)
Feb 05–06 Swiss Cosmology Days 2015
Geneva, Switzerland

Funding

FK14-081 University of Zurich Candoc reseach grant (Forschungskredit Candoc)

FK15-087 University of Zurich Candoc reseach grant (Forschungskredit Candoc)